Evolution of Dark Spots
in
Organic Light Emitting Devices

Liew Yoon Fei

NATIONAL UNIVERSITY OF SINGAPORE

2004

Evolution of Dark Spots
in
Organic Light Emitting Devices

Liew Yoon Fei

(M.Sc., NUS)

A THESIS SUBMITTED

FOR THE DEGREE OF DOCTOR OF PHILOSOPHY

DEPARTMENT OF ELECTRICAL AND COMPUTER ENGINEERING

NATIONAL UNIVERSITY OF SINGAPORE

2004

Acknowledgements

I gratefully acknowledge and express deep appreciation to many wonderful people who had helped to make this project succeeded. First and foremost, I am deeply indebted for the indulgence of my family, and particularly to my parents, for their understanding and supporting throughout the years. I would like to express my deepest gratefulness to my wife, Shiau Yee for her unquestioning faith and support throughout the whole project.

I would like to express my heart-most gratitude to my supervisors Professor Chua Soo Jin and Dr. Zhu Furong for their invaluable guidance and advices. My appreciation also goes to Professor Xu Gu and Dr. Tok Eng Soon for their friendship, help, encouragement and discussion during my entire candidature. What I have learned from them is truly beneficial to the rest of my life.

I would like to thank Institute of Materials Research and Engineering (IMRE) for offering me the opportunity to pursue my research work in IMRE. My appreciation also goes to the staffs in IMRE, Jianqiao, Weiwei, Roshan, Siew Wei, Bee Ling, Li Wei, Kian Soo, Xiao Tao and Yanqian for their enormous help and support all this while.

Table of Contents

Summary

The demand for cost effective information displays has driven an increase in effort of research into improving the performance of organic light-emitting devices (OLEDs). Despite these attempts, the gradual decrease in electroluminescence efficiency and increase in operating voltage remain the major hurdles that limit the long-term stability of the OLEDs. Apart from the intrinsic instability of the organic materials, the growth of non-emissive areas known as dark spots in OLEDs is another limiting factor that deteriorates the device performance. Various mechanisms have been proposed to address the ambient-induced growth of dark spots. Recent studies show that organic/cathode interface is mainly responsible for the formation of dark spots. These interfacial deteriorations in OLEDs are often considered a result of cathode delamination or insulating layer formation at the organic/cathode interface.

It is known that the dark spots in OLEDs grow when they are not operated or are stored in ambient conditions. Many studies on the growth of dark spots have focused mainly on devices under various operating modes. However, the initiation and the growth mechanisms of the dark spots in OLEDs formed before the operation of the devices are not well investigated and fully understood. In order to pursue the study of the origin and growth behavior of these dark spots in OLEDs without external stimulus, it is thus essential to eliminate electrical influences via non-operation mode.

In this study, an optical image analysis technique is developed to study the growth of dark spots in OLEDs under non-operation condition. Under reflected light of a microscope, a direct relationship between dark spots, found in the emitting area of

the OLEDs, and circular features, seen in the same locations of non-operated devices, is identified. By using this technique, the electrical field effect on dark spot formation is eliminated. Investigation of organic/cathode and anode/organic interfaces with respect to their morphologies and chemical states was carried out in order to reveal the mechanism of dark spots formation in OLEDs. Atomic force microscopy (AFM) was employed to study the morphology of ITO and organic films deposited on ITO. X-ray photoelectron spectroscopy (XPS) was used to obtain the materials chemical states.

Results reveal that thickness and roughness of organic films do not seem to have significant impact on the growth of dark spots. It is found that the growth of dark spots is dependent on the anode/organic contact. Results confirm that the degradation site for the formation of dark spots indeed occurred at the organic/cathode interface, but has great influence from the anode/organic interface. There is no evidence of indium and oxygen diffusion from either the cathode or the anode to the organic layer. Therefore, indium diffusion can not be the cause of dark spot formation in OLEDs under non-operating condition.

Based on the experimental results obtained from this study, a model of dark spots formation in OLEDs under non-operating condition is proposed. The growth of dark spots is associated to the corrosion or oxidation process of reactive cathode. The growth of dark spots is accelerated by the formation of a galvanic cell between cathode and anode in OLEDs. The galvanic cell is formed due to the presence of an internal built-in potential, induced by a pair of dissimilar electrodes in OLEDs.

Abbreviations

ac	alternative current
AFM	Atomic force microscopy
Alq_3	Tris-(8-hydroxyquinoline) aluminum
BE	Binding Energy
CuPc	Copper phthalocyanine
CRT	Cathode ray tube
dc	direct current
EL	Electroluminescent
ETL	Electron transporting layer
HOMO	Highest occupied molecular orbital
HBL	Hole blocking layer
HTL	Hole transporting layer
ITO	Indium tin oxide
J-V-L	Current density-voltage-luminance
LCD	Liquid crystal display
LED	Light-emitting device
LUMO	Lowest unoccupied molecular orbital
NPB	N, N'-di(naphthalene-1-yl)-N, N'-diphenylbenzidine
OLED	Organic light-emitting device
PDA	Personal digital assistant
PDP	Plasma panel display
PLED	Polymer light-emitting device
PPV	poly(*p*-phenylene vinylene)

RL	Reflected light
RMS	Root mean square
TFEL	Thin film electroluminescent
XPS	X-ray photoelectron spectroscopy

List of Figures

List of Tables

List of Publications

1. *Investigation of the sites of dark spots in organic light-emitting devices*
   Yoon-Fei Liew, Hany Aziz, Nan-Xing Hu, Hardy S.O.Chan, Gu Xu, Zoran Popovic
   Applied Physics Letters, Volume 77, pp2650-2652 (2000)

2. *Reduced reflectance cathode for organic light-emitting devices using metalorganic mixtures*
   Hany Aziz, **Yoon-Fei Liew**, H. Michelle Grandin, Zoran D. Popovic
   Applied Physics Letters, Volume 83, pp186-188 (2003)

3. *Novel Cathode for Organic Light Emitting Devices with Reduced Optical Reflectivity*
   Hany Aziz, **Yoon-Fei Liew**, Zoran Popovic
   Proceeding of SPIE's 48th annual meeting, Organic Light Emitting Materials and Devices VII, San Diego, California, 3-8 August 2003Proc. SPIE Int. Soc. Opt. Eng. 5214, pp277 (2004)

4. *Effect of surface electronic properties of ITO on luminance efficiency of OLED*
   Furong Zhu, Hu Jian Qiao**, Liew Yoon Fei**, Kian, Soo Ong, Hao Xiaotao
   Proc. SPIE 5277, pp163-173 (2004)

5. *Effect of organic layer combination on dark spot formation in organic light emitting devices*
   Yoon-Fei Liew, Furong Zhu , Soo-Jin Chua
   Chemical Physics Letters, Volume 394, pp275-279 (2004)

6. *Alq_3-modified indium tin oxide for enhancing the efficiency and reliability of organic light emitting devices*
   Yoon-Fei Liew, Furong Zhu, Soo-Jin Chua
   Applied Physics Letters, Volume 85, pp4511-4513 (2004)

7. *Fundamental of dark spot formation in organic light-emitting devices*
   (manuscript in preparation)

Chapter 1

Introduction and Research Overview

1.1 Information Display

Information display is an important communication interface between man and machine. The discovery and development of cathode-ray-tube-based television, transmitting the full visual content of an event, have brought knowledge and entertainment directly to the general population. The related communication and display technologies also have used for delivering the news from around the world to the living room. The introduction of liquid crystal displays (LCDs) enabled information exchange applying for the portable electronics. Now the organic light-emitting device (OLED), a novel flat panel display technology, promises to bring full imagery and graphical content to truly convergent products, comprising video, text and data.

OLEDs have many advantages over the existing display technologies. They are lightweight and much thinner compared to the bulky CRT or LCD displays. They are self–emissive with high luminous efficiency and can be operated at a few volts, unlike CRTs that are usually operated at thousand of volts. With the advances of chemistry and physics, OLEDs can emit light in many colors, from deep blue to infrared. Other advances of organic thin film displays include high resolution, fast switching speed and flexibility. However, OLEDs will have to compete with exciting, well-established technologies like CRTs and LCDs. The market for displays is huge, estimated to be some US$30 billion per annual [Gymer, 1996, Burrow *et al*. 1997], and the lure of success is sufficient to persuade industry to invest significantly in the development of OLEDs. Expected applications range from simple backlights for portable battery-operated equipment, through alphanumeric displays, to complex full

color video screens for computer and televisions. The first commercial OLED product was launched in 1999 by Pioneer Corporation using Kodak licensed technologies.

1.2 Display Devices

The commonly used display devices can be classified into four different types according to their operating mechanisms, namely cathodoluminescent, non-emissive, plasma and electroluminescent displays. Their operation mechanisms are described briefly in the following sections.

1.2.1 Cathodoluminescent Display

The cathode ray tube (CTR) is an example of cathodoluminescent display which is commonly used in television and computer monitor. The first CRT was developed by Ferdinand Braun, a German scientist, in 1897. It was applied for the television sets in the late 1940s. The mechanism of such devices is based on cathodoluminescence, electrons are generated from an electron gun and are falled onto phosphor screen leading to light emission. In a colored television, there are three electron guns, each of them is controlled for emitting three primary colors, red, green, and blue. When the operation of these three electron guns is controlled, the system enables to produce color images for display applications.

CRTs are the most widely used display devices at present time due to its matured technology and inexpensive price, even though the technology has been around for nearly 70 years. However, CRT displays are very heavy and bulky. CRTs

require a vacuum tube and a long neck for deflecting and focusing the electron beam. The electron optic system makes CRTs unsuitable for large flat panel displays. Another major disadvantage of CRTs is the high operation voltage of up to 30kV. The strong magnetic field used in the CRTs also creates harmful electromagnetic radiation.

1.2.2 Non-emissive Display

Non-emissive displays, as the name implied, are devices that are inherently incapable of emitting light. Liquid crystal displays, LCDs, are the most common non-emissive display devices. Liquid crystal was first discovered in the late 19th century by Friedrich Reinitzer, an Austrian botanist. The term "liquid crystal" was coined shortly by Otto Lehmann, a German physicist. Liquid crystals are almost transparent substances, exhibiting the properties of both solid and liquid matter. Liquid crystal molecules tend to align parallel to each other due to their chemical structure. They usually orient themselves randomly on a mechanically rubbed substrate, resulting in an optical anisotropy – despite the fact that the molecules form a liquid. The molecular orientation in liquid crystals is very sensitive to an applied electric field. Thus a liquid crystal cell works like a tiny optically tunable shutter that can be controlled by a locally applied electric field. The liquid crystal cell is sandwiched between a pair of polarizers to form a single pixel. The operation of such devices is therefore based on the presence of a separate illumination source. When electric field is applied locally, the orientation of the liquid crystal molecules can be controlled, leading to an optically opaque or transparent transformation. By installing a color filter of red, green, or blue for each pixel, full color images can be displayed.

LCDs are currently widely used in watches, calculators, laptop computers and television. Although lightweight, compact size with low power consumption are considered to be their strong assets over the CRTs, LCDs have a major disadvantage of high cost compared to CRTs. Furthermore, LCDs bear limited viewing angle and limited operation temperature range of -20 to +50°C. These drawbacks, in addition to their dependence on a separate illumination source, result in LCDs having limitations in application.

"Electronic paper" is another non-emissive display technology. It offers excellent resolution and high visual contrast display with a wide viewing angle. It does not require an external power to retain its image, and it is lightweight, inexpensive and remarkably flexible. This technology, being developed for electronically configurable paper-like displays, relies on microscopic beams that change colors in response to the charges on nearby electrodes. There are two types of beans used: the first type is a two-tone solid bean invented by Nicholas Sheridon. Each bean is two-toned with one half white and one half black, with opposite polarity charges on each half, that twist around in place when respond to electrical field. The second type of the beans, developed by Joseph Jacobson, consists of see-through microcapsules containing charged pigment chips that move through a liquid medium when an electrical field is applied.

This technology is being used as signboard in department store, character and segmented displays for advertising. Commercial prototypes have been developed for high-resolution active matrix displays including personal digital assistants (PDAs), mobile telecommunication devices, and portable electronic books.

1.2.3 Plasma Displays

Plasma display panels (PDPs), similar to CRTs, also use phosphor materials for light emission. Essentially, a PDP can be considered as a matrix of tiny fluorescent tubes, which are controlled in a sophisticated fashion. Each cell comprises a small capacitor with a pair of parallel electrodes and a mixture of inert gases, such as argon, neon or xenon sealed in the cell. When a high electric field is applied between two electrodes, electrons and ions are accelerated and bombard gas molecules to break down gas molecules producing weakly ionized plasma. Once energized, the cells of plasma release ultraviolet light, which then strikes and excites red, green and blue phosphors along the face of each pixel, and visible light is emitted when the excited molecules relax to the ground state.

Compared to conventional CRT displays, the thickness of PDPs is ~ 4 inches, which is about one-tenth thinner than that of CRTs. A 40 inches PDP is about 67 pounds, this is about one-sixth of the weight of a typical CTR display. PDPs use over 16 million colors and have a 160° viewing angle. Because of their dependence on an electric discharge in a gas medium, plasma displays essentially require high operating voltage of over 100 V and demonstrate low brightness (up to 150 cd/m^2). Another ultimate limitation of plasma display has proved to be pixel size. At present, it is very challenge to get pixel sizes below 0.3mm, even in the long term. A biggest obstacle that plasma displays have to overcome is their inability to achieve a smooth ramp from full white to dark black. Low shades of gray are particularly troublesome, a noticeable posterised effect being present during the display of movies or other video programming with dark scenes.

1.2.4 Electroluminescent (EL) Displays

The mechanism of operation of the fourth class of display devices, the electroluminescent devices, depends on the radiative relaxation (in the form of visible light) of excitation generated by an electrical stimulus. The EL displays can be further classified into two classes, according to the active materials used, i.e. inorganic and organic electroluminescent devices.

1.2.4.1 Inorganic Light Emitting Devices

There are two types of inorganic electroluminescence devices. In the first type, light is produced by the direct recombination of electrons and holes, which move towards each other from conduction band and valence band respectively. the carrier are transported through a diffusion process which can be controlled by an external applied direct current (dc) electric field. The recombination of holes and electrons in p-n junction in inorganic light emitting diodes (LED) is one of the examples. The electroluminescent materials are usually made of III-V semiconductor compounds. Due to the fact that the diodes must be made of single crystal materials, which are difficult to obtain in sizes exceeding few millimeters, the inorganic light emitting diodes are mainly used for semiconductor lasers, indicator lights, and light sources for optical communication. In the second type, the electroluminescence mechanism is based on placing a doped phosphor materials, between two dielectric layers onto which two electrodes are deposited from outside. This type of devices is also called thin film electroluminescent device (TFEL). Electrons and holes are generated by means of impact ionization or by quantum mechanical tunneling under the effect of a strong externally applied high alternate current (ac) electrical field (~10^6 V/cm). The recombination of electrons and holes take place at the dopant sites thereby producing

light. The phosphor materials, from the II-VI semiconductor compounds group (e.g. ZnS), usually have a large band gap. Although such devices can be made in relatively large size, their use is limited due to a requirement of high ac drive voltage (>100V). In addition, most inorganic light emitting devices are linked to a narrow range of substrates due either to stringent lattice-matching requirements, or high temperature processes associated with semiconductor growth.

1.2.4.2 Organic Light Emitting Devices (OLEDs)

Organic semiconductor based light emitting device is the most recent class of display devices. The device structure and operation mechanism are quite similar to the first type of inorganic LED, except that the active electroluminescent materials are organic semiconductors. In the most basic device structure, a thin layer of an organic electroluminescence material (50-100nm) is sandwiched between two metal electrodes in which at least one is transparent. Figure 1.1 shows a schematic diagram of a typical OLED structure. Under the influence of an externally applied dc field, electrons and holes are injected from the opposite electrodes, and transported towards each other to form electron-hole pair called exciton. Light is produced and emitted through the relaxation of the exciton process from the transparent electrode side.

Obtaining electroluminescence in an OLED required placing the organic electroluminescent materials between two conducting electrodes with different work functions. The difference in work function is required for the efficient injection of electrons and holes. When an electric field is applied, electrons are injected from electrode with lower work function, called cathode, into the conduction band of the organic materials, while holes are injected from electrode with higher work function,

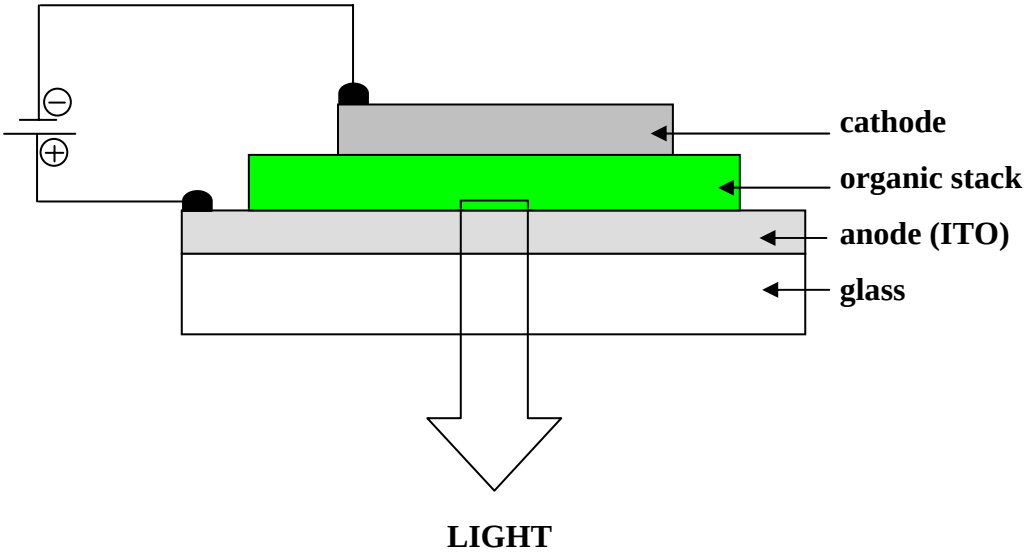

Figure 1.1: A cross sectional view of a typical OLED.

an anode, into the valence band of the organic materials. The electrons and holes are transported towards each other, driven by the electric field, and recombined to form excited state of electron-hole pairs, termed excitons. Because the excitons are in an unstable state, the excitons will then relax radiatively to ground state, producing photons. If energy of the photon is in the range of 1.8 to 3.2eV, visible light is produced. In order for the photon to emit out from the device, at least one of the electrodes is made transparent. Indium-tin-oxide, ITO (90% In_2O_3, 10% SnO_2) is a commonly used transparent electrode for the hole-injection, with a band gap >3eV, a work function of about 4.8eV, and transmission of more than 90% in the visible wavelength range.

Organic light emitting devices can be divided into two groups according to the size of the organic molecules used. The first group is the small molecule based device, commonly called "Organic Light Emitting Devices (OLEDs)", usually with molecular weight in the range of 200-800. The second group is from the large molecules (polymer) devices, and is called "Polymeric Light Emitting Devices (PLEDs)", with molecular weight > 10^5. Typical examples of most widely used small molecular and polymeric electroluminescent materials are tris(8-hydroxyquinoline)aluminum, Alq_3 and poly(*p*-phenylene vinylene), PPV, respectively. The fabrication process for OLEDs and PLEDs are different but relatively simple. OLED is fabricated by vacuum deposition and PLED is fabricated via spin-coating process. All these process do not require high temperature, and can be maintained at room temperature during deposition. The films of organic and polymeric materials are amorphous, therefore they can be deposited on any substrate without lattice matching requirement, which is required for the growth of conventional inorganic semiconductor LEDs. As a result, a

wide variety of substrate materials can be selected, for example lightweight, flexible, and robust plastic substrates. The simplicity of the device fabrication process, availability of the organic materials and flexibility of substrate choice enable to fabricate OLED inexpensively. In addition, the thickness of the organics active layers is less than 1μm, which distinguishes OLED technology from TFEL technology, in which the active layers are usually several microns thick. Because OLEDs are so thin, a voltage of only 2-10V applied between the electrodes can result in an electric field high enough to inject charges into the organic layers. OLEDs are self-emissive devices, thus do not require backlight, which is necessary for LCDs. This can reduce the power consumption and the volume of the display module enabling the OLED viewable over a wide angle. Furthermore, OLEDs exhibit fast sub-microsecond switching speed, which allows for high quality video images and movies.

1.3 Development of OLEDs

The phenomenon of electroluminescence was first discovered in inorganic materials in 1936, when Destriau observed high field electroluminescence from ZnS phosphor powder dispersed in an isolator and sandwiched between two electrodes [Destriau 1936]. In 1962, the first commercial inorganic LED based on inorganic semiconductor GaAsP was introduced by General Electric [Holonyak and Bevacqua 1962]. Electroluminescence from organic crystals was first observed from anthracene in 1963 [Pope *et al*. 1963]. However the efficiency and lifetime of resulting devices were significantly lower than those obtained from inorganic system at that same time, research activities had been focused on the inorganic materials. Electroluminescence

from devices made of anthracene can only be seen in dark room and only last for few seconds. In the late 1980s, Tang and VanSlyke with their research on electroluminescence of organic compounds, developed a new generation of light emitting devices [Tang and VanSlyke 1987]. High luminous efficiencies of 1.5 lm/W and brightness of more than 1000 cd/m^2 at a driving voltage of less than 10 V with their double layer OLEDs was reported. Shortly afterward, in 1990 the Friend's group announced a conducting polymer-based light emitting devices [Burroughes *et al.* 1990]. Since then research in OLEDs was sparked off and has led to many advanced developments on OLEDs, including the improvements in color gamut, luminescence efficiency and device reliability. One of the key enablers in the history of OLED advancement can be attributed to the continuing discovery of new and improved electroluminescent materials, which were made possible by the dedication and ingenuity of many organic chemists who provide the design and skilled synthesis. Indeed, from small molecules, oligomers to conjugated polymers, intense research in both academia and industry has yielded OLEDs with remarkable color fidelity, device efficiencies and operational stability. The growing interest is largely motivated by the promise of the use of this technology in flat panel displays. As compared to conventional LED, the development of OLEDs is significant over the past few years as illustrated in Figure 1.2 [Sheats *et al*. 1996].

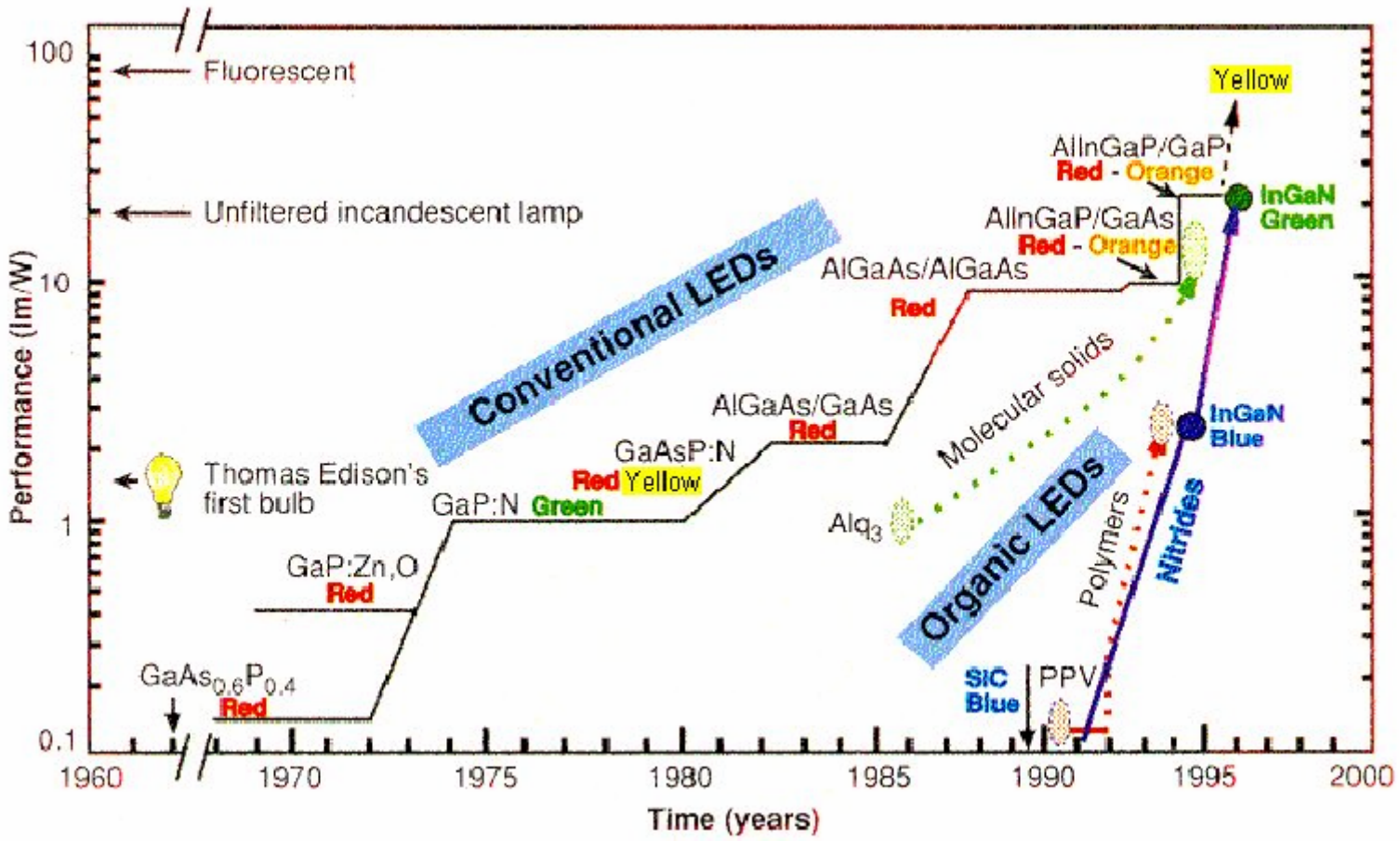

Figure 1.2: Comparison between the progress in EL efficiency for inorganic and organic LEDs [Sheats et al. 1996].

1.4 Remaining Challenges for OLEDs

Although OLED technology has been developed rapidly over the past decade, and it has many advantages over the existing display technologies, there still remain challenges for OLEDs towards the commercialization. The current challenges for OLEDs include (a) achieving full color display, (b) improving EL efficiency, and (c) extending device operation lifetime.

1.4.1 Achieving Full Color Displays

There are a few fundamental issues in achieving full color in OLEDs. One of those issues is related to the design of organic EL materials. If OLEDs can emit three primary colors i.e. red, green, and blue, principally, full color display can be achieved. Similar to inorganic LED, in order for the devices to emit different color, the band gap of the emitter is varied. Therefore, a wide range of emitters with the desired band gap could be designed chemically. [Shoustikov *et al*. 1998]. Besides synthesizing new emitter, the emission color can be changed by doping the EL materials with appropriate dopant. For example, the emission of Alq_3 can be changed from green to yellow by doping rubrene in Alq_3. [Vestweber and Rieb 1997] Even though organic emitter with a wide range of color can be synthesized, high color purity and material stability are still the open challenge.

Besides the organic materials issues, the architecture of OLEDs is another important factor for achieving full color display. With the demonstration of blue OLEDs, the most difficult color to produce due to it high band gap, the issue on achieving different color becomes easier. One of the architecture designs of full color display is to use blue OLEDs and fluorescent color filters where all OLEDs emit the

same blue color, and the change of color is accomplished by fluorescent color filters. Another design involves the construction of RGB (Red, Green, Blue) pixel array, in which three basic color devices have to be presence. [Burrows *et al*. 1997, Gu and Forrest 1998].

1.4.2 Improving EL Efficiency

In order to improve the EL efficiency, two major issues must be addressed, the energy level matching and the quantum efficiency of emitter materials. This is related to the design and synthesis of new materials. Apart from synthesizing new organic materials with different charge mobilities to improve device performance, the understanding on device operation can also be utilized to improve the efficiency of the devices. For example, the introduction of bilayer structure can sufficiently improve EL efficiency [Tang and VanSlyke 1987].

Electrode modification is another commonly used approach to obtain more balanced electron-hole current in OLEDs. The effect of cathode having different work function, on device performance has been widely investigated. [Tang and VanSlyke 1987] Nevertheless, modification of indium-tin-oxide (ITO), the commonly used anode in OLED, is also employed to improve the device performance. [Kim *et al.* 1998] For further improvement, it entails the understanding of the fundamental mechanisms leading to electroluminescence in vacuum deposited organic thin films, which is not fully understood.

1.4.3 Extending Device Operation Lifetime

Besides improving the devices efficiency, stability of the devices is another important factor that determines OLEDs performance. OLEDs suffer from poor stability due to the fall in luminescence efficiency with time during operation and also during storage at ambient environment. In general, there are two main types of degradation processes, namely "intrinsic" [McElvain *et al*. 1996, Aziz and Popovic 2004] and "dark spot" [Burrow *et al*. 1994, McElvain *et al*. 1996, Aziz and Popovic 2004] degradation. "Intrinsic" degradation refers to the decrease in the efficiency of the emitting materials to convert electric energy to light with time. While "dark spot" degradation refers to the formation and growth of non-emissive area, which leads to the reduction in the active area thus reducing the device luminescence with time.

The intrinsic degradation is usually attributed to the instability of the EL materials. In this regards, searching and designing of new materials is one of the approaches that would improve the stability of OLEDs. Besides searching and synthesis of new materials, device structure modification is another approach which can extend the lifetime of OLEDs. [Aziz *et al*. 1999]

Apart from the intrinsic instability of the organic materials, the growth of non-emissive areas known as dark spots in OLEDs, is another limiting factor that deteriorates the device performance. Recent studies show that organic/cathode interface is mainly responsible for the formation of dark spots. These interfacial deteriorations in OLEDs are often considered as a result of cathode delamination or insulating layer formation at the organic/cathode interface. [Liew *et al.* 2000, Kolosov *et al.* 2001, Kim *et al.* 2002]

1.5 Research Objective

It is known that the dark spots in OLEDs grow when they are not operated or are stored in ambient conditions. Many studies on the growth of dark spots have focused mainly on devices under various operating modes. However, the initiation and the growth mechanisms of the dark spots in OLEDs formed before the operation of the devices are not well investigated and fully understood. In order to pursue the study of the origin and growth behavior of these dark spots in OLEDs without external stimulus, it is thus essential to eliminate electrical influences via non-operated mode.

The objective of the research was to investigate and understand the nature and the origin of dark spots degradation, leading to the reduction in device active area, hence reducing the device luminescence with time. Even though the ambient-induced growth of dark spots can be controlled by means of encapsulation, the origin of dark spot is still not fully understood. It is certain that dark spots in OLEDs do not increase in number, but their size is time dependent. Therefore, a better understanding on the origin of dark spots is important for controlling the nucleation and growth of dark spots. However, the focus of this study was on the growth of dark spots rather then the nucleation.

This work was focused on studying the nature of dark spots formation in small molecule based OLEDs. An optical image analysis technique was developed to study the growth of dark spots in OLEDs. A direct relationship between dark spots, found in the emitting area of the OLEDs, and circular features, seen in the same locations of

non-operated devices, was identified. The image analysis technique enables to study the evolution of the dark spots formed in OLEDs before device operation. By using this technique, the electrical field effect in dark spot formation is eliminated.

In this study, investigation of organic/electrode interfaces with respect to their morphologies and chemical states was carried out in order to reveal the mechanism of dark spots formation in OLEDs. Atomic force microscopy (AFM) was employed to study the morphology of ITO and organic films deposited on ITO. X-ray photoelectron spectroscopy (XPS) was used to obtain the materials chemical states. From the experimental results of this study, the main cause of dark spot evolution in OLEDs is elucidated, and new phenomenon is observed associated with the formation of dark spots.

1.6 Thesis Outline

This thesis consists of eight chapters. In Chapter 1: *Introduction and Research Overview*, the operation mechanisms of various types of displays are reviewed. The major development of organic light emitting devices (OLEDs) is presented. In the later part, some of the remaining challenges of OLEDs toward commercialization are discussed. In the last part, research objective is presented, followed by the thesis outline.

Chapter 2: *Literature Review*. In this chapter, the fundamental physics of OLED is discussed. It includes the physics of conduction and light emission in organic materials, followed by the discussion on the construction of efficient devices. The development on enhancing device efficiency will be touched on. Stability issues on OLEDs, including the intrinsic and the dark spots degradation will be further elaborated here.

Chapter 3: *Experimental*. This chapter presents the detail of the experimental methods used in the study. In the first part, sample preparation procedures are presented. In the latter part, the characterization techniques used to study the OLEDs are described.

In Chapter 4: *Evolution of Dark Spots*, an optical image analysis technique is developed to study the growth of dark spots in OLEDs under non-operation condition. By using this technique, the electrical field effect in dark spot formation is eliminated. In addition, a series of experiments that were conducted for studying the dark spot

behavior in OLEDs are described, including the substrate effect, organic layer thickness effect and multilayer effect on the degradation of dark spots. Some new observations are discussed.

In Chapter 5: *Surface and Interfacial Analyses*, investigation of organic/cathode and anode/organic interfaces with respect to their morphologies and chemical states was carried out in order to reveal the mechanism of dark spots formation in OLEDs. Atomic force microscopy (AFM) was employed to study the morphology of ITO and organic films deposited on ITO. X-ray photoelectron spectroscopy (XPS) was used to obtain the materials chemical states. Based on the experimental results, a model of dark spots formation in OLEDs under non-operating condition is proposed in Chapter 6: *Model of Dark Spot Formation*. The main cause of dark spot evolution in OLEDs is elucidated, and new phenomenon is observed associated with the formation of dark spots.

Chapter 7: *Anode Modification*. In this chapter, Alq_3–modified ITO is used to fabricate the OLEDs. The performance of the devices in relation to the EL efficiency, intrinsic stability and environment stability are characterized.

Chapter 8: *Conclusion*. This chapter summarizes the major findings of this work, and presents the most important conclusions.

Chapter 2

Literature Review

2.1 Principle and Operation of OLEDs

Semiconducting or conducting properties associated with organic materials usually derive from the presence of extended π orbitals formed in carbon-containing compounds that have $sp^2 + p_z$ hybridization. In aromatic hydrocarbon, e.g. organic electroluminescent materials, the characteristic alternation of single (σ bond) and double (σ and π bonds) bonds between the carbon atoms is termed conjugated bonding. Because the π electron system of one molecule is highly delocalized, the double bond and single bond in these molecules are interchangeable and can also interact with other neighboring molecules [Pope and Swenberg 1982]. Although such intermolecular interaction can facilitate the transfer of electrons from one molecule to another, leading to macroscopic electronic conduction in the materials, its role in amorphous organic solids, e.g. OLEDs, is negligible. This is because amorphous solids do not have long-range structural order.

According to Pauli exclusion principle, two electrons with different spins may occupy the same atomic energy level. When two isolated molecules are brought into close proximity of one another, electrons are acted upon, perturbed, by the electrons and nuclei of adjacent atom. This influence results in the splitting of their orbitals of each molecule into two; bonding and anti-bonding orbitals. When n molecules come in close proximity to one another, each district orbital may split into a series of closely spaced orbitals, each of which can be effectively seen as a continuous band, to form what is termed energy band. Just as in an atom, the lower energy bands are filled and the higher energy bands are empty. Empty energy bands are called conduction bands, and the occupied bands are called valence bands. Both conduction and valence bands

are separated by a forbidden energy gap, E_g. The highest energy orbital in the valence band is called the highest occupied molecular orbital (HOMO) and the lowest energy orbital in the conduction band is called the lowest unoccupied molecular orbital (LUMO). Both HOMO and LUMO play the most important role in determining electronic properties of an organic semiconductor material. Since electronic transitions between the valence and conduction bands of the molecule, require the absorption or the emission of a photon, with energy comparable to the forbidden energy gap, the optical properties of the materials depend on the height of the gap. For a material to be electroluminescent in the visible range of the electromagnetic spectrum, the energy gap must be in the range of 1.9 eV to 3.1 eV, which corresponds to a visible wavelength range of 650nm (red) to 400nm (violet) accordingly.

2.1.1 Transportation, Recombination and Electroluminescence

Although the energy band theory is sufficient to explain the intramolecular electronic conduction in conjugated polymer, it is still not totally suitable to describe the conduction behavior in small molecule based organic semiconductors because of the weak intermolecular interaction. Since the conduction of electron require the charge transfer from one molecule to another, the intermolecular charge transfer is assumed to occur via a hopping mechanism [Gutmann and Lyons 1967].

In the hopping mechanism, the moving entity is called polaron. Polaron is caused by excess electron in a polar medium. It is not bound to any atom and does not interact with any positively charged partner, but it interacts with the polarization created by itself. A polaron is an electron (or hole) trapped in a self-induced potential well, and the electron moves and serves as a carrier of conductivity. In a hopping

transport case, the time an electron (or hole) spends at a lattice site is much longer than the time it spends jumping from one site to another, resulting in strong electron-lattice interaction. This is due to the fact that the residence time of an electron on a lattice site is larger than the period of intramolecular nuclear vibrations. This suggests that during the time in which an electron stays at a particular molecular site, the nuclei of the molecule will move to a new equilibrium state with an opposite polarization. This induced polarization of the molecule will act back on the electron itself and reduces its energy, and hence the electron is trapped in a self-induced potential well. The combination of the electron (or hole) and the induced polarization is the polaron [Kao and Hwang 1981]. This is a nonlinear phenomenon from the very beginning, being closely related to solitons. However, polarons are caused by long-range interactions, which make them different from solitons caused by local interactions.

The polaron is a charge trapped in a potential well. The polaron can only move when it overcomes an energy barrier. The height of the energy barrier is approximately equal to the sum of the coulombic potential attracting the electron to its self-induced trap and the potential of electron affinity of the originally neutral molecule. Because an excited electron has higher energy, therefore, the energy barrier for electron at the excited state is relatively lower than that of an electron in the ground state, hopping predominantly occurs via an excited state. The longer the polaron spends in an excited state, the higher the probability of hopping.

Although polaronic effect has been used to describe the conduction in organic crystals, it is of secondary importance in amorphous solids. Due to the absence of long-range order in amorphous solids, hopping sites are located in statistically

different environments, thus both the site energy and intersite distances are subjective to a distribution. Conduction in amorphous solids is therefore governed primarily by the energy disorder formalism. The formalism is based on the argument that in the absence of long-range order, the transport manifolds are split into Gaussian distributions of localized states. The energy distribution at the hopping site arises from disorder-induced fluctuations of dipole-dipole intermolecular potentials, which result from the carrier-induced polarization of the electronic orbitals of surrounding molecules. Due to the weak van der Waals coupling amongst hopping sites, electronic states of amorphous organic solids are essentially localized. Both the energy and spatial distribution of states can be assumed to have Gaussion distribution because each of them depends on a large number of entities (energy levels or configurational coordinates), each varies randomly by a small amount. The energy involved in the charge transport is usually dependent on the hopping process. When a charge hops to a lower energy site, the process does not require activation energy and therefore it is not enhanced by electric fields, whereas the charge carrier hops to a site with higher energy, in the absence of thermal activation, it requires the assistance of a field. As an external electric field affects the energy distribution within the material, it reduces the average barrier height for hopping in the field direction, therefore the carrier mobility in amorphous organic solids is strongly field-dependent.

When an electron and hole get in close proximity, because of the coulombic interaction between the electron and hole, they recombine to form an electron-hole pair called an exciton. Excitons can be classified into two groups based on two different limiting approximations: group one, which is based on the tightly-binding approximation, is referred to as Frenkel exciton and the other, which is based on the

weakly-binding approximation known as the Wannier exciton. Frenkel excitons are found in organic molecules, where electron and hole are usually localized in the same molecule and move from one molecule to another as a pair. These excitons are also called small radius excitons. In Frenkel excitons, an electron removes from the filled orbital and occupies a previously empty orbital with higher energy. This leaves a hole in the original orbital (ground state) and the excitation is confined within the molecule. Wannier excitons are found in inorganic semiconductor, where electron and hole of the excitons are usually separated by a large distance compared to the period of crystal lattice. This is because the molecules (or atoms) are packed so closely that interaction among molecules is strong. This reduces the coulombic interaction between electron and hole and hence increases their separation. This type of excitons is also termed large radius excitons.

In general, excitons can be generated by direct optical, indirect optical and carrier injection processes. Singlet or triplet excitons may be produced. Once at the excited state, the electron tends to relax back to ground state by losing energy via radiative or non-radiative processes. The radiative transition is produced from singlet excitons, while the non-radiative transition is from the triplet excitons. In a radiative transition, the electron in the higher electronic state loses its energy by emitting a photon, therefore giving out light. Simple spin statistic arguments predict that the ratio of production of triplet to singlet excitons is 3:1, since the triplet state is threefold degenerated. Since the triplet excitons decay non-radiatively, the maximum internal quantum efficiency that can be produced is therefore 25%. However, this limit will increase up to 35% if triplet excitons annihilate to create emitting singlets [Glinski *et al*. 1978].

Before considering the microscopic organics of electroluminescence, it is worthwhile to discuss the related process of photoluminescence. Photoluminescence refers to a radiative relaxation (fluorescence or phosphorescence) of an electron from a higher electronic state to which the electron was promoted by means of absorbing of a photon. On the other hand, electroluminescence, the central phenomenon in OLEDs, refers to a radiative relaxation of an electron from a higher electronic state that has been generated electrically by the recombination of injected positive and negative charge carrier. A schematic representation of the process of photoluminescence in organic molecular solids is shown in Figure 2.1 [Sibley *et al*. 1999]. A high energy photon is absorbed to excite the molecule from ground state manifold S_0, to an excited state, S_1. Excitation can also be into a higher manifold, i.e., S_2, S_3, etc., however, this is normally followed by rapid relaxation to S_1. Typically there is some structural rearrangement that occurs in the excited state, and hence the equilibrium geometries of the ground and excited states will be different, leading to different r value (r is related to the interatomic separation in the given molecule) for the minima of the S_1 and S_0 manifolds. The result of this displacement of S_1 relative to S_0 is that the dominant transition will often be from the ground vibrational level of S_0 to a higher vibrational level of S_1 (point a in Figure 2.1).

The excited molecule rapidly relaxes to the ground vibrational level of S_1 (point b, Figure 2.1), to release energy via either radiative or non-radiative process. Alternatively, the molecule can be relaxed via a low energy state, such as a triplet, excimer, or charge transfer state. A molecule in S_1 state is referred to as a Frenkel exciton. Radiative relaxation of the molecule from the ground vibrational level of the S_1 state leads to a vibrationally excited level of the S_0 state, which rapidly relaxes to

the ground vibrational state. It is clear from this simple picture that the excitation energy must be larger than the one for emission. The molecules with a large structural change in their excited states will result in a corresponding large energy difference between the excitation and emission processes.

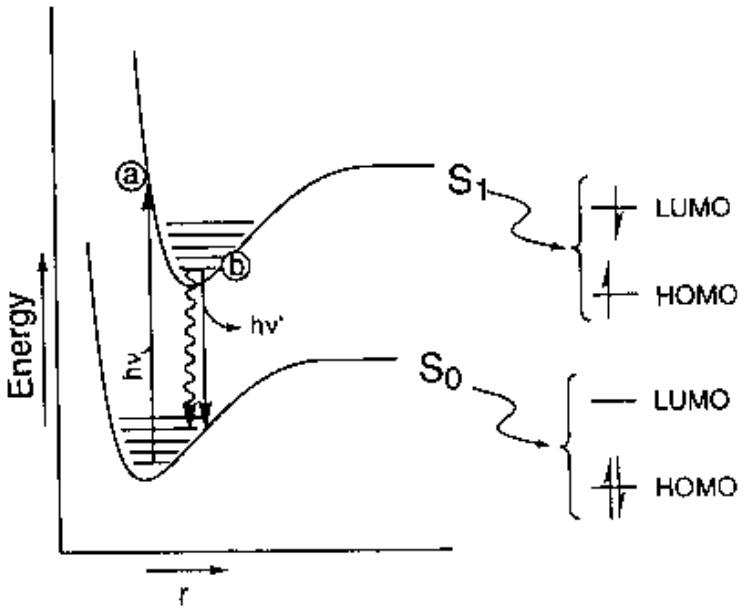

Figure 2.1: Schematic energy representation of excitation and luminescence process in an organic semiconductor.

Generally, the shape of the electroluminescent spectrum is identical to that observed in photoluminescence for an organic material. For closed shell molecules, S_0 has two electrons in HOMO and a completely vacant orbital for the LUMO. In the S_1 state, both HOMO and LUMO are singly occupied, as shown in Figure 2.2. Considering a simple OLED consisting of a thin organic film between an ITO anode and a metal cathode. When a potential is applied to the device, the material is oxidized at the anode and reduced at the cathode, leading to the injection of holes and electrons, respectively, into the thin film. Since these films consist of weakly interacting molecules, the oxidized and reduced versions of the molecule correspond to the case where holes and electrons, respectively, are located at that molecular site. The holes and electrons injected into the thin film drift in the presence of the applied field via a hopping mechanism until they are lost to the opposite electrode or encounter an oppositely charge carrier within the film. In the latter case, electron transfer from the reduced (electron carrier) to the oxidized molecule (hole carrier) occurs, leading to molecule in its ground electronic state, S_0, and an adjacent one in the S_1 or Frenkel state. The S_1 state then relaxes exactly as described above for photoluminescence. The close relationship between electroluminescence and photoluminescence is not surprising since the emission comes from the same excited state (or Frenkel exciton) in both processes.

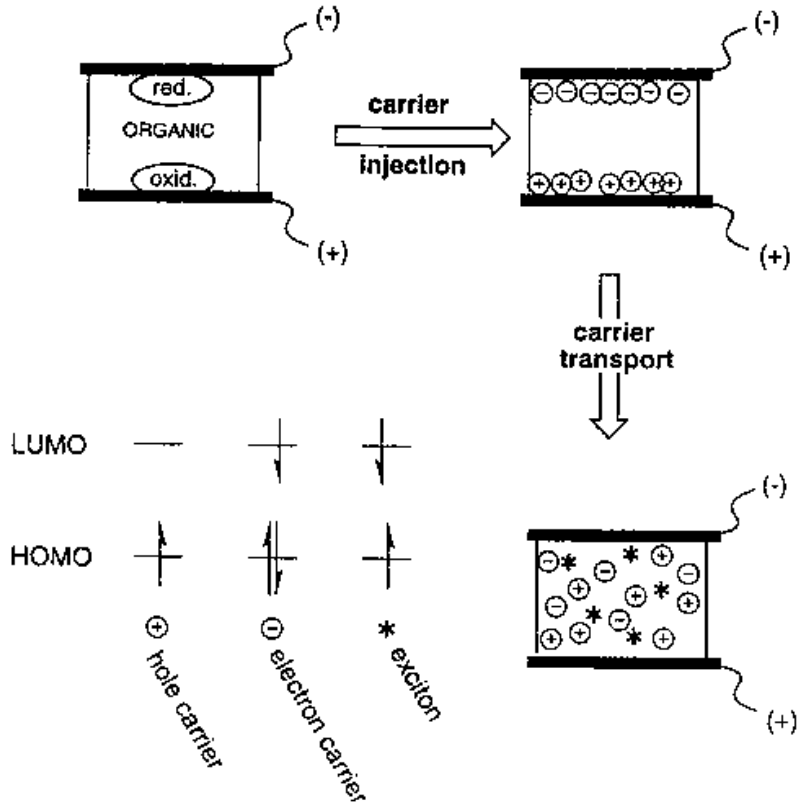

Figure 2.2: Injection and migration of charges in an organic thin film device.

2.1.2 Quantum Efficiency

In the process of light generation in OLEDs, carriers with opposite charge are injected from opposite direction through electrodes. Injected electrons and holes recombine to form excitons, thereby producing electroluminescence when excitons relax to ground state.

The internal quantum efficiency η is defined as the ratio of the number of photon emitted within the device to the number of electrons injected and is given by [Greenham and Friend 1995].

$$\eta_{int}=\gamma r_{st} q$$

where, γ: ratio of the number of excitons formed within the device, to the number of the electrons provided by the external circuit. The number of excitons formed in the thin film system is determined by the number of minority carrier.

r_{st}: luminance efficiency of excitons or the fraction of excitons formed as singlet. Approximately one singlet exciton is created for every three triplet excitons during electrical excitation, but only relaxation of singlet excitons conserves spin and generates fluorescence. Therefore, 75% of the electron-hole pairs losses to triplet excitons, which does not decay by emitting light.

q: efficiency of radiative decay of singlet excitons. In the absence of competing radiationless transitions, its value is approximately 1.

The internal quantum efficiency can be strongly affected by re-absorption, scattering, losses and waveguiding of emitted light in the sample and glass substrate. They have also been observed to substantially distort to spatial distribution of excitons, fluorescence spectra, and photoluminescent efficiency. Thus, the overall quantum efficiency, called the external quantum efficiency, is introduced to characterize the performance of real EL system.

The external quantum efficiency of an OLED is defined as [Shoustikov *et al*. 1998]

$$\eta_q = \eta_{int}\eta_e$$

where η_e : light extraction efficiency is defined as a ratio of power loss due to the light transmission within electroluminescence specimen to the total power losses in the bulk and at the surface. It is fixed for a given system. This factor can be estimated by Fresnel loss ($1/2n^2$) which is about 20% as the reflective index of most organics materials is in the range of 1.6 – 1.7.

From the above discussion, there are basically two ways to increase the external quantum efficiency, either by increase the internal quantum efficiency or increase the light extraction efficiency.

2.2 Device Configuration for Efficient Operation

The single layer OLED as shown in Figure 1.1 may generate light when a suitable potential is applied, but it will most likely not be very efficient. In practice, a number of different criteria need to be satisfied in order to have an efficient electron–hole recombination within the active organic layer and hence electroluminescence. First, energy barriers for injection of holes and electrons at the anode and cathode, respectively, need to be roughly equal to ensure a balance between the injected electron and hole densities. Figure 2.3 shows a schematic representation of energy diagram in a single layer OLED showing carriers injection and recombination. In

order to obtain high efficient electroluminescence, with respect to the energy level of organic materials, a low work function electrode is used as cathode for the injection of electrons. On the other hand, high work function electrode is utilized as the anode for hole injection. Because the energy barriers at the two electrode/organic interfaces for electron and hole injection are different, usually with a higher hole injection barrier, charge injection in single layer OLEDs is usually unbalanced, leading to inefficient electroluminescence. Besides, thickness of the organic layer also plays an important role in determining the EL efficiency of the devices. The Frenkel excitons nucleate on individual molecules due to Coulombic attraction between electron and hole. They are free to migrate through the film prior to the light emission. If the diffusion length of the exciton is larger than the film thickness, excitons will reach the electrode interface and can be quenched non-radiatively. This process can lead to a loss in device efficiency. For molecular solids, exciton diffusion length is typically over the range of 100 to 1000Å, e.g. a measured exciton diffusion length in Alq_3 was reported to be ≈300Å. [Saito *et al*. 1993, Burrows and Forrest 1994].

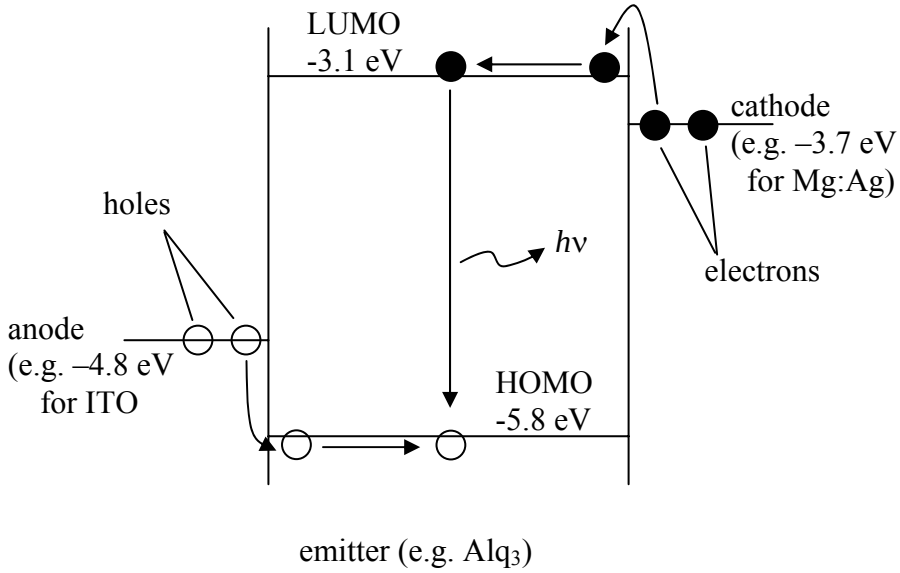

Figure 2.3: Schematic representation of energy diagram of a single layer OLED.

The first efficient bilayer OLED was reported in 1987 [Tang and VanSlyke 1987]. Since then, much effect has been focused on researching and developing high performance OLEDs due to their potentials for low power consumption, high contrast, lightweight and flexible displays [Sheats *et al*. 1996, Salbeck 1996]. In the bilayer structure device, an organic hole transporting layer (HTL), in their case a diamine compound, is introduced between the electroluminescent layer and the anode. Figure 2.4 shows a schematic representation of energy diagram for a bilayer OLED. In this bilayer structure, the emitting layer is Alq_3, which also serves as electron transporting layer (ETL). The HTL and ETL have high mobilities for holes and electrons, respectively, but very low mobilities for the oppositely charge carriers. Because the ionization potential of the hole transporting material lies between that of the electroluminescent material and the work function of anode, the injection of holes into the electroluminescent material is thus facilitated by means of energy cascading. In comparison to the electroluminescent material, hole transporting materials has a smaller electron affinity, as such the HTL acts as an electron blocking layer to reduce or avoid the electron in the electroluminescent layer to loss to the anode. As a result, a high electroluminescence efficiency device can be obtained.

The choice of materials used as anode and cathode in OLEDs is based on the energies of the filled and vacant states of the organic materials relative to the work functions of the contacts. ITO with the work function of about 4.8eV is well matched with the HOMO of HTL for hole injection, and low work function metals such as Mg, Al, and Ca having a better match with the LUMO of emitter are used as cathode for electron injection.

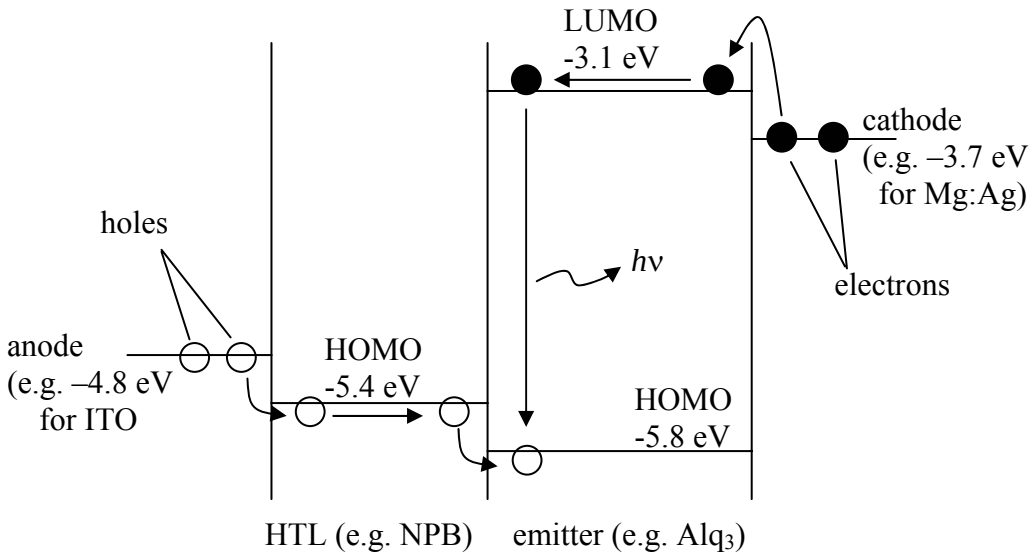

Figure 2.4: Schematic representation of energy diagram of a bilayer OLED.

As discussion above, in order to improve the device efficiency, the excitons are confined within the HTL and electroluminescent material interface that reduces the excitons diffusion length. Alternatively, the confinement of exciton can be achieved by doping a luminescent molecule into the host materials [Tang *et al*. 1989, Hosokawa *et al*. 1995, Kido *et al*. 1995, Burrows *et al*. 1996]. As long as the energy gap of the host material is higher than that of the dopant, excitons will be effectively trapped or confined in the dopant molecules leading to higher EL efficiency. The improvement of EL efficiency can be explained by confinement of recombination center and energy transfer mechanism. The excitons are trapped in the organic material to avoid the quenching through diffuse process. Besides, excitons can be formed at the dopant sites by either Förster energy transfer from the host matrix to the dopant [Pope and Swenberg 1982], or as a result of carrier trapping by the dopant. The efficiency of the energy transfer is optimized by matching the emission energy of

the host, and the absorption energy of the dopant. The criteria for the dopant as an efficient trap for electron or hole, is that the HOMO and LUMO states of the dopant must fall within the band gap of the host material, as shown in Figure 2.5.

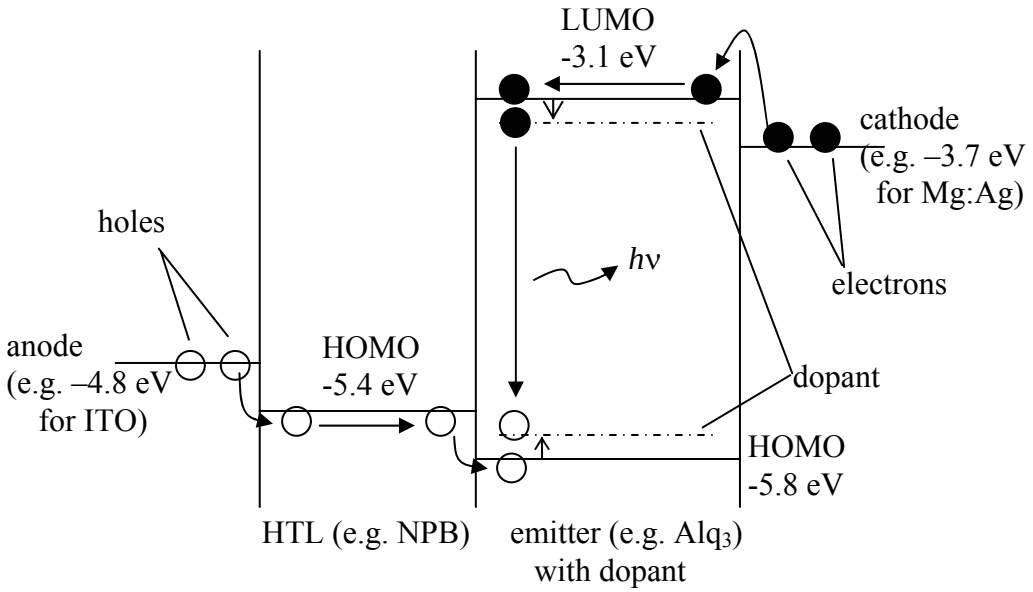

Figure 2.5: Schematic representation of energy diagram of an OLED with a doped emitter.

As described previously, triplet excitons contribute 75% of radiative loss in the OLEDs efficiency. Therefore, utilizing triplet excitons for emitting light is another approach for enhancing EL efficiency of OLEDs.

The solution to the utilization of phosphorescent materials in OLEDs is found by doping the phosphorescent material into a charge transport host material. Baldo et al. have described the major difference between fluorescence and phosphorescence in terms of materials and devices [Baldo *et al.* 1999, 2000]. Emission occurs by exciton formation in the host and energy transfer to the luminescent guest through triplet–

triplet transfer (Dexter energy transfer). This is a short-range process where excitons diffuse from donor (host) to acceptor (dye) sites via intermolecular electron exchange at a rate proportional to the orbital overlap of the donor and acceptor molecules. It differs from the mechanism described for singlet–singlet transfer (Forster energy transfer), which is a long range (~40 A), dipole–dipole coupling of donor and acceptor. The doping concentrations required for an maximum quantum efficiency are extremely high compared to the devices doped with fluorescent dyes, which are and excited by long-range Forster transfer. High efficiencies are obtained by transition from the host singlet and triplet states to the phosphor triplet states via energy transfer, intersystem crossing and by direct trapping of charge on the phosphor dyes.

High efficiency has been demonstrated in OLEDs using the phosphorescent dyes. The OLED consists of a HTL, a light-emitting layer doped with phosphorescent dyes, a barrier layer to exciton diffusion, and an ETL (Fig. 26). Owing to long lifetimes, the diffusion lengths of triplets in organic materials are substantially longer than that of singlets. To increase EL efficiency, OLED is then optimised to trap triplets within the luminescent layer, thereby increasing the probability for energy transfer from the host to the phosphor. A material suitable for this purpose is a hole blocking layer (HBL), which has a large ionization potential. Furthermore, because of its wide bandgap, it should act as a barrier to exciton diffusion. The use of a barrier layer to exciton diffusion is particularly important when the orbital overlap of the donor and acceptor molecules is weak.

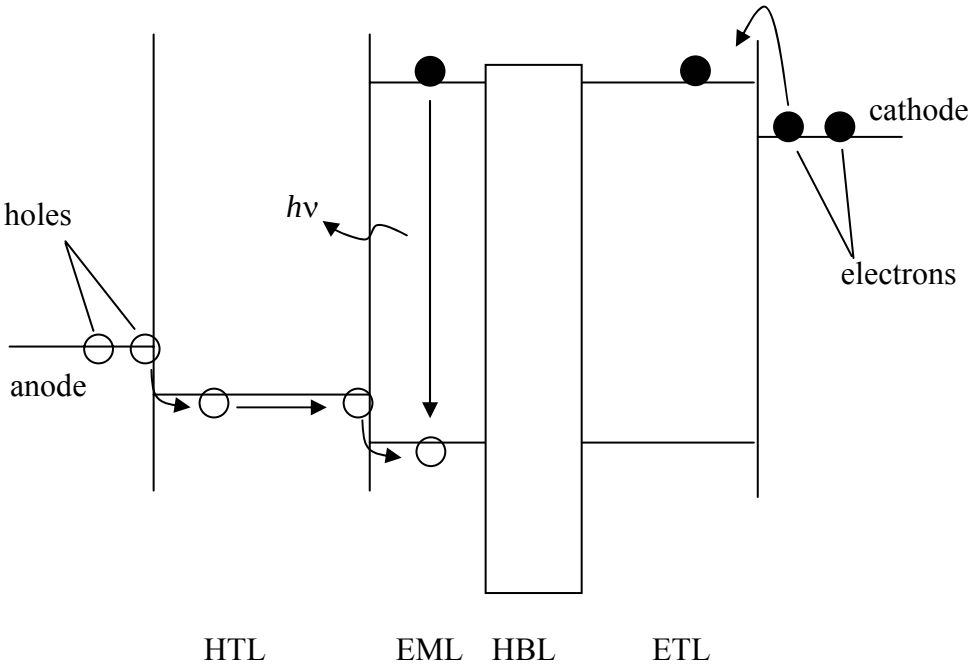

Figure 2.6: Schematic representation energy diagram of an electrophosphorescent OLED.

Besides increasing the internal quantum efficiency, optical coupling technique is applied to boost the light extraction efficiency. A considerable portion of the light originating from emissive centers in a solid film never escapes due to total internal reflection at the air–film interface. The internal trapped light scattered as an edge emission or dissipated to the waveguide. This is one of the major reasons causing low luminous power efficiency in OLEDs.

An OLED is a typical multi-layer thin film that consists of, a layer of ITO (t_{ITO} ~100 nm, n_{ITO} ~ 1.9), an organic medium (t_{org} ~ 0.1 nm, n_{org} = 1.6–1.8), and a reflecting cathode formed on a planar glass substrate (t_{sub} ~ 1 mm, n_{sub} =1.51), where t refers to the layer thickness and n refers to the refractive index. The coupling problem

can be easily analyzed provided that one can ignore both the microcavity effect and diffuse scattering at interfaces. If all surfaces are planar, light emitted from the backside of the substrate will originate only from light emitted at angles less than the organic-air critical angle, θ_1, given by $\sin^{-1}(n_{air}/n_{org})$ (ray I in Fig. 27). Light emitted at angles larger than θ_1 but smaller than the organic-substrate critical angle, θ_2, given by $\sin^{-1}(n_{sub}/n_{org})$ is trapped in the substrate (ray II in Fig. 27). Light emitted at angles larger than θ_2 is trapped in the organic and ITO layers collectively (ray III in Fig. 27), and will likely be quickly absorbed by the ITO or at the cathode [Madigan *et al.* 2000]. It can be determined that the fraction of light escaping from the substrate (coupling efficiency) is 18.9%, and the fraction of light trapped in the substrate is 34.2%. Nevertheless the fraction of light trapped in the organic/ITO layers is 46.9%, for glass substrate and $n_{org} = 1.7$.

A model based on a quantum mechanical microcavity theory has been established to compute the distribution of light emission among the three modes, and to examine the effects of the ITO thickness and the refraction index of the substrate on this distribution [Lu and Sturm 2001]. Finally, the modeling results are correlated with experimental measurements determined both by the far-field emission pattern and the edge emission of light trapped in the glass substrate. The coupling efficiency is found to range from 24 to 52%, which is much larger than the 18.9% expected from classical ray optics. The main difference between the classical and quantum mechanic models arises from the relative suppression of modes at large angles from the normal by the microcavity effect.

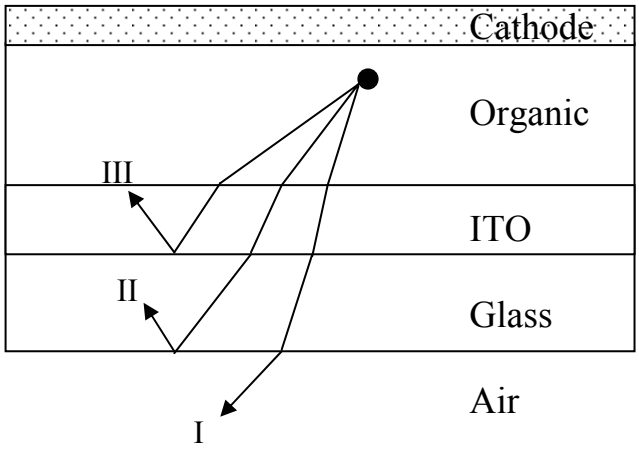

Figure 2.7: Ray diagrams in thin film OLED system showing losses by light-trapping (ray II and III), and only light emitted at sufficiently small angle will escape (ray I)

2.3 Recent Development of OLEDs

OLEDs are next generation displays touted to replace LCDs and CRTs. This is because OLEDs are self-luminescent rather than the backlighting needed by current televisions and displays. Many progresses have been made in OLED but some challenges still remain in OLEDs towards their commercialization. The current development of OLEDs is focused on (a) enhancing EL efficiency, and (b) extending device operation lifetime.

2.3.1 Enhancement of EL Efficiency

In order to enhance the EL efficiency, two major issues must be addressed, the energy level matching and the quantum efficiency of emitter materials. This is related

to the design and synthesis of new materials. The understanding on device operation can also be utilized to improve the efficiency of the devices. For example, the introduction of bilayer structure can sufficiently improve EL efficiency [Tang and VanSlyke 1987].

Due to their low molecular weight, thin films of small molecule based organic electroluminescent materials can be prepared by thermal evaporation. This preparation technique was first used by Tang and VanSlyke at Kodak for fabrication of their bilayer structure OLEDs in 1987 [Tang and VanSlyke 1987]. Bis(triarylamine) was used as hole transport layer, i.e. ITO/amine/Alq_3/Mg:Ag, resulting in high external quantum efficiencies (1%), with remarkable luminous efficiencies (1.5 lm/W) and brightness (>1000cd/m^2) at an operating voltage below 10V. Since then, Alq_3 has been extensively used as an active material in OLEDs. Alq_3 based EL devices exhibit high luminous efficiency, brightness, and external quantum efficiency [Doi *et al*. 1997, Kido and Iizumi 1998].

Along with Alq_3, other metal chelates complexes have been used as electron transport emitter in OLEDs, for example zinc complex and boron [Tao *et al*. 1999] complex. Zinc revealed a yellow luminance of 16200 cd/m^2 in the standard device configuration (ITO/TPD/Znq2/Mg:In) [Hamada *et al*. 1993-a]. By far the most noteworthy emitter besides Alq_3 is beryllium complex, which achieved a brightness of 19000 cd/m^2 and a luminous efficiency of 3.5 lm/W in a bilayer device using TPD as HTL and Mg:In as cathode [Hamada *et al*. 1993-b].

Dopants are also often used to improve device efficiency. Highly efficient organic fluorescent materials, in particular in the solid state, tend to suffer from various degrees of quenching, which typically causes broadening of emission bands and bathochromic shifts. By using dopant, quenching can be minimized by means of energy transfer. It is demonstrated that the external quantum efficiency of OLED can be increase from 1% to 2.5% by doping the Alq_3 layer with a highly fluorescent coumarin and 4-dicyanomethylene-4H-pyran (DCM) derivatives [Tang *et al*. 1989]. The dopant concentration is usually small (typically 0.5 – 1%), because higher concentration were found to affect the device performance unfavorably, as various quenching mechanisms became prevalent. So far, there are quite a number of dopants that have been used with different electron and hole transporting materials in OLEDs, e.g. porphyrins [Shoustikov *et al*. 1997], benzoxazoles [Yang *et al*. 1997], stilbenes [Hosokawa *et al*, 1997], derivatives of quibacridone [Wakimoto *et al*. 1997, Tokito *et al*. 1997, Shi and Tang 1997], coumarin [Mori *et al*. 1997, Kido and Iizumi 1998, Hamada *et al*. 1998], DCM [Frederiksen *et al*.1994, Yamashita *et al*. 1997, Mori *et al*. 1997, Baldo *et al*. 1998] etc. So far the most commonly used dopant is rubrene [Vestweber and Rieb 1997, Hamada *et al*. 1997, Jang *et al*. 1997, Aria *et al*. 1997, Fatemi *et al*, 1997, Zhang *et al*. 1997, 1998, Murata *et al*. 1998 , Katsuma and Shirota 1998, Hamada *et al*. 1999], which improve device stability and luminous significantly.

An alternative to the small molecule and polymer EL materials is the rare-earth (Lanthanide) complex emitter. Rare-earth chelates have attracted much attention for OLEDs recently. The use of rare-earth containing EL materials offers an opportunity to circumvent the theoretical upper limit of 25% of the internal quantum

efficiency. This could be accomplished via energy transfer from the triplet state of the ligand to the singlet state of the emitting lanthanide cation. The first OLED with an external quantum efficiency of 7.1%, which already exceeded the theoretical value of 5% was reported by Kido J. [Kido and Iizumi 1998].

Apart from synthesizing new organic materials to improve device performance, the luminescence efficiency of the device also is dependent on the energy level matching at the metal/organic interface. Furthermore, charge injection and charge transport play an important role in determining the device efficiency of an OLED. An unbalanced injection results in an excess one type of carriers that does not contribute to light emission. This will then cause an enhanced non-radiative recombination due to interaction of excitons with the excess charge carriers. Electrode modification is another commonly used approach to engineer the interfacial properties for improving hole-electron current balance and hence the EL performance of OLED.

Charge injection and transport are the limiting factors in determining operating voltage and luminance efficiency. In OLEDs, the hole current is limited by injection, and the electron current is strongly influenced by the presence of traps owing to metal–organic interactions. In order to enhance carrier injection the selection of efficiently electron-injecting cathode materials and the use of appropriate surface treatments of anode are of great importance. The effect of metal having different work function, used as cathode, has widely investigated. [Tang and VanSlyke 1987, Hung et al. 1997, Jabbour et al. 1997, 1998, Stossel *et al.* 1999, 2000] For example, Stossel and coworkers have investigated the Alq_3-base OLEDs, prepared at 5 x 10^{-9} mbar, with the cathode work function ranging from 2.63 to 4.70 eV. The results indicate that

the lower the work function of the metal is, the higher the current density will be. [Stossel *et al.* 1999, 2000]

Nevertheless, modification of indium-tin-oxide (ITO), the commonly used anode in OLED, is also employed to improve the device performance. [VanSlyke *et al.* 1996, Wu *et al.* 1997, Kim *et al.* 1998, Nuesch *et al.* 1999, Forsythe and Abkowitz 2000, Hung *et al.* 2001] Work function of ITO is an important factor to determine the barrier at ITO/organic interface, hence the devices efficiency. Since the work function is strongly influenced by the electronic properties at its surface, surface treatment of ITO is used to improve device performance. Acid, base and plasma treatments were proven to have dramatic effect on the device performance. [Wu *et al.* 1997, Kim *et al.* 1998, Nuesch *et al.* 1999] Besides, inserting of a buffer layer between ITO and HTL was shown to have impact on device performance as well. Organic materials like copper phthalocyanine (CuPc) and CHF_3 has been used as the buffer layer. [VanSlyke *et al.* 1996, Forsythe and Abkowitz 2000, Hung *et al.* 2001] Thin layer of insulating inorganic materials (e.g. silicon dioxide, silicon nitride) has also been employed in OLEDs. [Deng *et al.* 1999, Jiang *et al.* 2000] Both organic and inorganic materials as buffer layer in OLED have been shown to improve device efficiency by blocking or reducing the injection of holes into HTL. Usually mobility of holes in HTL is a few orders of magnitude higher than mobility of electron in ETL. [Hosokawa *et al.* 1992, Kepler *et al.* 1995, Chen *et al.* 1999, Deng *et al.* 1999] Therefore reducing holes in HTL helps to improve electron–hole current balance.

2.3.2 Extension of Device Operation Lifetime

OLEDs suffer from poor stability due to the fall in luminescence efficiency with time during operation and also during storage at ambient environment. In general, there are two main types of degradation processes, namely "intrinsic" [McElvain *et al*. 1996, Aziz *et al*. 1999] and "dark spot" [Burrow *et al*. 1994, Do *et al*. 1994, McElvain, 1996, Aziz *et al*. 1998-a, Aziz *et al*. 1998-b, Fujihira *et al*. 1997, Kawaharada *et al*. 1997] degradation. "Intrinsic" degradation refers to the decrease in the efficiency of the emitting materials to convert electric energy to light with time. While "dark spot" degradation refers to the formation and growth of non-emissive area, which leads to the reduction in the active area thus reducing the device luminescence with time.

2.3.2.1 Intrinsic Degradation

A major suspect of the intrinsic degradation in OLEDs has been attributed to the morphological instability of the organic layer, especially the hole transporting layer. In this regards, designing of new materials is one of the approaches that would improve the stability of OLEDs. In general, there are a few requirements for designing new EL materials. First of all, the materials must be stable chemically and electrochemically. The materials must not react easily with other materials especially electrochemical reaction during device operation when high electric field is applied.

In many cases, the degradation of OLEDs is attributed to the thermal instability in the HTL. Morphological changes especially the crystallization of the HTL as the cause for the decrease of the device performance has been reported [Han *et al*. 1994, 1995-a, 1996]. In other words, the film tends to undergo morphological

changes (e.g. crystallization) at high temperatures. Crystallization of HTL will result in detachment of the HTL from the electrode, and locally interrupt the electrical conduction [Han *et al*. 1994], or create non-rariative trapping sites [Salbeck 1996], hence reduce the effective contact area and electroluminescent efficiency. The morphological changes of HTL occur even at ambient temperature, and are generally characterized by relatively low glass transition temperature (T_g) (usually < 100°C) [Shirota *et al*. 1994, Adachi *et al*. 1995, Oktusu *et al*. 1997, Sato *et al*. 1998]. The organic layers in OLEDs are highly amorphous due to the nature of vacuum evaporation process, thus they are thermodynamically less favorable than more ordered structures. Morphological changes could be promoted by the movement of molecules due to rapid molecular motion near T_g, to a more stable conformation. Therefore, it was expected that a high T_g HTL is required for improved stability of OLEDs [Shirota *et al*. 1994, Adachi *et al*. 1995, Tanaka *et al*. 1996, VanSlyke *et al*. 1996, Okutsu *et al*. 1997, Itano *et al*. 1997, Hu *et al*. 1999].

In addition, an important phenomenon observed for the intrinsic degradation of OLED, that is due to the morphological change in HTL was reported in 1995 [Hamada *et al*. 1995]. In their devices, the HTL was doped with a molecular dopant, and the OLEDs lifetime was increased by two orders of magnitude. The improvement in stability was explained in term of the role of dopant in preventing the crystallization of the HTL by an entropy effect [Sato and Kanai 1994]. Since then, dopants were widely used to achieve stable devices [Shi and Tang 1997, Sato *et al*. 1997, Wakimoto *et al*. 1997, Zhang *et al*. 1998, Popovic *et al*. 2000-a]. However, another study performed on a number of hole transporting materials showed no

correction between the T_g of HTL and the durability of the OLEDs [Adachi *et al*. 1995].

Energy level matching for organic semiconductor materials is another criterion for efficient OLEDs. The ionization potentials of hole transport materials should be in the range of 5.0 eV to 5.6 eV for better holes injection. On the other hand, the electron affinity of electron transport materials is at the range of 3.0 eV to 3.5 eV for electron injection. The charge transport mobility also is an important parameter for synthesis of new materials. Last but not least, the materials should be synthesized easily for cost consideration and can be purified easily for performance consideration.

Besides searching and synthesis of new materials, the optimal design of device structure is another approach that helps to achieve high performance OLEDs. Doping of HTL, as discussed previously is one example. Another approach for improving the stability of OLEDs is to use a buffer layer between the HTL and the hole injecting electrode (ITO anode) [VanSlyke *et al*. 1996]. By using copper phthanocyanime (CuPc) as the buffer layer in a device with a non-doped HTL, lifetime of about 3500 hours was achieved. This improvement was explained in term of the instability at the HTL/ITO that may be attributed to the formation of deep carrier traps which lead to the accumulation of positive space charges in the HTL bulk near the ITO contact. Another explanation was attributed to the degradation at the HTL/ITO interface due to poor adhesion. Since then, inserting a buffer layer between the HTL and ITO became a widely followed approach to obtain stable OLEDs [Sato *et al*. 1997, Haskal 1997, Aria *et al*. 1997, Vestweber and Rieb 1997, Zhang *et al*. 1997].

Inter-diffusion between the HTL and the electroluminescent layer has been attributed as the cause of the degradation in OLEDs [Han *et al*. 1995-b, Do *et al*. 1996, Fujihira *et al*. 1996]. However, such hypothesis failed to explain why the introduction of buffer layer between the ITO and HTL gives more stable devices.

In a recent report on the degradation of Alq_3 based OLEDs, the instability of cation Alq_3 was proposed as the key factor in the intrinsic degradation [Aziz *et al*. 1999, Popovic *et al*. 2000-b]. Stable device was obtained by placing a mixed layer (made of HTL:Alq_3) between the HTL and the electroluminescent layer (in this case Alq_3). The stability of the devices was explained in terms of the imbalance charge at the emission site of Alq_3, where the holes have higher mobility than that of Alq_3. Therefore the ratio of hole to electron is high at the site of Alq_3 near the HTL/Alq_3 interface, and irreversible oxidation of Alq_3 occurred due to the instability of cation Alq_3 [Papadimitrakopoulos *et al*. 1996]. It is also able to explain improved stability of devices with the additional buffer layer and devices with doped HTL. The insertion of CuPc layer between ITO/HTL interface is able to impede hole injection into HTL, while dopant in HTL reduce the mobility of holes in HTL. Thus, both have the common feature of slowing the transport of holes to the HTL/Alq_3 interface, where they are injected into the Alq_3. Hole injection in Alq_3 appears to be responsible for the intrinsic degradation of OLEDs.

2.3.2.2 Dark Spots Formation

Apart from the intrinsic instability of the organic materials, the growth of non-emissive areas known as dark spots in OLEDs, is another limiting factor that deteriorates the device performance. Morphological changes in organic layers,

including HTL [Sato and Kanai 1994] and Alq_3 [Aziz *et al*. 1998-a], have been reported as the cause of dark spots degradation. Crystallization of organic layer will result in detachment of the HTL from the electrode. Besides, the electronic characteristic of organic films will change upon crystallization [Nguyen *et al.* 1998], where increased charge mobility is observed in organic crystal, thus localized heating (Joule heating) will occurred when the device is operated [Papadimitrakopoulos *et al*. 1998]. The high current hot spots will eventually lead to dielectric breakdown, local short circuits in which the cathode penetrates the organic layers and contact with the anode. Alternatively, the electrode may delaminate from the receding organic layer that forms a barrier between the cathode and emitter layer, resulting in voltage increase [Sato and Kanai 1994].

Other than the mechanism discussed above, decomposition of Alq_3, the most widely used electroluminescent materials, was reported [Papadimitrakopoulos *et al*. 1996]. In that experiment, Alq_3 was found to react with oxygen and water to form non-emissive polymeric byproduct. However such mechanism could not account for the degradation in encapsulated devices, where there is no continual supply of oxygen and water. Furthermore, the reaction occurred only at high temperature (>100°C). This model is no longer generally accepted as entirely valid.

Other reports attributed the dark spots degradation to inter-diffusion between HTL and EL layer [Han *et al*. 1995-b, Do *et al*. 1996, Fujihira *et al*. 1996]. It was proposed that the active EL materials became non-emissive after inter-diffusion with the HTL, hence, the formation of dark spots. However such mechanism seem to

contradict with some results that HTL:ELM mixed layer was found to be emissive [Naka *et al*. 1994], and even more stable [Aziz *et al*. 1999].

Delamination of cathode from the organic layer as the cause of formation of dark spots has also been reported [McElvain *et al*. 1996, Do *et al*. 1996, Aziz *et al*. 1998-a, Liew *et al.* 2000, Schaer *et al.* 2001]. In McElvain's report, cathode defect especially pin holes are believed to play an important role in the formation of dark spots. Cathode oxidation (or corrosion) was found to be the cause for cathode delamination [Burrows *et al*. 1994, Do *et al*. 1994, Do *et al*. 1996, Aziz *et al*. 1998-b]. Moreover, the mechanism of cathode delamination is supported by the fact that the electroluminescent materials are still active at the dark spots site [McElvain *et al*. 1996, Aziz *et al*. 1998-a, Liew *et al.* 2000].

Recent studies show that the formation of dark spots is attributed to the corroded cathode with an insulating oxide or hydroxide formed at the cathode/organic interface.[Kolosov *et al.* 2001, Murase *et al.* 2001] However, in a separate report, Scheblykin et. al. found that the thin insulating layer was a product of degraded polymer from the active polymer.[Scheblykin *et al.* 2001] Kim et. al. suggested that the insulating layer formed as a product of the reaction between polymer and the reactive cathode.[Kim *et al.* 2002] The observed chemical changes at cathode/organic interface support their argument.

Cathode defects, especially pinholes, are believed to play a role in the formation of dark spots, but investigations so far have not been conclusive as to whether the cathode pinholes originate during cathode fabrication or are created as a

result of defects in the underlying layers of the device. The incomplete understanding of the processes behind the nucleation of dark spots is perhaps, the reason why encapsulation is used to slow down growth rate rather than control nucleation processes of dark spots [Burrows *et al*. 1994]. Although the dark spots problem can be controlled by operating OLEDs in inert atmosphere, it is still of great importance to understand the details of the dark spots origin, in order to eliminate their formation all together.

Among these three challenges, the stability issue is the most crucial. Resolving it will clear the path towards commercialization of OLEDs. Besides the intrinsic degradation, the dark spots degradation also plays an important role in device performance.

Chapter 3

Experimental

3.1 Sample Preparation

OLEDs with a structure of glass/ITO anode/organic layers/metal cathode were prepared. Two types of organic materials (supply from LumTec Corp.) are used in this study: 1) N,N'-di(naphthalene-1-yl)-N,N'-diphenylbenzidine(NPB), a commonly used hole transport material and 2) tris-(8-hydroxyquinoline) aluminum (Alq_3), an electron transport as well as emitting material. The metal cathode was made of calcium and caped with thick layer of silver. ITO-coated glass substrate was provided by Merck Display Technologies.

Patterned-ITO substrate was first ultrasonic cleaned in acetone and deionized water for about 30 minutes each. The ITO substrate was blow dry with nitrogen before loading into a multi-chamber vacuum system for device fabrication. Prior to the deposition of organic materials, the patterned-ITO glass substrates were treated by oxygen plasma for 10 minutes with plasma power of 100W at oxygen flow rate of 60 sccm. Without breaking the vacuum the ITO substrates were transferred to organic chamber where NPB and Alq_3 were thermally evaporated at a base pressure of about 6×10^{-7} Torr. After organic films deposition on oxygen plasma treated ITO, the devices were transferred to an electrode chamber for calcium and silver depositions. Unless specified, the thickness of Ca and Ag used in this study were fixed at 10 nm and 200 nm respectively. All the organic materials and metals were deposited at the rate of about 0.1nm/s. Each ITO substrate contains 8 active diodes, and the emission area for each device was 2mm × 2mm.

The devices were then transferred to the adjacent glove box for measurement. The characterizations of the devices were carried out e.g. current-voltage measurement in the glove box. The devices were stored in an ambient environment (~23^{o}C and ~75% RH) without encapsulation to allow the growth of dark spots.

In the case of morphological characterization using atomic force microscope, only organic materials were deposited on ITO substrate. Metal cathode i.e. Ca and Ag were not deposited. Organic materials (NPB or/and Alq_3) with thickness ranging from 0.5 nm to 100 nm were fabricated. These samples were used to study the organic film morphological changes at film thickness changes.

3.2 Device Characterization

3.2.1 Current–Voltage–Luminescence and Optical Microscopy

Immediately after the device fabrication, current–voltage–luminescence (I-V-L) characteristics of the devices were measured using a calibrated Keithley 2000 multimeter, following by the examination of dark spots. An optical microscope was used to monitor the device through the glass side under reflected light (RL). In the case where device is lighted up, the devices were then operated at a constant current density of 20 mA/cm^2 for less than 5 seconds in order to obtain the electroluminescent (EL) images of the operated devices using the optical microscope. They were monitored continuously in air for at least 24 hours and the optical microscope images were taken at different time intervals.

3.2.2 Atomic Force Microscopy (AFM)

AFM gives a view on virtually any surface in near-atomic detail. It is based on the minute but detectable forces-order of magnitude nano Newtons between a sharp tip and atoms in the surface.

The morphological features of ITO and organic films were evaluated by a Digital Instrument Dimension 3000 Multimode AFM. The measurements were performed in Tapping® Mode using triangle cantilevers at room temperature. Different scan sizes of each AFM image were taken, and the sizes are 10μm ×10μm, 4μm×4μm and 1μm×1μm, with scan rate ranging from 1.0 to 2.0 Hz. All images were taken under ambient conditions. Root-mean-square (rms) roughness was calculated with the AFM software.

3.2.3 X-ray Photoelectron Spectroscopy (XPS)

XPS is one of the most frequently used surface analysis techniques. It offers information on the surface elemental composition, the oxidative state of the elements and the electronic interaction between ions in samples.

XPS measurements were employed to investigate the chemical state at anode/organic and organic/cathode interfaces of an OLED. All XPS measurements were performed in a VG ESCALAB 220i-XL spectrometer equipped with two UHV chambers, the analysis and the preparation chambers. XPS spectra were recorded in the constant pass energy mode of a hemispherical analyzer and a monochromated Al Kα (1486.6eV) X-ray source. The X-ray anode was operated at 200W (15kV, 13.3mA), the analyzer was operated at constant pass energy of 150eV for survey

spectra and 20eV for narrow scan spectra. The background pressure in the chamber was normally at 1.5×10^{-10} mbar. XPS peak intensities were calculated by integrating the peak areas after proper subtraction of the base line by Shirley background subtraction method.

Chapter 4

Evolution of Dark Spots

4.1 Optical Image Analysis

It is known that the dark spots grow even under non-operation condition but are accelerated when the device is operated at ambient. The introduction of electrical stress in an operating device creates some additional uncertain factors in the study of the dark spots formation. The origin of the formation of dark spots is not fully understood, particularly the mechanism of dark spots formation under non-operation condition. Therefore, in order to study the origins of the formation of dark spot, the electrical effect has to be eliminated.

In this section, an optical image analysis technique was developed to study the evolution of dark spots in OLEDs under non-operation condition. The circular features observed in the optical images of non-operated devices correlated directly to the dark spots seen in the same locations in the electroluminescent images. By eliminating the electrical field, the optical image analysis technique enables to study the growth of the dark spots formed in OLEDs before device operation.

Bilayer OLEDs of structure glass/ITO/NPB(60nm)/Alq_3(60nm)/Ca/Ag were made. Immediately after the device was taken out from vacuum chamber, an optical microscope was used to monitor the device from the glass side of the device under reflective light (RL) – non-operation, and the RL images were captured. The same device was then operated at a constant current density of 20 mA/cm^2 for less than 5 seconds in order to obtain the electroluminescent (EL) images of the OLEDs using the optical microscope. They were monitored continuously in air for 24 hours and both RL and EL images taken for devices at different time intervals for comparison.

Figure 4.1 illustrates the optical microscope images showing the circular features (RL, left column) and dark spots (EL, right column) taken for the same OLED at different time intervals during the monitoring period, i.e. as-made (shown in Figures (a) and (d)), 7 hours (Figures (b) and (e)) and 24 hours (Figures (c) and (f)) after it was fabricated, respectively. The RL images were recorded just before taking the EL images. It is obvious from the images in Figure 4.1 that dark spots in OLED grew even under non–operation condition during storing in ambient.

It is interesting to note that the size and the location of the circular features captured in the RL correspond directly to the dark spots found in the same location in the EL images of the device. In order to ascertain whether the circular features shown in the optical images were induced initially by external electric field, another identical device was made and monitored continuously under open circuit condition in air for about 24 hours. In this experiment, the circular features were still observed to grow with time. The device was then biased to acquire the EL images. As expected, dark spots, with the same location and same size as the circular features when non–operated, were observed under biased. These dark spots observed in the emitting OLED had similar growth behavior to that of the circular features, i.e. both were time dependent and circular in shape. Therefore, it shows clearly that the circular features, grew in non-operated OLED, correspond to the dark spots in the emitting device. In addition to the findings of dark spots induced by electric stress or joule heating, it is also demonstrated that dark spots also grew in OLEDs without the presence of external electric field.

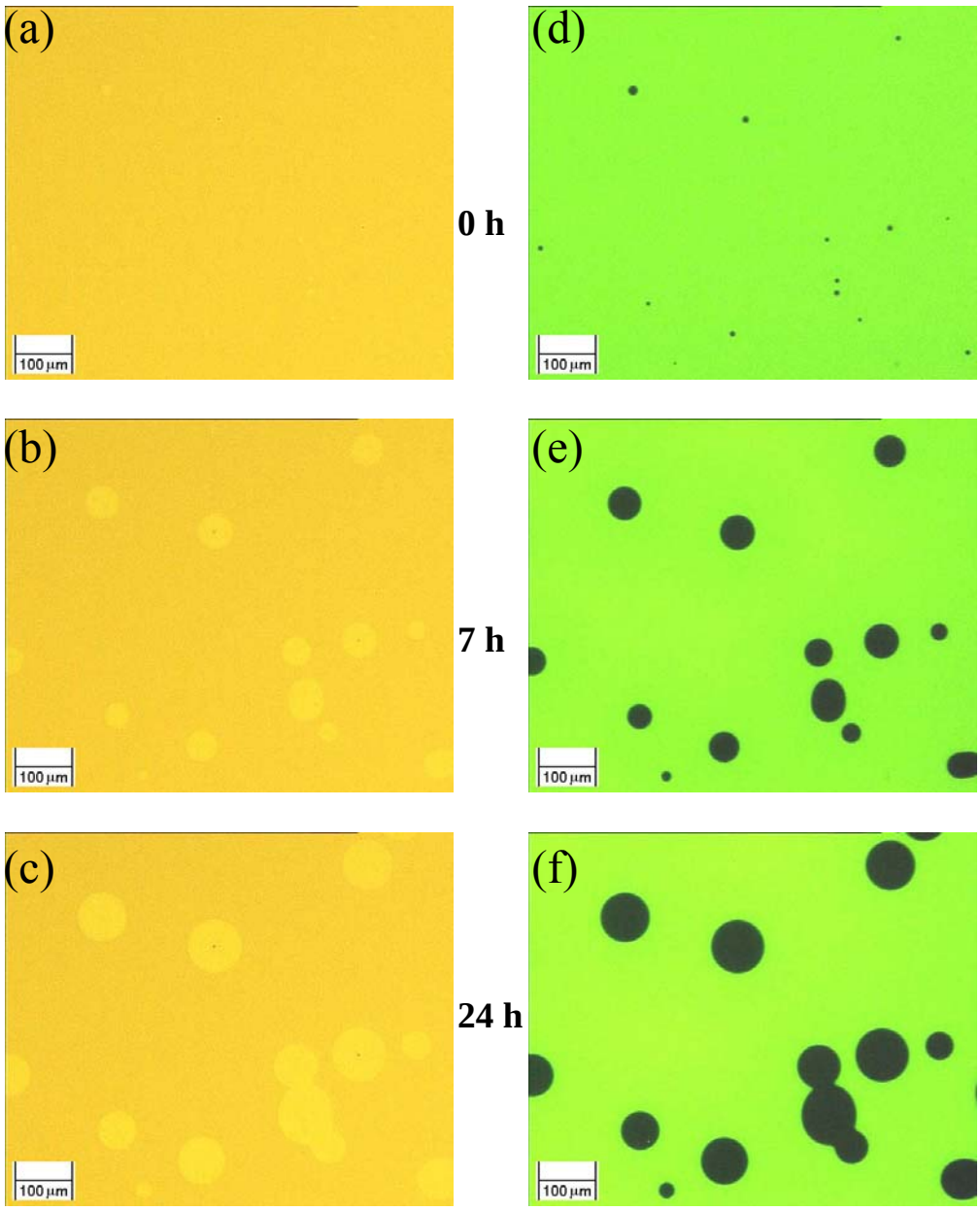

Figure 4.1: RL images showing the circular features (left column) and EL images showing the dark spots (right column) taken for the same OLED at different time intervals after it was fabricated, (a) and (d) as-made, (b) and (e) 7 hours , (c) and (f) 24 hours.

The circular features observed in the optical images of non-operated devices behave somewhat similarly to the dark spots found in the OLEDs, i.e. they also have circular shape, grow with time, and are sensitive to the moisture and oxygen. The circular features seen in the optical images reflect the difference of the corroded or decomposed electrode occurred at organic/cathode interface. The deterioration of the organic/cathode contact is usually associated with the chemical changes at the organic/cathode interface resulting in a cathode delamination or oxidation. The variation in the optical properties of the corroded and the surrounding non-corroded parts of the electrode initiates a difference in the visual contrast leading to the circular features seen in the optical images. The direct correlation between the circular features and dark spots enables to use optical image analysis to study the behavior of dark spot growth for OLEDs at a non-operation condition.

4.2 Organic Layer Thickness Effect

For an operating device, the study of the effect of organic layer thickness on the growth of dark spot is extremely difficult. This is mainly due to the fact that the driving voltage is dependent on the thickness of organic layers used in the devices. Changes in the electrical stress created more uncertain factors in the study of dark spots formation. Small increment in the organic layer thickness is usually employed to study the thickness effect on the formation of dark spots. However, the growth behavior of dark spots becomes insignificant when the organic layer thickness varies over a small range. As discussed above, it is shown that optical image analysis can be used to study dark spots in OLEDs under non–operation condition. Therefore, in this

work, the optical image analysis method was employed to investigate the growth behavior of dark spots with respect to variation of thickness in devices containing single organic layer.

To investigate the effect of organic layer thickness on the formation of dark spots, a device with single organic layer of Alq_3 was fabricated, i.e. ITO/Alq_3/Ca/Ag. A control device of ITO/Ca/Ag was also fabricated. Figure 4.2 shows the optical microscope images (RL) of a set ITO/Alq_3/Ca/Ag devices, with different Alq_3 layer thicknesses of 0 nm (without Alq_3) (a), 6 nm (b), 60 nm (c) and 600 nm (d), taken 24 hours after they were fabricated. Figure 4.2 clearly indicates that the size of the circular features is not dependent on the Alq_3 layer thickness. However, no bright circular features were observed in device without the Alq_3 layer i.e. ITO/Ca/Ag device. In addition to Alq_3, other organic materials were also used to study the independency of thickness on the growth of circular features. The growth of the circular features in a set of dummy devices made with NPB and copper phthalocyanine (CuPc), i.e. ITO/NPB/Ca/Ag and ITO/CuPc/Ca/Ag, was investigated. Results verify that the growth of circular features is actually independent on the organic layer thickness.

In many cases, the growth of dark spots in OLEDs is attributed to morphological defects on cathode (e.g. pinholes). These defects provide entry paths for moisture and oxygen, allowing penetration into the cathode to degrade and oxidize the reactive metal cathode at the organic/cathode interface. Figure 4.2 (a) shows that there is no growth of circular features in device without the organic layer even though pin-holes are detectable in this device. The reason why there is no circular features

observed on the device without the organic layer could be due to stronger bonding between ITO and the cathode compared to the weak organic-cathode bonding. In general, organic material is "required" in the device enabling the dark spots to grow. Nevertheless, results also reveal that the growth of circular features observed in non-operated OLEDs is not dependent significantly on the thickness of organic layer used in this work.

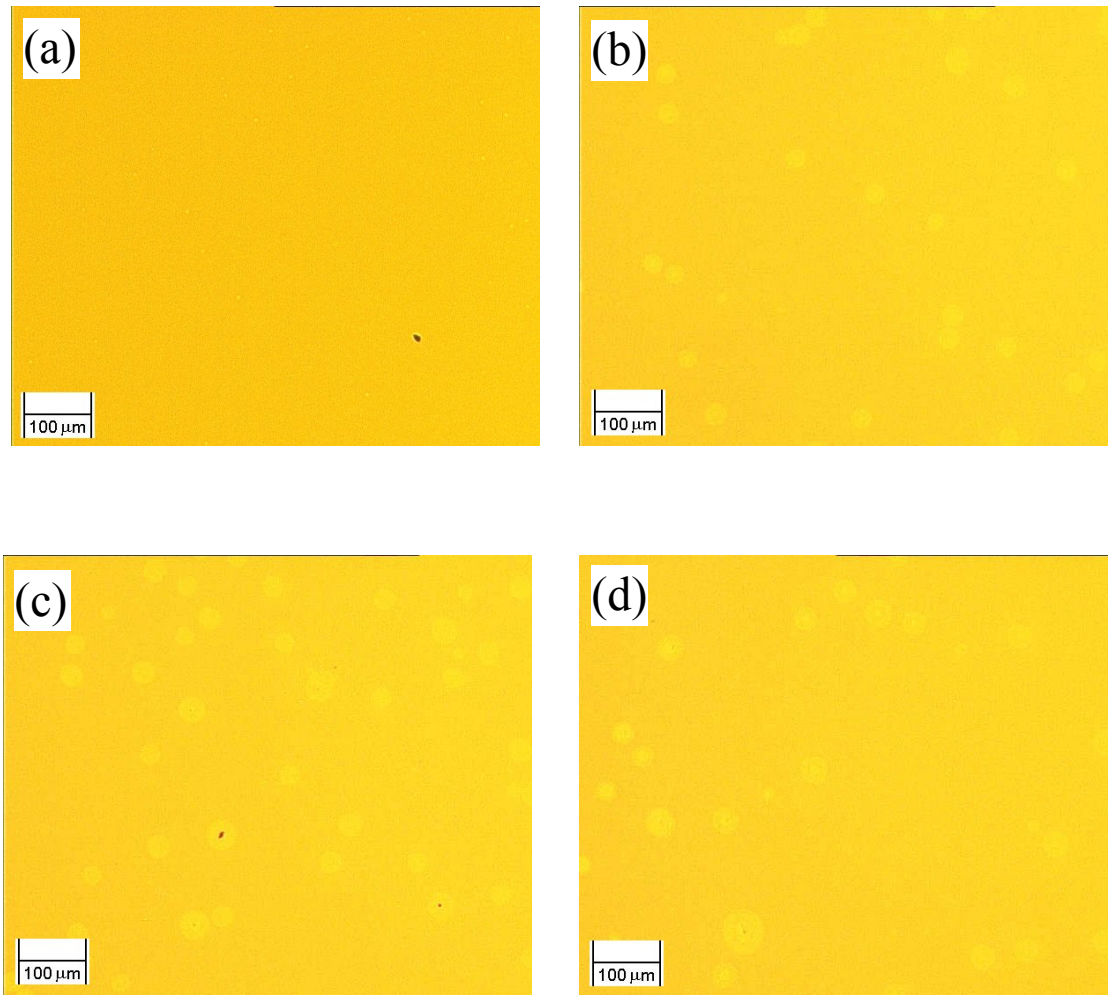

Figure 4.2: Optical images of ITO/Alq_3/Ca/Ag devices, with Alq_3 layer thickness of (a) 0 nm (without Alq_3), (b) 6 nm, (c) 60 nm and (d) 600 nm, 24 hours after being exposed to ambient environment.

4.3 Substrate Effect

The optical image analysis method was extended to investigate the growth behavior of these circular features on different substrates. In this experiment, two types of substrate were used, i.e. glass and ITO substrates. Alq_3/Ca/Ag stack or NPB/Ca/Ag stack were fabricated on glass and ITO substrates, and the thickness of organic materials was kept constant at 60nm.

Figure 4.3 shows the optical microscope images taken for Alq_3/Ca/Ag stack deposited on ITO and glass substrates, 24 hours after being exposed to ambient environment. In this experiment, all the materials were deposited on patterned-ITO and glass substrate simultaneously and they were not biased during the monitoring period. It is obvious that the size of the circular features for devices made on both ITO and glass substrates are almost the same. The growth rates of the circular features observed in glass/Alq_3/Ca/Ag and ITO/Alq_3/Ca/Ag devices were about 0.6 μm^2/min. It seems that either ITO or glass substrate does not have any significant effect on the growth of dark spots in device made with Alq_3 single layer.

Figure 4.4 shows the optical microscope images taken for NPB/Ca/Ag stack deposited on ITO and glass substrates, 24 hours after being exposed to ambient environment. It illustrates evidently that the circular features observed in ITO/NPB/Ca/Ag device grow faster than that seen in glass/NPB/Ca/Ag one. Their growth rates were 6.0 μm^2/min and 1.3 μm^2/min, respectively. This result indicates that the growth of circular features is related to the substrate materials. However, no significant difference on the growth of circular features was observed when Alq_3 deposited on different substrates. These two results reveal that, the growth of circular

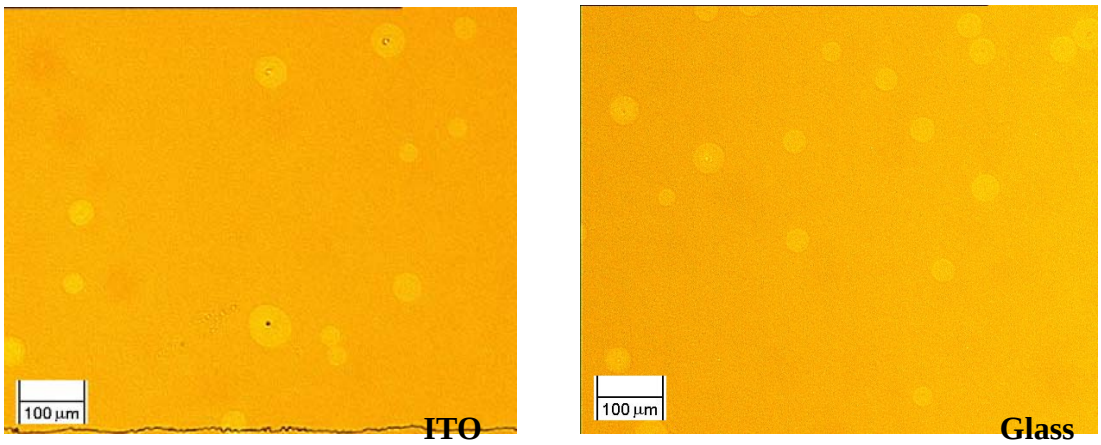

Figure 4.3: Optical images taken for Alq_3/Ca/Ag stack deposited on ITO and glass substrates, 24 hours after being exposed to ambient environment.

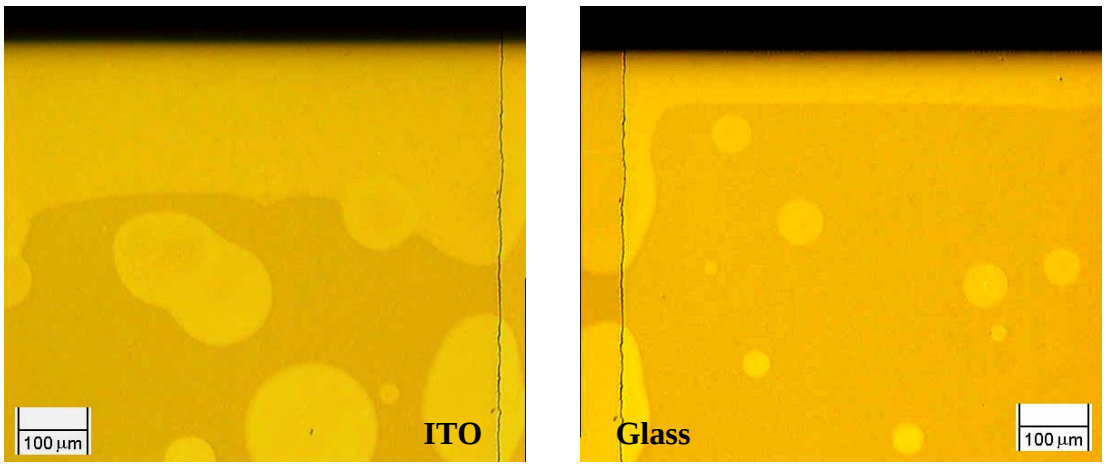

Figure 4.4: Optical images taken for NPB/Ca/Ag stack deposited on ITO and glass substrates, 24 hours after being exposed to ambient environment.

features no only depend on substrate, but also depend on the organic materials used.

Figure 4.5 shows the area of circular features as a function of time measured for NPB/Ca/Ag and Alq_3/Ca/Ag stacks deposited on both ITO and glass substrates. It is obvious that growth rates of the circular features observed in ITO/Alq_3/Ca/Ag and glass/Alq_3/Ca/Ag systems are respectively slower than that observed in ITO/NPB/Ca/Ag and glass/NPB/Ca/Ag ones.

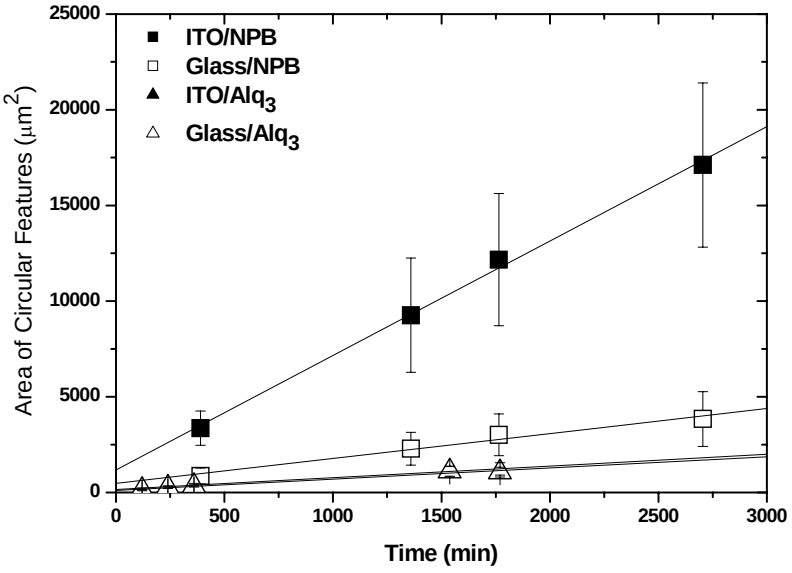

Figure 4.5: The area of circular features as a function of time measured for NPB/Ca/Ag and Alq_3/Ca/Ag stacks deposited on both ITO and glass substrates.

4.4 Multilayer Effect

From section 4.3, it has been shown that the growth of circular features not only depend on substrate, but also depend on the organic materials used. One may argue that the difference in the growth rate when different organic materials used, might be due to the difference in the organic/cathode contact. As reported in the literature, the organic/cathode interface is responsible for the formation of dark spots. In order to gain an insight to better understand this problem, devices made with dual-layer and tri-layer configurations were used to study the circular features growth behavior.

For the investigation of device with dual-layer configuration, two sets of devices were fabricated. In the first set, ITO/Alq_3/NPB/Ca/Ag devices with fixed NPB thickness (60 nm) and different Alq_3 thickness ranging from 1 nm to 90 nm were made. Similarly, in ITO/NPB/Alq_3/Ca/Ag devices, the Alq_3 thickness was fixed (60 nm) and the thickness of NPB was varied from 1 nm to 90 nm as well. The growth of the circular features was monitored in air. Results revealed that, the growth of circular features observed in ITO/Alq_3/NPB/Ca/Ag is slower than that in ITO/NPB/Alq_3/Ca/Ag under the same experiment condition, with the rate of 0.6 μm^2/min and 6.0 μm^2/min respectively. As expected, changing the thickness of organic layer does not seem to have impact on the growth of circular features. The effect of thickness on the growth of circular features was discussed in section 5.2. It is also interesting to note that the growth rate of circular features for ITO/Alq_3/NPB/Ca/Ag device is comparable to that of ITO/Alq_3/Ca/Ag device.

Similarly, the growth of circular features for ITO/NPB/Alq_3/Ca/Ag device is also in the same order of magnitude of ITO/NPB/Alq_3/Ca/Ag device.

In order to gain an insight to better understand the effect of device architecture on the behavior of dark spots and their growth rates, tri-layer configurations devices were made, i.e. ITO/Alq_3/NPB/Alq_3/Ca/Ag and ITO/NPB/Alq_3/NPB/Ca/Ag. In this study, all the thickness of organic layer was kept constant at 60 nm. Similarly, the growth of circular features was monitored in ambient. For these tri-layered devices, the circular features in ITO/Alq_3/NPB/Alq_3/Ca/Ag were found to grow slower than that in device made with ITO/NPB/Alq_3/NPB/Ca/Ag. It is noticed that the circular features observed in the multi-layer devices, e.g., ITO/Alq_3/NPB/Alq_3/Ca/Ag and ITO/Alq_3/NPB/Ca/Ag, are similar to that observed in device made with single Alq_3 layer i.e. ITO/Alq_3/Ca/Ag, at the growth rate of about 0.6 μm^2/min. Likewise, the growth of circular features in ITO/NPB/Alq_3/NPB/Ca/Ag and ITO/NPB/Alq_3/Ca/Ag are also comparable to that in ITO/NPB/Ca/Ag, with the rate of about 6.0 μm^2/min. The growth rates of the circular features observed in single and multi-layered devices with different layer combinations are summarized in table-1. From this experiment, it can be concluded that the growth of circular features is dependent on the first layer that was deposited on the substrate. And the organic/cathode interface does not seem to affect the growth rate of circular feature discussed in this study.

It is shown that the growth of circular features in multi-layer OLEDs is dependent on the contact between the first organic layer and the substrate. This implies that ITO/organic interface has a direct implication on the growth of the dark spots in OLEDs. In this work, ITO/Alq_3 interface has been demonstrated having

advantage over ITO/NPB contact for used in durable multi-layer OLEDs. For single or multi-layer devices, if they were started with ITO/Alq_3 contact, as shown in table-1, the different organic/cathode interfaces, in this case, NPB/cathode and Alq_3/cathode, did not have significant influence on the growth of the circular features.

Device structure			Growth rate of circular features (μm^2/min)
Anode	Organic Stack	Cathode	
ITO	Alq_3	Ca/Ag	~ 0.6
	Alq_3/NPB		
	Alq_3/NPB/Alq_3		
ITO	NPB	Ca/Ag	~ 6.0
	NPB/Alq_3		
	NPB/Alq_3/NPB		

Table 1: Growth rates of circular features in devices with different organic layer combinations.

Chapter 5

Surface and Interfacial Analyses

5.1 AFM Studies

It is found from previous section that the growth of dark spots in OLED depends on the contact between anode substrate and the first organic layer deposited on substrate, in other words the anode/organic interface. It is not dependent on the subsequent organic layers formed on top of the first layer. It is known that organic/cathode is responsible for the formation of dark spots. However, the underlying reason for dark spots formation influenced by anode/organic interface remains unclear. In this study, investigation of ITO substrate and organic films with respect to their morphologies is carried out to reveal the mechanism of dark spots formation in OLEDs influenced by the anode/organic interface. "Spikes" at ITO surface are considered to play a role in dark spots formation. Therefore, AFM was employed to study the surface morphologies of ITO and organic films on ITO.

5.1.1 ITO Substrate

ITO glass substrate was used for the deposition of the organic layers, therefore its physical and chemical properties at surface are especially important for the device performance. The surface roughness of a clean ITO substrate was measured by AFM. Figure 5.1 shows AFM images of an ITO sample with different scan area, a) 10 μm × 10 μm, b) 4 μm × 4 μm, and c) 1 μm × 1 μm. The grainy structure of the surface is clear recognizable, and there were not noticeable "spike" on the surface. The root-mean-square (RMS) roughness obtained for these samples, on the right side of the AFM images, are 1.54 nm, 1.58 nm and 1.34 nm respectively. The morphology and roughness of ITO are used as the reference for organic films deposited on ITO substrate.

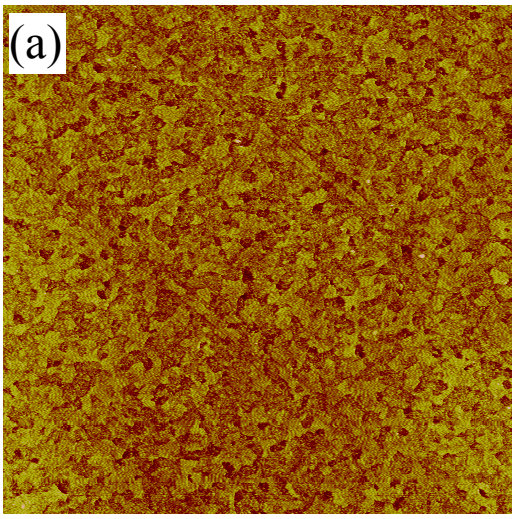

RMS = 1.54 nm

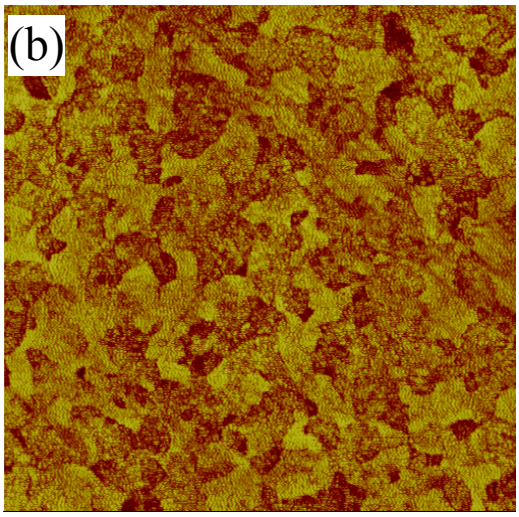

RMS = 1.58 nm

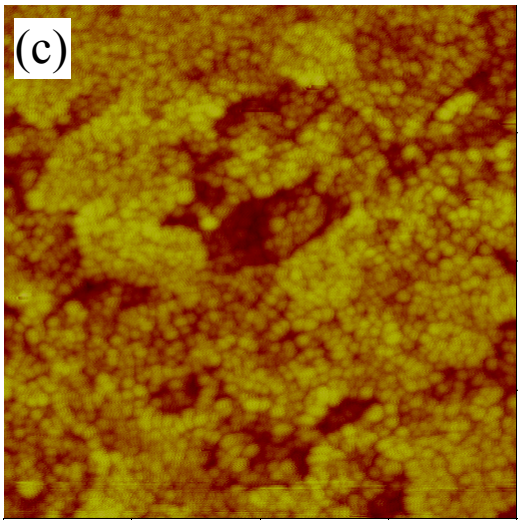

RMS = 1.34 nm

Figure 5.1: AFM images of ITO scanned over the different areas of a) 10 μm × 10 μm, b) 4 μm × 4 μm, and c) 1 μm × 1 μm.

5.1.2 Alq_3 Films

In this experiment, Alq_3 films with thickness ranging from 0.5 nm to 100 nm were deposited on clean ITO substrate. The morphologies of these films were recorded by AFM using tapping mode. Figure 5.2 and Figure 5.3 are the AFM images taken for Alq_3 films, with different thicknesses ranging from 0.5 nm to 100 nm, deposited on clean ITO substrates. The thicknesses of Alq_3 layers used in this experiment were, a) 0.5 nm, b) 2 nm, c) 5 nm, d) 10 nm, e) 50 nm, and f) 100 nm. Figure 5.2 shows the AFM images with scan size of 4 μm, and Figure 5.3 shows the same images with a scan size of 1 μm. As can be seen, the film becomes smoother as Alq_3 layer thickness increases. For example, the RMS measured in the 4 μm scan size sample for 100 nm Alq_3 film is 1.18 nm which is much smoother than 0.5 nm thick Alq_3 film, which has a RMS of 1.46 nm. RMS for a bare ITO is 1.58 nm. The RMS values obtained for films with different Alq_3 thickness (for both 1 μm and 4 μm scan size), are plotted in Figure 5.4. It illustrates clearly that smoother surface is obtained when the Alq_3 layer thickness increases. However, this change in the RMS roughness is not relevant to the growth rate of dark spots in OLEDs. This analysis agrees with earlier discussion in showing that the growth rate of circular features in ITO/Alq_3/Ca/Ag device is not dependent on the Alq_3 layer thickness.

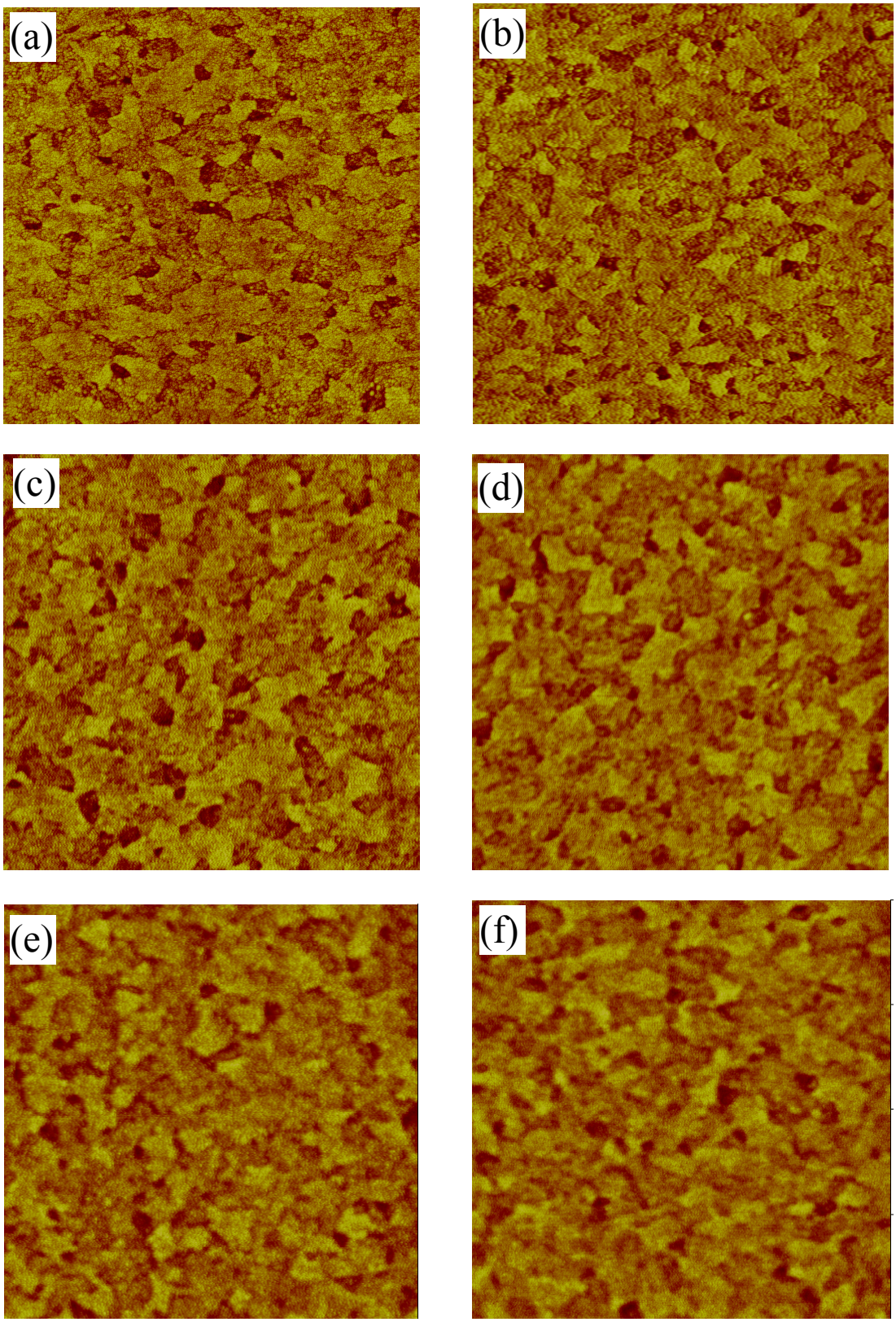

Figure 5.2: AFM images of Alq_3 films scanned over the area of 4 μm × 4 μm, with the thickness of (a) 0.5 nm, (b) 2 nm, (c) 5 nm, (d) 10 nm, (e) 50 nm and (f) 100 nm.

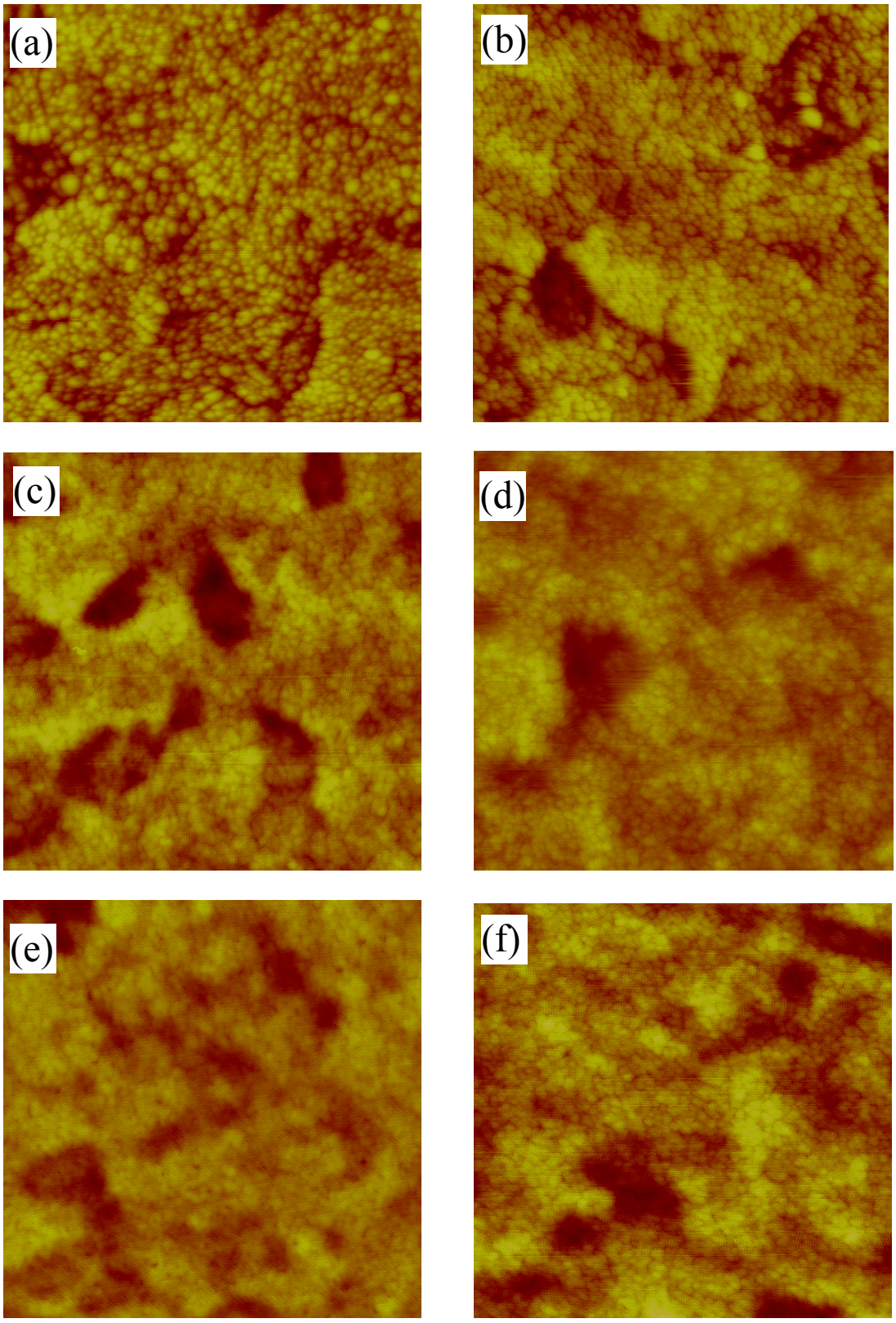

Figure 5.3: AFM images of Alq_3 films scanned over the area of 1 μm × 1 μ, with the thickness of (a) 0.5 nm, (b) 2 nm, (c) 5 nm, (d) 10 nm, (e) 50 nm and (f) 100 nm.

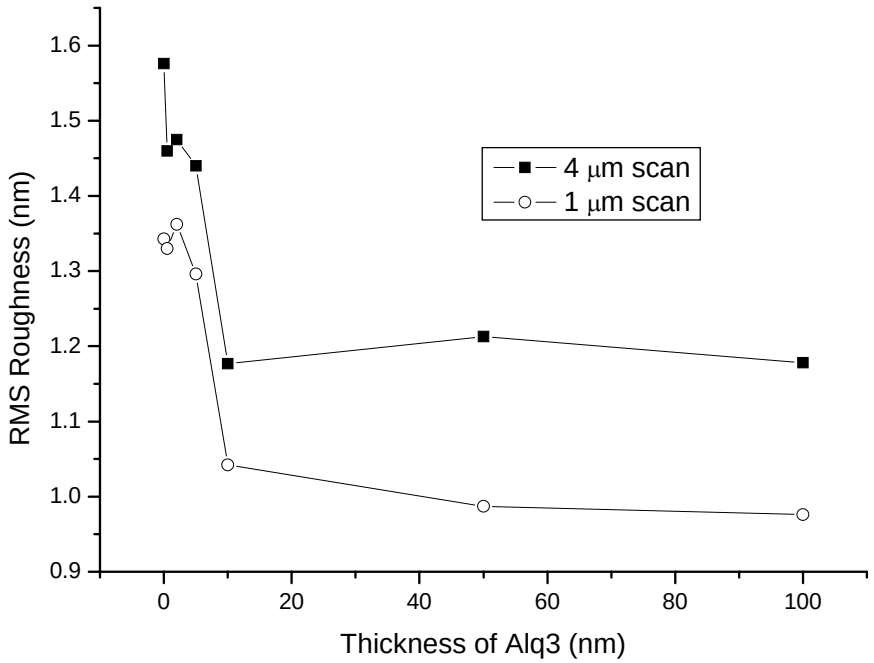

Figure 5.4: The RMS roughness as a function of Alq_3 thickness obtained from AFM measurements over the different scanned areas of 1 μm × 1 μm and 4 μm × 4 μm, respectively.

5.1.3 NPB Films

Figure 5.5 illustrates the AFM images taken for NPB films with different thickness on ITO substrate. The thicknesses of NPB films are a) 2, b) 20 and c) 60 nm, and their RMS are 1.34 nm, 1.21 nm and 1.09 nm respectively. Similar to Alq_3 film, as the thickness of NPB increases, film morphology becomes smoother, as indicated from the AFM images and numerically from the RMS roughness. For a clear presentation, the RMS roughness for these films are plotted against NPB thickness and shown in Figure 5.6. However, the variation in the RMS roughness as a function of NPB thickness also does not explain the growth rate of circular feature in ITO/NPB/Ca/Ag devices.

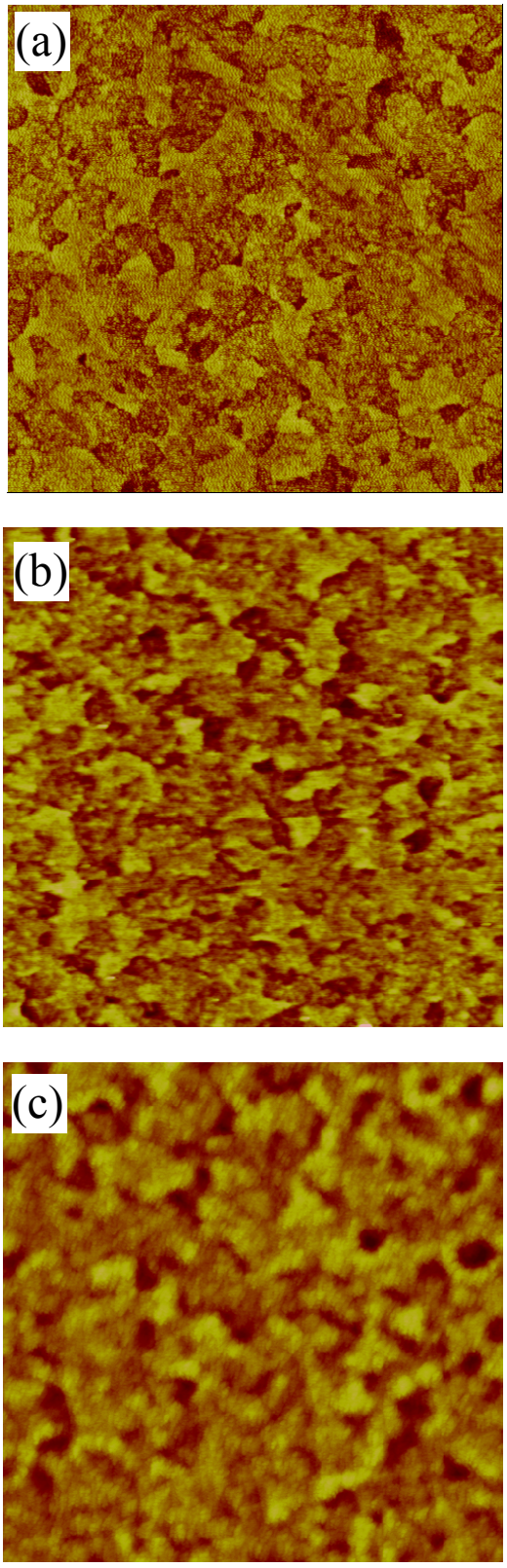

Figure 5.5: AFM images of NPB films scanned over the area of 4 μm × 4 μm, with the thickness of (a) 2 nm, (b) 20 nm and (c) 60 nm.

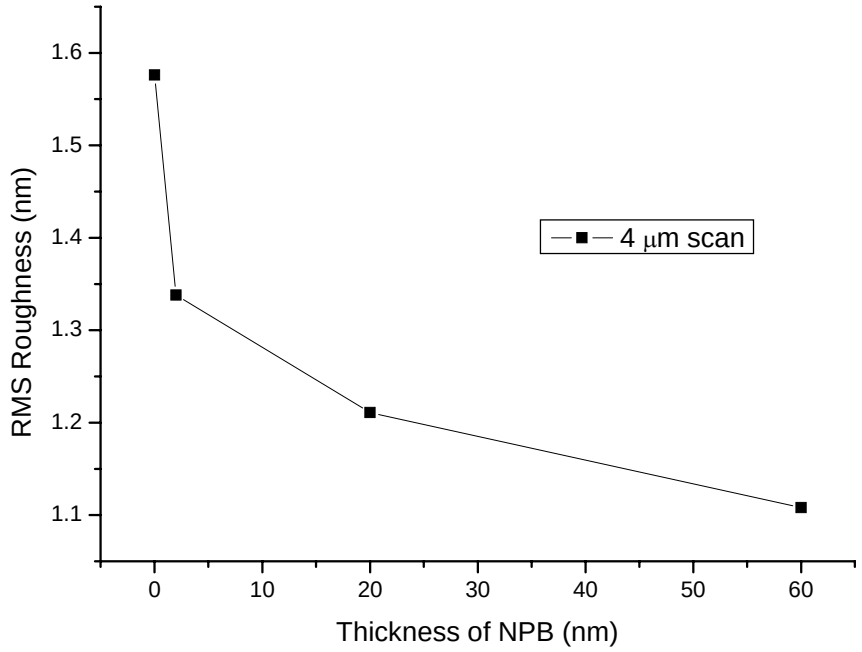

Figure 5.6: The RMS roughness as a function of NPB thickness obtained from AFM measurements over the scanned areas of 4 μm × 4 μm.

5.1.4 Bilayer Structure

It was demonstrated that the dark spots in device with structure of ITO/Alq_3(2nm)/NPB(60nm)/cathode grew about 10 times slower than that in ITO/NPB(60nm)/cathode device. The growth rates of circular features for these devices are about 0.6 μm^2/min and 6.0 μm^2/min respectively. Therefore it is interesting to compare the morphologies of ITO/Alq_3/NPB and ITO/NPB films. Experiment shows that AFM topography for both films are similar. The RMS roughness for ITO/Alq_3/NPB and ITO/NPB films are 1.07 nm and 1.09 nm respectively. One would expect that the morphologies for both films should be different if the difference in dark spots growth rate is associated to the morphologies of films. However, from this experiment, it shows that the RMS roughnesses for these films are in fact similar. For a better comparison, ITO/Alq_3(50nm)/NPB(60nm) structure was prepared, and the RMS roughness was measured to be 1.11 nm. In a device with a configuration of ITO/Alq_3(50nm)/NPB(60nm)/cathode, the growth rate of circular feature was about 0.6 μm^2/min. It was shown that the RMS roughness of ITO/Alq_3(50nm)/NPB(60nm) film is comparable to ITO/NPB(60nm) film, however, devices made from these films show significant difference in the growth of circular features. Figure 5.7 shows those AFM films, i.e. a) ITO/NPB(60nm), b) ITO/Alq_3(2nm)/NPB(60nm) and c) ITO/Alq_3(50nm)/NPB(60nm). In conclusion, inserting of either a thin (2nm) or a thick (50nm) Alq_3 layer in between ITO and NPB does not change the NPB film morphology significantly. However, the presence of thin Alq_3 interlayer between ITO and NPB in a device, i.e. of ITO/Alq_3/NPB/Ca/Ag can dramatically reduce the growth rate of dark spot as compared to ITO/NPB/Ca/Ag device. Therefore, the variation in RMS roughness observed at ITO and organic/ITO surfaces is not the main reason that initiates the dark spots in OLEDs.

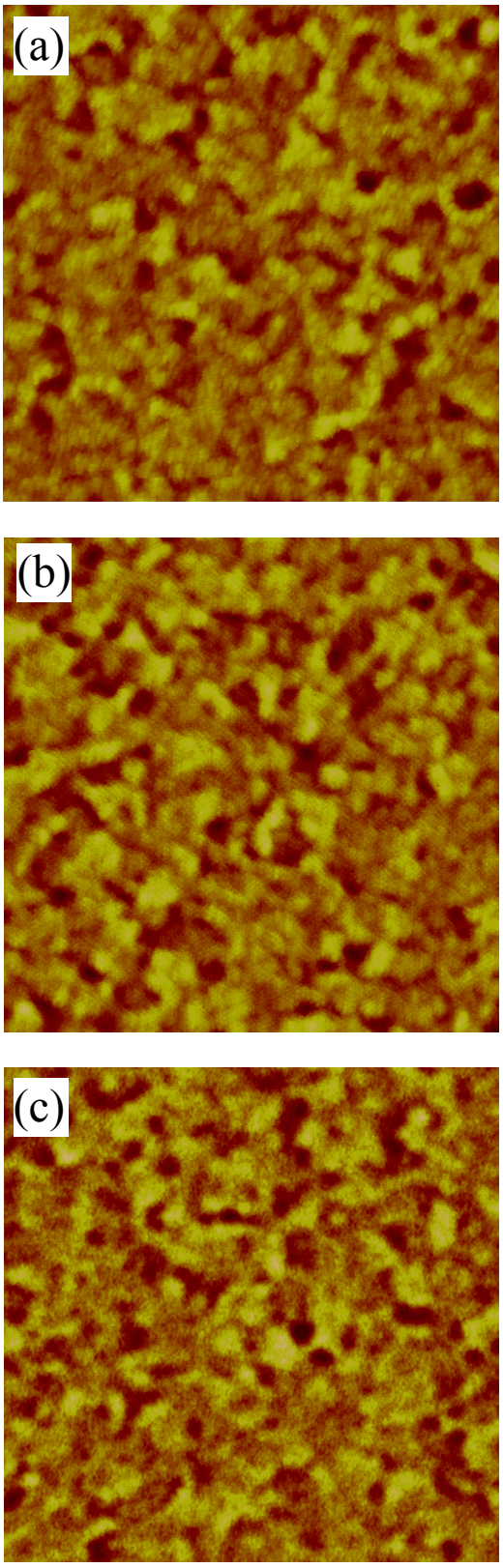

Figure 5.7: AFM images of NPB films with the structure of a) ITO/NPB(60nm), b) ITO/Alq_3(2nm)/NPB(60nm) and c) ITO/Alq_3(50nm)/NPB(60nm), the images were obtained over a scanned area of 4 μm × 4 μm.

5.2 Interfacial Analysis

It is discussed in the previous section that morphologies of organics films do no correlate to the growth rate of dark spots in OLEDs. The underlying reason for dark spots formation, which was influenced by anode/organic interface, still remains unclear. Literature studies show that the formation of dark spots involves chemical reaction, particularly at the organic/cathode interface due to the presence of the moisture and/or oxygen species. These interfacial deteriorations in OLEDs are often considered as a result of cathode delamination or insulating layer formation at the organic/cathode interface. This research shows that the growth of dark spots in OLED depends on the contact between anode and the first organic layer. The effect of organic/cathode properties on the formation of dark spots in OLEDs has been widely studied. However, the effect of anode/organic contact on the dark spots evolution is not fully understood. The finding on a correlation between anode contact and dark spot formation has created new knowledge in this field. In order to explore the effect of anode on the growth of the dark spots, XPS were carried out to study the properties at both anode/organic and organic/cathode interfaces.

5.2.1 XPS – Alq_3 Thickness

Due to the fact that our XPS system does not equip with organic films deposition source, the ex-situ XPS measurements were carried out. After Alq_3 films were deposited on ITO in the multi-chamber vacuum system, the samples were transferred to the XPS chamber using a nitrogen box. The transferred time taken was usually less than 5 minutes, and the exposure time to air was less than 1 minute. Therefore, it is essential to verify that no significant changes or damages to the

sample during the transferred time. In this experiment, the Alq_3 films on ITO with different exposure times in air were investigated using XPS, and all the samples were 100 nm thick. The exposure time was 0.0, 0.5, 2.0, 5.0, 24.0 hours and 1 week respectively.

Figure 5.8 show the evolution of (a) O 1s, (b) N 1s, (c) C 1s and (d) Al 2p XPS peaks measured for the Alq_3 films. It shows clearly that the binding energy (BE) of all the analyzed elements, measured for films exposed in air from 0 – 24 hours, did not change. However, there is a clear shift in BE measured for the films one week after they were made. Firstly, O 1s peak was shifted from 531.5eV for an "as-deposited" film to 532.3eV for film one week after it was made. O bounded to Al^{3+} is assigned for the 531.5eV peak, and 532.3eV is typical BE position for surface absorbed oxygen. For the N 1s spectrum, N 1s peak shifted 0.5 eV to higher BE region for film 1 week after it was made, at initial BE of 400.2eV. The shift of 0.5eV might due to O-rich environment surrounding it. A small hump were found present at ~407.5eV. Nitrates are suspected to be present on O-rich surface. The BE of C 1s peak shifted 0.3eV and 0.6eV to higher BE region for film 1 day and 1 week, respectively, after is was made, at the initial BE of 285.1eV. The shift might due to C-O types of bonding. C on O-rich surface such as ITO falls at 285.9eV. There was no evidence of Al-C at it usually has BE <283eV. Al peak was shifted from 74.3eV for an "as-deposited" film to 74.8eV for film 1 week after is was made, a 0.5eV shift. The shift of O 1s, N 1s, C 1s and Al 2p peaks to higher BE after one week of exposure to air may be attributed to moisture [Liao *et al.* 2001]. In conclusion, there are significant changes in BE of all elements from t = 0 to 24h. Table 2 summarized the peak center of Alq_3 sample with different exposure time.

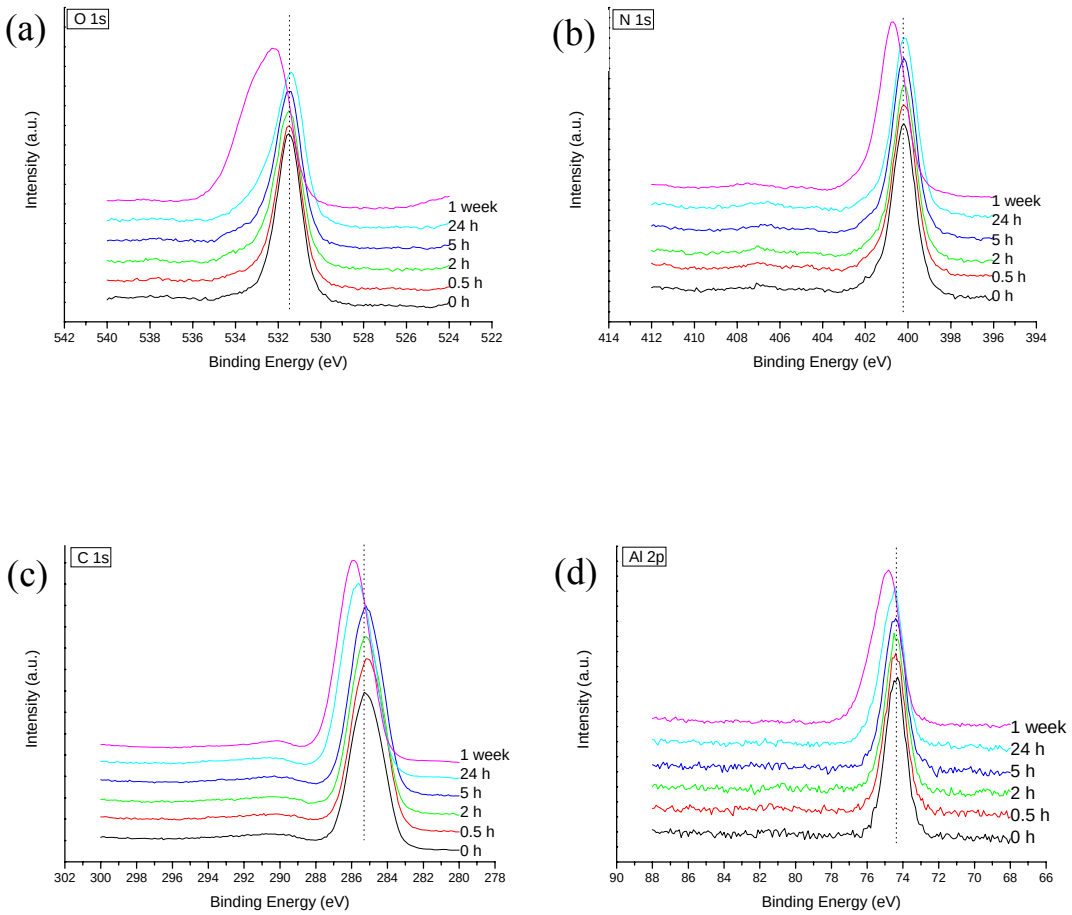

Figure 5.8: Evolution of (a) O 1s, (b) N 1s, (c) C 1s and (d) Al 2p XPS peaks, measured for Alq_3 films, as a function of exposure time.

Time (hr)	Peak center				FWHM			
	O 1s	N 1s	C 1s	Al 2p	O 1s	N 1s	C 1s	Al 2p
0.0	531.50	400.20	285.30	74.30	1.40	1.20	2.20	1.40
0.5	531.50	400.20	285.10	74.40	1.40	1.20	2.20	1.40
2.0	531.50	400.20	285.20	74.50	1.40	1.20	2.20	1.40
5.0	531.40	400.20	285.20	74.40	1.40	1.20	2.20	1.40
24.0	531.40	400.20	285.60	74.40	1.60	1.40	2.20	1.40
1 week	532.30	400.70	285.90	74.80	2.60	1.40	2.20	1.80

Table 2: O 1s, N 1s, C 1s and Al 2p XPS peak binding energies measured for Alq_3 films exposed at different time intervals.

From these observations in BE, it can be concluded that, the Alq_3 sample does not undergo significant changes or damages within a few hour of exposure in air. In the next experiment, the Alq_3 thickness was varied, it was "saved" to perform the ex-situ XPS measurements for samples that were exposed to air for less than 5 minutes during the sample transfer.

In order to investigate the chemical interaction between Alq_3 and ITO at the Alq_3/ITO interface, XPS study was carried out for Alq_3 films, with different thickness ranging from 0.5 nm to 50 nm, deposited on ITO substrate. In many cases, Ar^+ sputtering was employed to study the interface, however sputtered with high energy ion might damage the organic film. Therefore this thickness approach was used. When Alq_3 thickness becomes thinner, Alq_3/ITO interface properties can be resolved from the XPS data.

Figure 5.9 shows the XPS spectra of (a) O 1s, (b) N 1s, (c) C 1s, (d) Al 2p, (e) In 3d and (f) Sn 3d, respectively, for Alq_3 films with thickness of 0.5 nm, 1 nm, 2 nm, 5 nm, 10 nm and 50 nm. From figure 5.14 (a), the O 1s spectrum, at Alq_3 thickness of 0.5 nm, 1 nm, 2 nm and 5nm, O 1s signals from ITO at 530.7eV still can be seen. At 5 nm, O 1s signal from Alq_3 at 531.9eV was much stronger and O 1s signal from ITO appeared as a shoulder. Figure 5.10 shows spectral deconvoution of O 1s peak, for Alq_3 thickness of 1 nm, 5 nm and 10nm. As can be seen, O 1s signal from ITO becomes weaker as thickness of Alq_3 increases, while O 1s signal from Alq_3 is increased. It is interesting to note that the appearance of peak at 533eV region. This peak is assigned as Al_xO_y kind of bonding. In other word, Al_xO_y was formed at the Alq_3/ITO interface. From the N 1s spectrum, N 1s shifted 0.4eV to lower binding

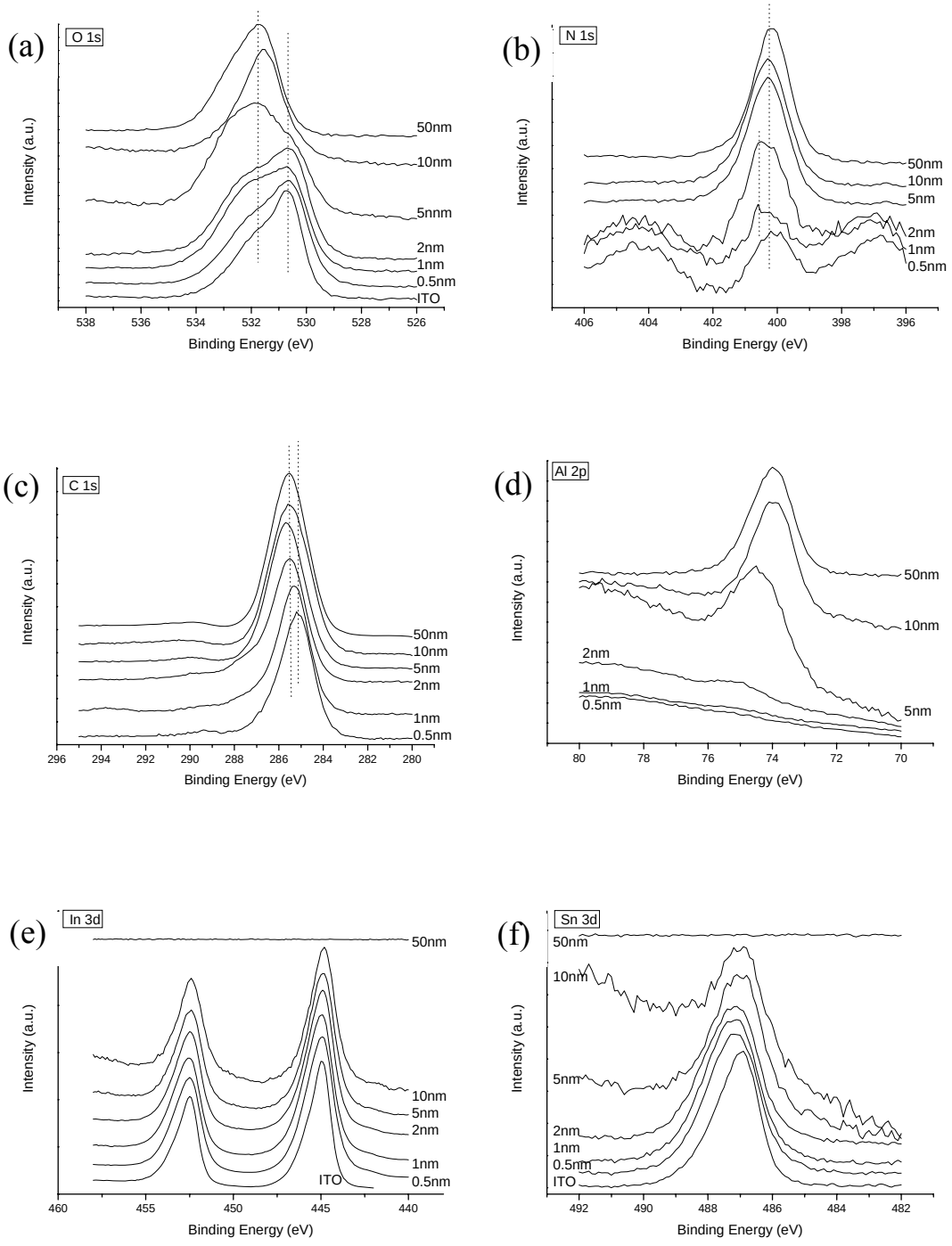

Figure 5.9: XPS spectra of (a) O 1s, (b) N 1s, (c) C 1s, (d) Al 2p, (e) In 3d and (f) Sn 3d respectively, measured for Alq_3 films with different film thicknesses of 0.5 nm, 1 nm, 2 nm, 5 nm, 10 nm and 50 nm.

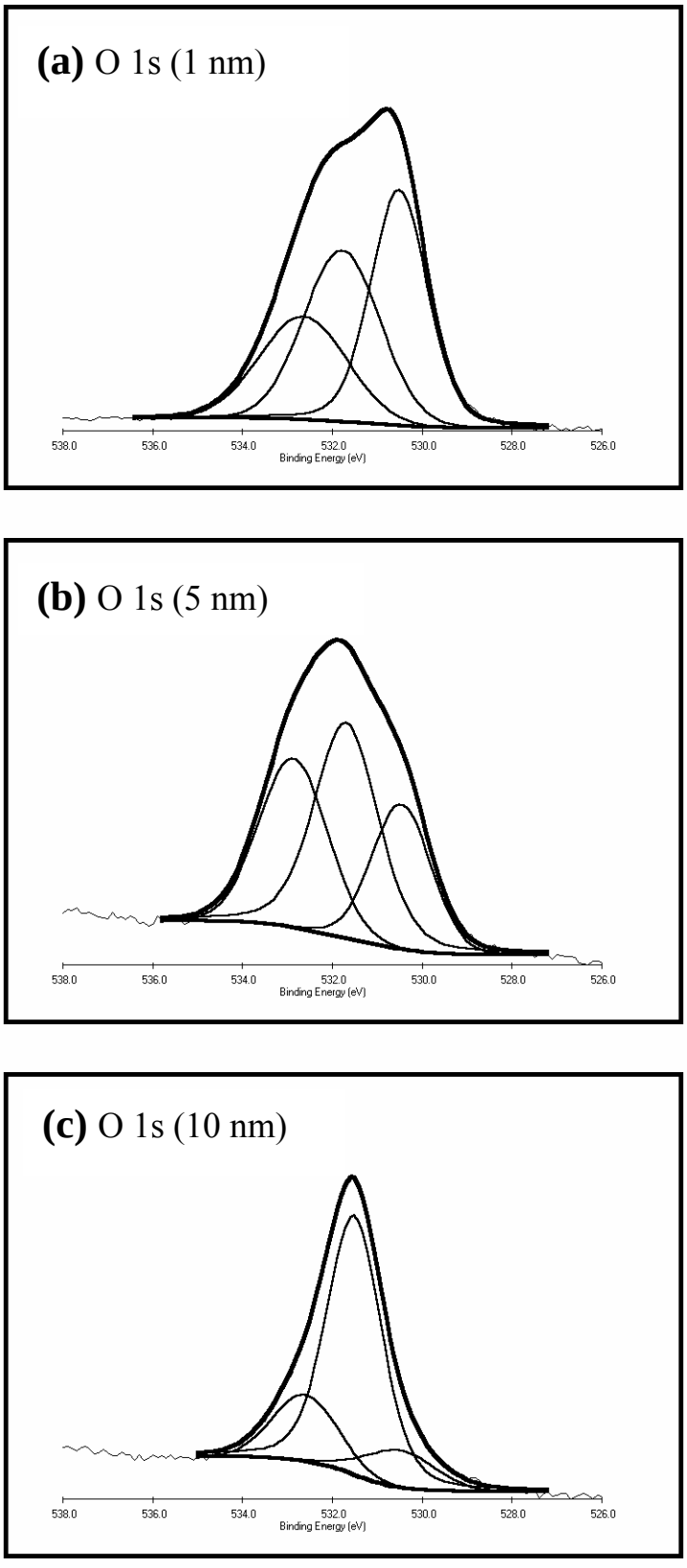

Figure 5.10: Spectral deconvoution of O 1s peak, measured for Alq_3 films with different film thicknesses of (a) 1 nm, (b) 5 nm and (c) 10nm.

energy side from 1 nm (400.6eV) to 50 nm (400.2eV). As discussed for the O 1s, Al_xO_y was formed at the Alq_3/ITO interface. Therefore, Alq_3 was broken down freeing 8-hydroxyquinoline (8-Hq), thus breaking the hydrogen bonding between Al and N atom. In the 8-Hq form, N atoms have more valence electrons, hence the core electrons need less energy to get excited. C 1*s* shifted +0.3eV from 285.2eV at the interface to ~ 285.5eV bulk value. A new feature appeared as a hump at 287.4eV region for thin Alq_3 i.e. 1 nm and 2nm. This hump diminished for bulk Alq_3 i.e. 10 and 50nm. If Alq_3 reacted with ITO at interface and formed free 8-Hq, then this peak may be assigned as C-OH type of bonding. Figure 5.11 shows the spectral deconvolution of C 1s peak measured for a 2 nm thick Alq_3, and the assigned bonding is shown. The BE for Al 2p were 74.9 eV, 74.5 eV, 73.9 eV and 74.0 eV for Alq_3 thickness of 2 nm, 5 nm, 10 nm and 50nm respectively. Al 2p shifted -0.9eV to lower energy region when the Alq_3 thickness increases. At 5nm thick Alq_3, BE of 74.5eV is assigned a typical Al 2p peak for Al_2O_3. The 73.9 and 74.0eV peaks can be assigned as Al-O-C bonding which is found in Alq_3. From the above analysis, there are signs of Alq_3 breakdown at the interface, then the free Al^{3+} bounded with oxides from ITO to form Al_XO_Y. Position of In 3d is not affected much. This observation might be the fact that In presents as bulk elements in ITO, hence loss of small amounts of O to Al does not very much affect its electronic states. Sn 3d is more sensitive towards change of chemical environment since it presents as a minor element in ITO. The Sn 3d peak shifted -0.4eV to lower energy region as thickness of Alq_3 increases. And this shift in BE can be explained if ITO breaks down and releases O to Alq_3. Hence, in environment of less O, Sn peak shifted to lower energy side.

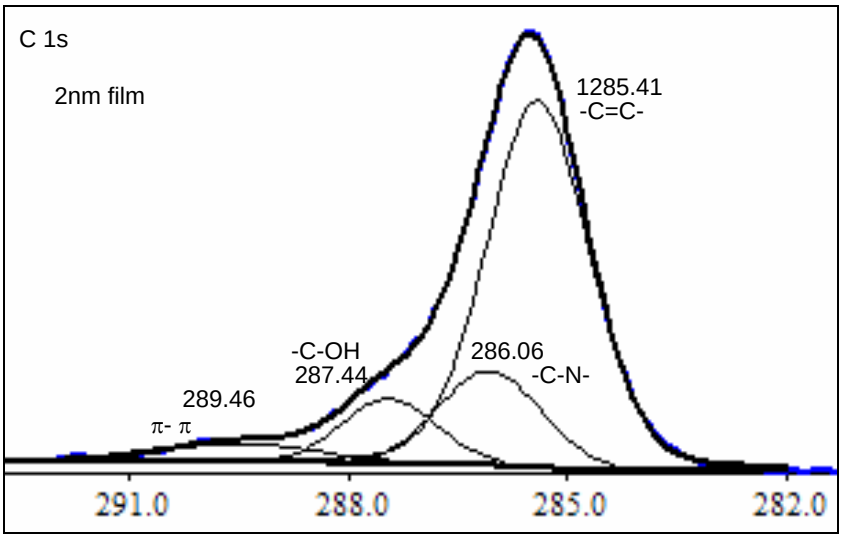

Figure 5.11: Spectral deconvoution of C 1s XPS peak measured for 2nm thick Alq_3 film.

5.2.2 XPS – NPB Thickness

Besides studying the interface between ITO and Alq_3, chemical reaction at ITO/NPB interface was also investigated. NPB films with different thickness ranging from 1 nm to 50 nm were deposited on ITO substrate, and the XPS spectra were recorded. Similar to Alq_3, when the thickness of NPB decreases to a few nanometers, NPB and ITO interaction can be seen from the XPS spectra recorded.

Figure 5.12 shows the XPS spectra of (a) O 1s, (b) N 1s, (c) C 1s, (d) In 3d and (e) Sn 3d respectively, for NPB films with thickness of 1 nm, 5 nm, 10 nm and 50 nm. From the O, In and Sn spectra, it can be concluded that 10nm of NPB completely covered the ITO surface as those XPS signals disappear at this thickness. Besides that, there are no significant changes in all the spectra presented in figure 5.12, suggesting that NPB does not interact chemically with ITO. There is about 0.1eV irregular shift in C 1s and N 1s spectra as the NPB thickness increases. This minor shift is within the experimental error. From this study, it is shown that NPB does not interact chemically when deposited on ITO. NPB remains as it is when reaching ITO.

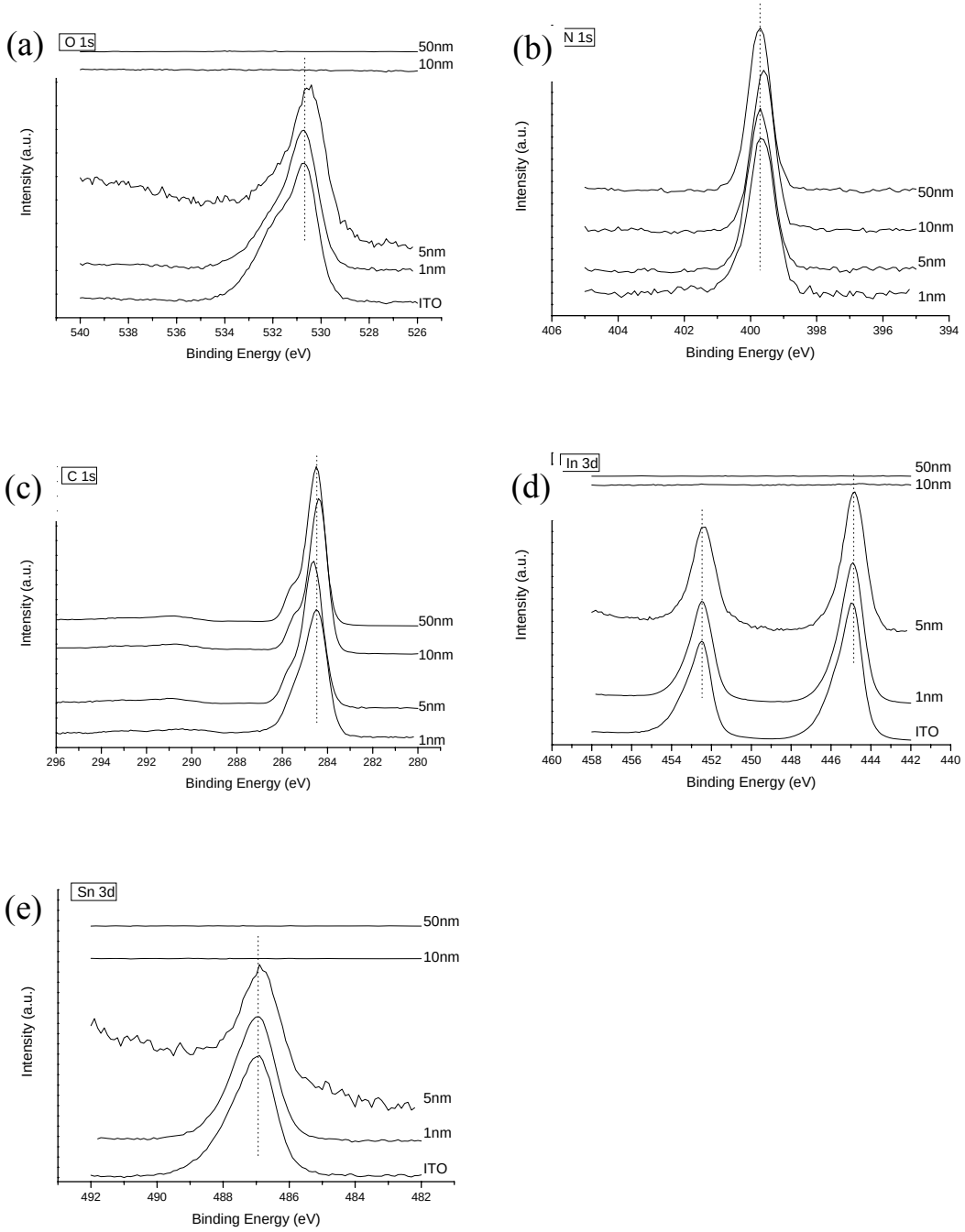

Figure 5.12: XPS spectra of (a) O 1s, (b) N 1s, (c) C 1s, (d) In 3d and (e) Sn 3d respectively, measured for NPB films with different film thicknesses of 1 nm, 5 nm, 10 nm and 50 nm.

5.2.3 XPS Depth Profile

In this section, XPS depth profile for freshly made device is compared with that of a degraded one. The two "fresh" and "degraded" devices had an identical structure of ITO/NPB/Ca/Ag. The thickness of NPB, Ca and Ag were 60 nm, 10 nm and 100 nm respectively. Immediately after devices fabrication, one of the devices was loaded to the UHV chamber for XPS measurement, and this device is referred as the fresh device. Another device was stored in an ambient condition for a few days until the device was fully covered by circular features. This device is referred as the degraded device. For the XPS measurement, in addition to a wide scan, Ag 3d, C 1s, Ca 2p, N 1s, O 1s, In 3d and Sn 3d XPS peaks were also recorded. After that the device was etched form the cathode side (starting from Ag side), using Ar^+ sputtering at ion energy of 1 kV. XPS measurement and etching process were repeated until the etching reaches ITO surface.

Figures 5.13 (a) and (b) show the compositional depth profile of a fresh and a degraded devices respectively. From the depth profile of OLEDs, it shows that sputtering time from 0 to 5 minutes is the silver layer, and Ca/NPB is represented by sputtering time from 5 to 8 minutes because of the appearances of Ca 2p3 peak. Sputtering time from 8 minutes to 14 minutes represents the organic layer, as C 1s and N 1s peaks show the maximum intensity. While sputtering time from 14 to 18 minutes indicates the NPB/ITO interface as In, Sn and O peak started to show up and C 1s and N 1s peak started to reduce and disappear. And the experiment stopped at sputtering time of 21 minutes when the organic or carbon signal started to disappear and only elements from ITO were detected. Analyzing Figure 5.13 (a), small trace of oxygen is detected at the Ca/NPB, and this could be due to the contamination when the sample

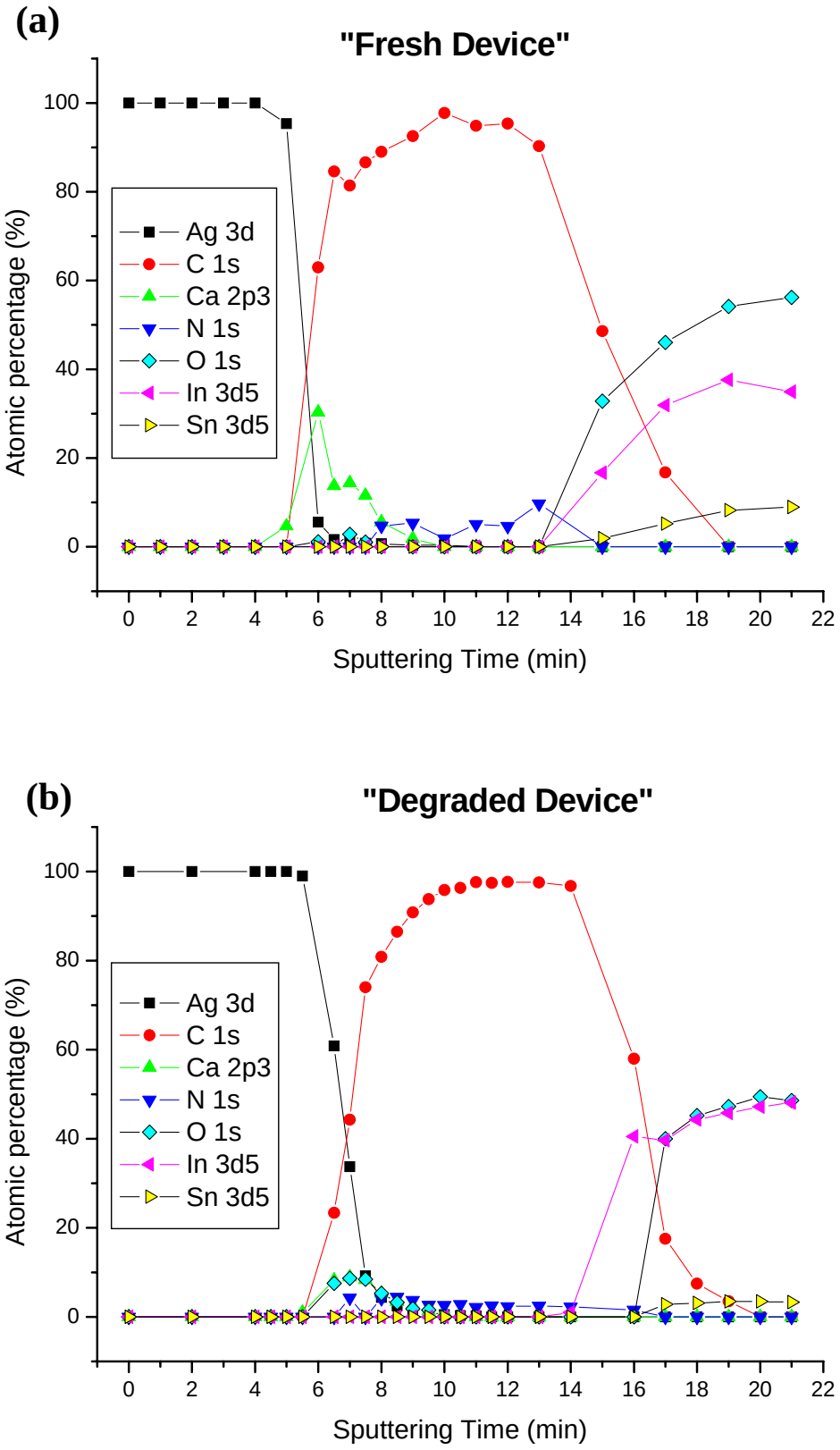

Figure 5.13: The compositional depth profile of (a) fresh and (b) degraded OLEDs.

was transferred from fabrication chamber to the XPS analysis chamber. Besides that, this depth profile clearly represents a device with structure of Ag/Ca/NPB/ITO.

From the degraded device (figure 5.13b), diffusion of In from ITO to the cathode through the organic layer (NPB in this case) was not observed. It clearly indicates that In diffusion is not the cause of dark spots formation in OLEDs. Besides, there is a significant increase in oxygen percentage at the Ca/NPB interface suggesting oxidation of calcium. This result suggests that Ca/NPB interface was indeed the degraded interface, which is in agreement with the literature finding that cathode/organic interface is responsible for the dark spots degradation in OLEDs. And the dark spots formation is mainly oxidation of the reactive metal used for cathode in OLEDs.

It is shown in the depth profile that there was no oxygen found at the organic layer and silver layer. As such, it is clear that oxygen did not diffuse either from ITO through NPB or from the ambient through the silver cathode. Figure 5.14 illustrates the evolution of O 1s spectra as a function of sputtering time for the entire degraded device. At the ITO site, the peak of O 1s is located at a binding energy of 530.7eV, corresponding to a typical binding energy of O atom in ITO. However, at the Ca/NPB interface, there were two peak associated to the O 1s peak with binding energy of 529.9eV and 531.9eV. These two peaks were assigned to OH^- and O^{2-} bounded to Ca^{2+}. Therefore the degradation process at Ca site was mainly due to the hydroxylation and oxidation of calcium that occurred at organic/cathode interface.

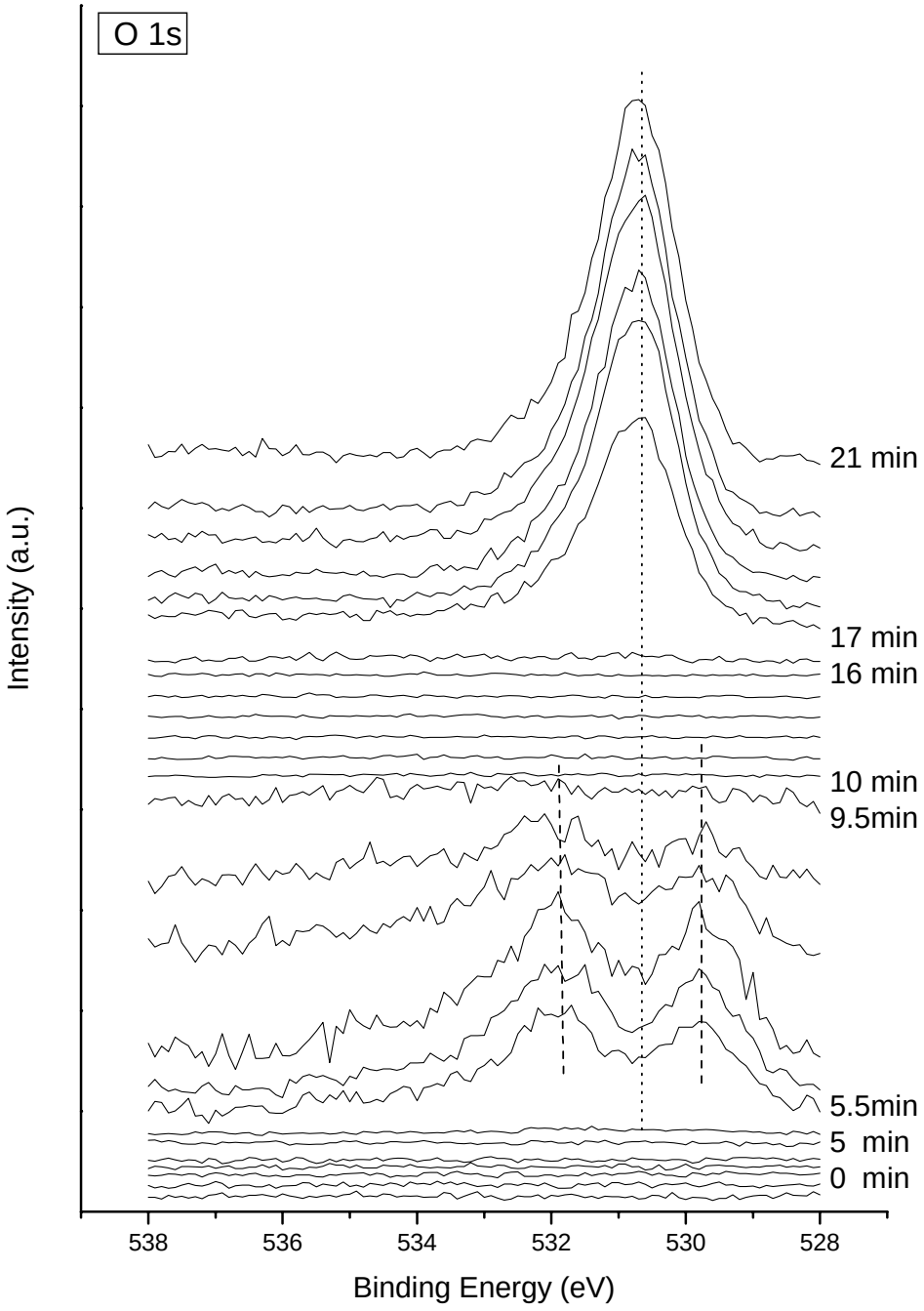

Figure 5.14: Evolution of O 1s spectra, measured for a degraded device, as a function of sputtering time.

The XPS results imply that the anode/organic interface plays an important role in the growth of dark spots in OLED. However, the degraded site responsible for dark spots formation is still at the cathode/organic interface, and the evolution of dark spots is influenced by the anode/organic interface. The next question is, how the anode/organic interface influences the cathode/organic interface in the growth of dark spots? In this regard, the NPB/ITO interface of both fresh and degraded is compared. By comparing the fresh and degraded devices, it is found that oxygen concentration at the NPB/ITO interface for the degraded device is less than that for the fresh device.

Figure 5.15 shows the evolution of atomic concentration of oxygen, indium and the ratio of O to In, O/In, at NPB/ITO interface region measured for the fresh and degraded devices. Those data were extracted from figure 5.13. The filled symbols represent the fresh device and the open symbols are for the degraded device. For the fresh device, as can be seen from the graph, O/In ratio reduced from about 1.96 at the NPB/ITO interface to about 1.44 at the bulk ITO. This observation is expected as the ITO was oxygen plasma treated before device fabrication. The O/In ratio of 1.44 in the bulk ITO extracted from the fresh device is comparable to that in an untreated bare ITO, which has a value of 1.37. For better comparison, the ratio of O, Sn, In and O/In in an untreated bare ITO were 0.55, 0.05, 0.40 and 1.37 respectively.

As shown in Figure 5.15, it is interesting to note that the oxygen content decreases from about 55% for the fresh device to 50% for the degraded device. This reduction in oxygen concentration is significant if the In concentration is taken into consideration, as can be seen in the O/In ratio. The O/In ratio reduces from about 1.4 to 1.0 for fresh and degraded devices respectively.

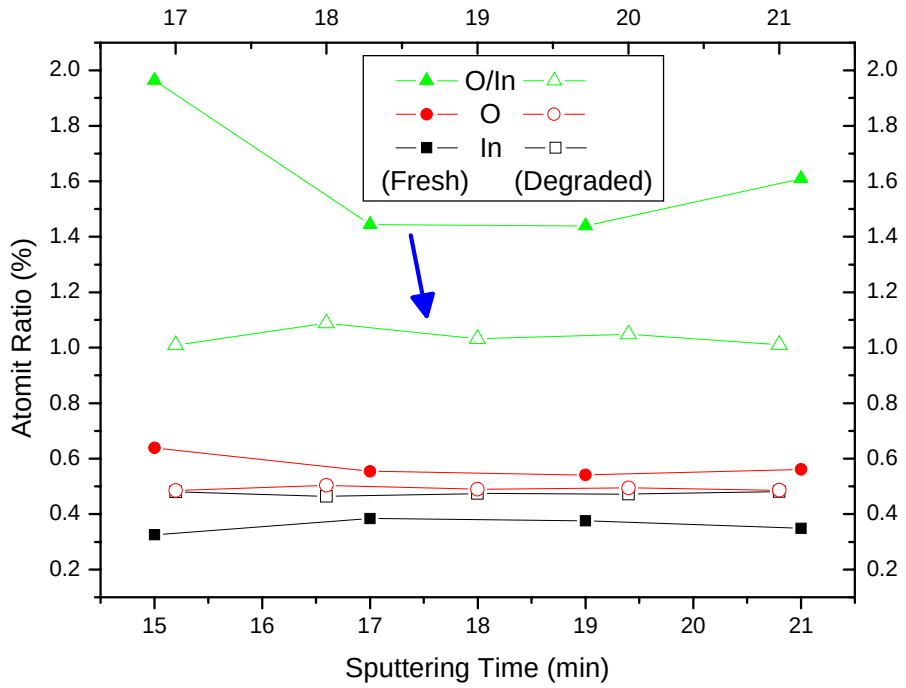

Fig 5.15: Evolution of atomic concentration of oxygen, indium and the ratio of O to In, O/In, at the NPB/ITO interface for the fresh and degraded devices.

In conclusion, XPS was employed to study the chemical states at anode/organic and organic/cathode interfaces in an OLED. At the anode/organic interface, results reveal that Alq_3 interacted chemically with ITO forming Al_xO_y when it deposited on ITO. However, it is clear that there was no chemical reaction occurred between NPB and ITO at the NPB/ITO interface. For OLED degraded due to the formation of dark spots, oxidation of Ca occurred at the cathode/organic interface forming CaO or $Ca(OH)_2$. On the other hand, reduction of ITO was observed at anode/organic interface. Indium and oxygen did not diffuse through the organic layer as no In and O in the organic layer were observed in the XPS depth profile of both fresh and degraded devices.

Chapter 6

Model of Dark Spot Formation

6.1 Galvanic Cell Formation in OLEDs

It is shown from the XPS analysis that there was an increase in oxygen at the Ca/NPB interface but loss in oxygen at the NPB/ITO interface. The oxidation and reduction processes occurred at two electrode/organic interfaces in OLEDs could be just a redox reaction due to the formation of an electrochemical galvanic cell. A galvanic cell is formed at the presence of a pair of dissimilar electrodes and an electrolyte. In this case, the cell with a low electrode potential metal (Ca), acting as an anode (which is just the opposite to that in an OLED, since Ca is corroded), and a higher potential electrode (ITO), the cathode (since it is protected).

In order to manifest the existence of galvanic cell in an OLED, an external voltage is applied to balance the built–in potential caused by the different potential in the two electrodes. In other words, a dramatic decrease of the growth rate should be observed by a positive bias (Ca : negative, ITO : positive) of 2 – 3 V to make the Ca "more cathode-like". Ideally, when the external voltage compensates the built–in potential, the galvanic cell is offset. Therefore, an external bias from 1 volt to 5 volts was applied to an ITO/NPB/Ca/Ag device, where ITO was connected to the positive terminal of a power source while Ca/Ag was connected to the negative terminal. The circular feature growth rate was measured for each of the devices. All the experiments were carried out in a humidity chamber at 25°C and relative humidity of 60%.

Figure 6.1 illustrates the growth rate of circular features observed in OLED as a function of applied voltage. The growth rate for a "zero" bias is referred to a control device without any external bias. The growth rate of circular features remains at about

6 μm^2/min for an external range from 0–2.5 V. However, a dramatic drop in the growth rate, from 6 μm^2/min to about 2 μm^2/min, when the external bias was increased from 2.5 V to 3.0 V. At 3.5 V, the growth rate was further reduced to about 1.5 μm^2/min. Unfortunately, the growth rate at a higher applied voltage was not measurable, due to the formation of dome-like bubble at the circular features. From this experiment, it clearly demonstrates the existence of galvanic cell in OLEDs. When the external bias reaches or is larger than the electrode potential difference between ITO and Ca, in this case, 3.0 V and above, the galvanic cell is offset.

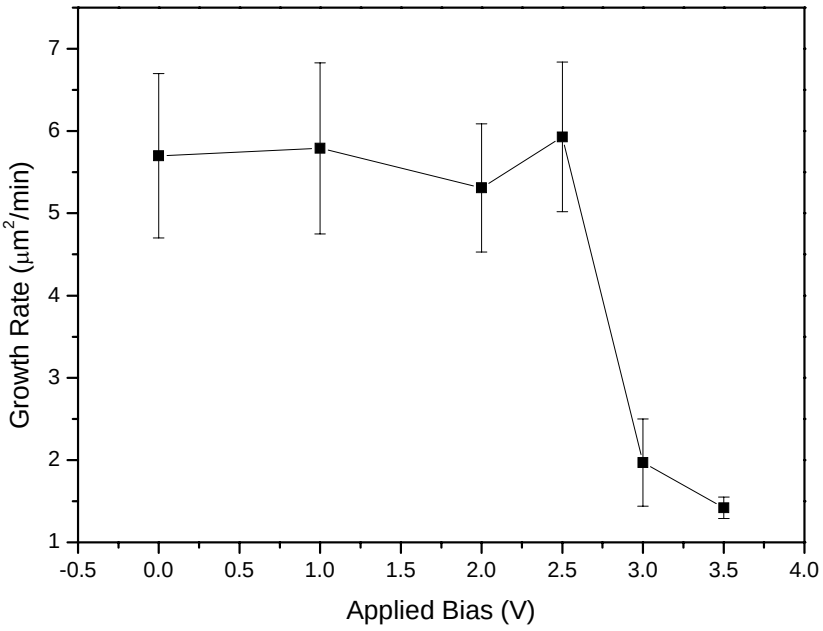

Figure 6.1: Growth rate of circular features as a function of external bias for the ITO/NPB/Ca/Ag device.

In the galvanic series, calcium is in the anodic site of the series, and can be oxidized easily. From the thermodynamic point of view, the Ca electrode is readily oxidized to Ca^{2+} because of its high standard electrode potential. It can be expressed as:

$$Ca \rightarrow Ca^{2+} + 2e^{-}, \qquad E = +2.87\ V \qquad (6.1)$$

where E is the standard electrode potential. In a galvanic cell, one of the electrodes is oxidized (anode) and the other reduced (cathode). In the case of OLED, which is related to the formation of dark spots, Ca is oxidized to Ca^{2+}, while ITO is reduced by release of oxygen. The loss in oxygen in the ITO has been verified in XPS depth profiles of OLEDs. The reduction potential for ITO is unknown, but it can be estimated from the above experiment. The galvanic potential of ITO/NPB/Ca is offset at an external bias of 3.0 V, but an external bias of 2.5 V is not sufficient to compensate it. Therefore the reduction potential for ITO can be estimated to be in the range of –0.37 V to +0.13 V while the oxidation potential for Ca is +2.87 V.

In order to further verify the formation of a galvanic cell in OLEDs containing ITO and reactive metal, e.g. Ca, investigation on the growth of dark spots with respect to different pairs of electrodes were performed. Glass/M/NPB/Ca/Ag and ITO/M/NPB/Ca/Ag were fabricated, where M represents Au, Ag, Al and Ca in this study. The thickness of M was kept constant at a few nanometers. After device fabrication, the growth of dark spots in the devices was monitored at 25°C and relative humidity of 60%.

Table 3 is a summary of the different electrode pairs used in this study and the corresponding growth rate of dark spots. As can be seen from Table 3, the growth rate of dark spots in the above devices is in the range of 0.8 – 1.2 μm^2/min, which is at the slow rate range compared to 6 μm^2/min for the devices with a configuration of ITO/NPB/Ca/Ag device. For sample 4, calcium was used for both electrodes, and calcium is highly reactive, it still shows slow dark spots growth rate. Ca/Ag is the oxidation electrode, in order to have a higher dark spots growth rate, calcium at the glass or ITO side should be reduced. However, thermodynamically, calcium is difficult to be reduced. Therefore, the device, sample 4, did not form a galvanic cell. This observation and explanation are true for samples 1, 2 and 3 as well. The main reason of the slow dark spot growth rate is due to the fact that those metals used (Au, Ag and Al) are not easy to be reduced, which is required in order to form an actual galvanic cell.

Sample	Electrode	Organic material	Electrode	Growth rate of dark spots (μm^2/min)
1	Glass/Au ITO/Au	NPB (60 nm)	Ca/Ag (10 nm/150 nm)	**0.8**
2	Glass/Ag ITO/Ag	NPB (60 nm)	Ca/Ag (10 nm/150 nm)	**1.1**
3	Glass/Al ITO/Al	NPB (60 nm)	Ca/Ag (10 nm/150 nm)	**1.2**
4	Glass/Ca ITO/Ca	NPB (60 nm)	Ca/Ag (10 nm/150 nm)	**1.0**

Table 3: OLED with different electrode pairs and the corresponding dark spots growth rate.

6.2 Model of Dark Spot Formation in OLEDs under Non-Operating Condition

It is well known that dark spots in OLEDs do not increase in number, but only increase in size. Pre-existed defects on substrate or the defects formed during films deposition are responsible for the nucleation of dark spots. The nucleation of dark spots in OLEDs is always associated with the presence of pin-hole defects in cathode.

Typical thickness of an OLED (including organic layers and metal cathode) is in the order of sub-micron. The size of dark spots that are usually seen under the optical microscope are more than a micron. The nucleation center for dark spot is not exactly a "pin-hole", rather, it is a "big hole" in comparison to the dimension of the thickness of the device. Figure 6.2 illustrates an enlarged cross sectional view of a dark spot center. Figure (a) is a typical dark spot observed in OLED. Figure (b) is an enlarged cross sectional view. Figure (c) shows schematically the edge from the center of the dark spot with absorbed moisture in the enlargement. From figure 6.2 (b), it can be seen that the nucleation site for dark spots is quite "big".

As discussed in the previous sections that the growth rate of dark spots can be grouped into two main groups: fast (~6μm^2/min) and slow (~1μm^2/min) growth rates. The discussion of model of dark spot formation in OLEDs under non-operating condition is separated into two parts, i.e. (a) Case I, devices made on glass/NPB/Ca/Ag, which show slow dark spots growth rate and (b) Case II, devices made on ITO/NPB/Ca/Ag, which have fast growth rate.

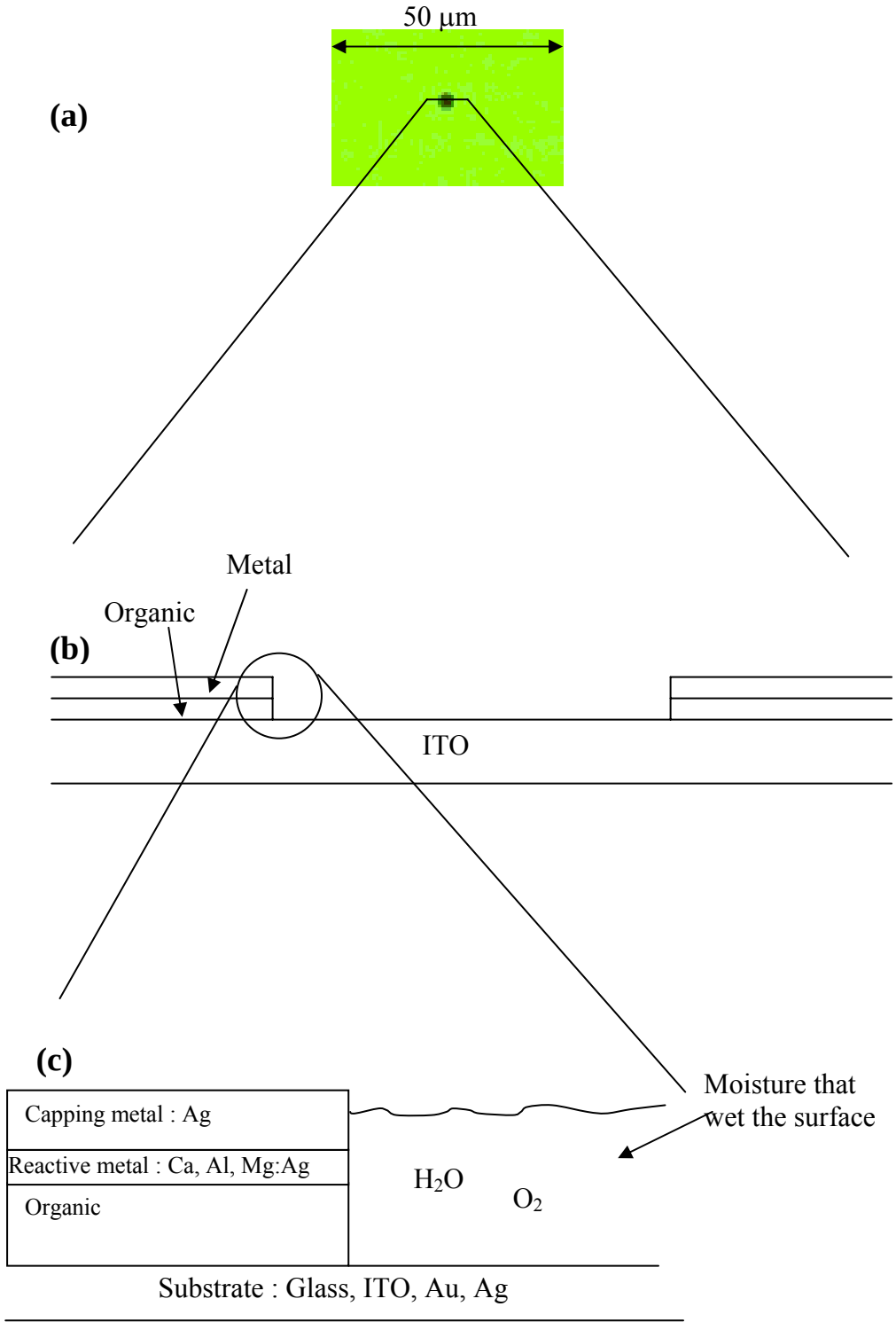

Figure 6.2: Illustration of an enlarged cross sectional view of a dark spot center, with (a) a typical dark spot observed in OLED, (b) an enlarged cross sectional view and (c) the schematic of the edge from the center of the dark spot.

It is known that the growth of dark spots in OLEDs can be controlled with proper encapsulation or storing in an inert environment. Therefore the effect of relative humidity on the growth of dark spots was studied. Figure 6.3 shows the dark spots growth rate as a function of relative humidity for NPB/Ca/Ag deposited on ITO and glass substrates. The inset is the same set of data plotted in log scale and the curve fitting equations are also shown in the inset. This experiment was done in a humidity chamber at 25°C. At a constant temperature, the relative humidity can be used as the amount of moisture or water present in the air. From the graph, it is clear that the dark spots grew exponentially with relative humidity. At a given relative humidity, the growth rate is always higher in ITO/NPB/Ca/Ag device compared to glass/NPB/Ca/Ag.

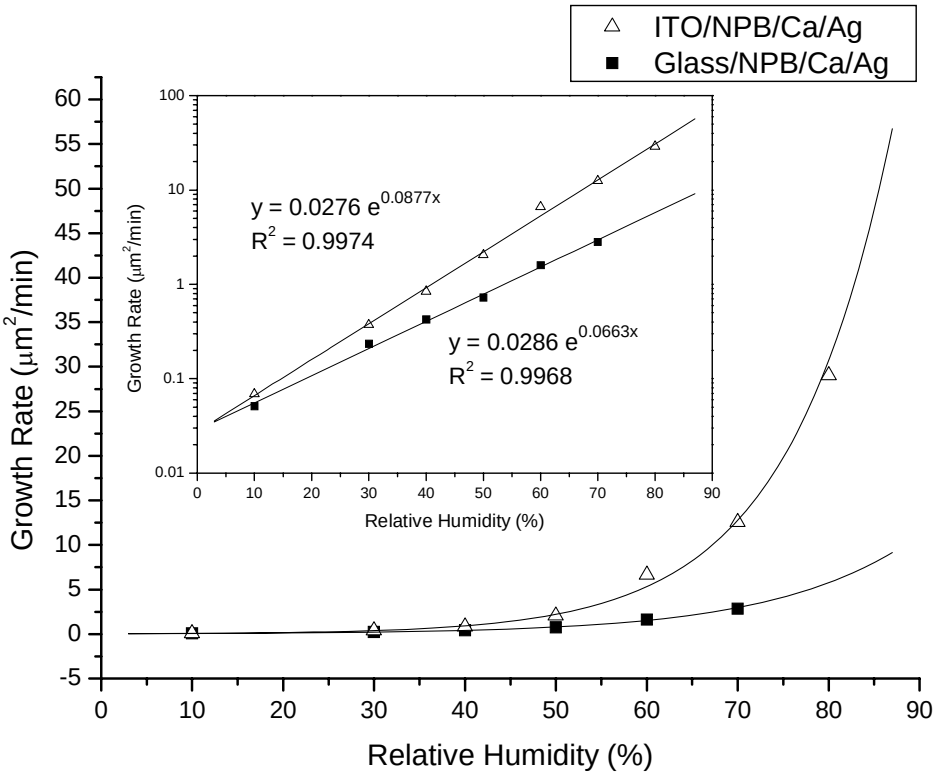

Figure 6.3: Growth rate of dark spots as a function of relative humidity measured for NPB/Ca/Ag deposited on ITO and glass substrates. The inset is the same set of data plotted in log scale.

6.2.1 Case I : glass/NPB/Ca/Ag Device

From the XPS analysis, it is found that calcium is corroded or oxidized to calcium hydroxide and calcium oxide. For metallic materials, the corrosion process is normally electrochemical, a chemical reaction in which there is transfer of electrons from one chemical species to another. In OLEDs calcium is oxidized according to the reaction:

$$Ca \rightarrow Ca^{2+} + 2e^{-} . \qquad (6.2)$$

The electrons generated from each metal atom that is oxidized must be transferred to and become a part of another chemical species, known as a reduction reaction. In the case of aqueous solution with dissolved oxygen, the following reduction will probably occur,

$$O_2 + 2H_2O + 4e^{-} \rightarrow 4OH^{-} . \qquad (6.3)$$

For a acidic solution in which oxygen is also dissolved,

$$O_2 + 4H^{+} + 4e^{-} \rightarrow 2H_2O . \qquad (6.4)$$

In the presence of moisture, the growth of dark spots in OLEDs is the oxidation process of reactive metallic cathode, which in this case is the calcium. As can be seen from figure 6.2 (c) that moisture can easily wet the edge from the center of the dark spot, and can act as electrolyte and electrode (cathode) in the process of corrosion. The corrosion process is taken place at the weakest interface, which is at the organic/metal interface, and this was verified by the XPS depth profile measured for the OLEDs.

Moisture in air is assumed to be neutral and there is always dissolved oxygen. The total electrochemical reaction can be written as:

$$2Ca + O_2 + 2H_2O \rightarrow 2Ca(OH)_2 . \qquad (6.5)$$

From the thermodynamic point of view, the process described by equation (6.5) is favorable because of its cell potential of +3.27 V. The electrode potentials in the processes shown in equations (6.2) and (6.3) are +2.87 V and +0.40 V, respectively. However, the electrode potential does not determine how fast the corrosion will take place. From the kinetic point of view, the concentration of the chemical species involved and the temperature play an important role in determining the corrosion rate. In the humidity experiments, the temperature and calcium thickness were kept constant. The only factor would affect the corrosion rate was the oxygen and water (moisture) concentration. As can be seen from Figure 6.3, the corrosion rate increases as moisture concentration increases.

6.2.2 Case II : ITO/NPB/Ca/Ag Device

As shown in section 6.1, galvanic cell exists in OLED with ITO and Ca as the two electrodes.

$$Ca \rightarrow Ca^{2+} + 2e^- , \quad E = +2.87 \text{ V}, \qquad (6.6)$$

$$ITO + e^- \rightarrow O_2, \quad E = -0.37 \text{ to } +0.13 \text{ V}. \qquad (6.7)$$

Thermodynamically, the above redox reaction is favorable. Figure 6.4 illustrates schematically the formation of a galvanic cell in OLED, a complete reaction that involves transform of electrons and ions is depicted.

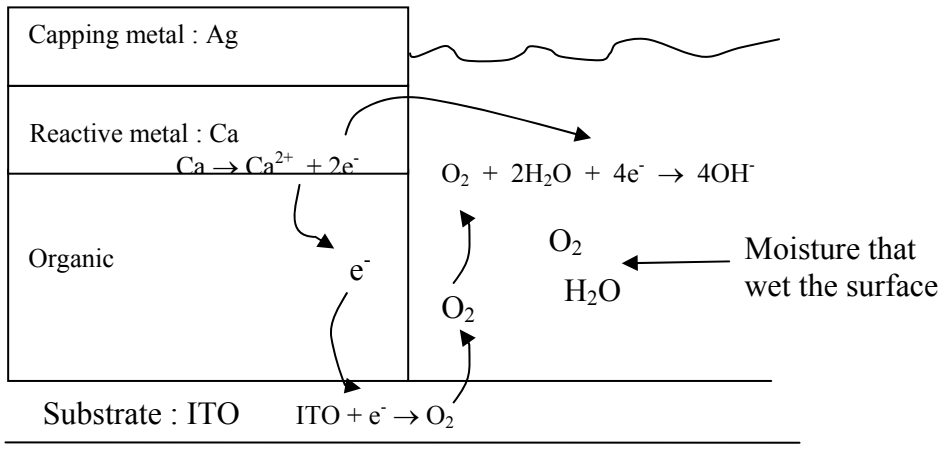

Figure 6.4: Schematic diagram of a galvanic cell formed in an OLED. A complete reaction that involves transform of electrons and ions is depicted.

In this model, the absorbed moisture acts as the electrolyte for the transfer of ion or oxygen. The semiconducting organic layer reacts as a conducting media for electron transportation. It has to be pointed out that when the conducting organic is replaced by non-conduction organic material, it does not show acceleration in the growth of dark spots. Besides, the organic materials can serve as electrolyte as well, as it might absorb moisture. When oxidation process occurs at calcium electrode, electrons are transported to the ITO through the conducting organic layers. This process is driven by the electrode potential difference existed between Ca and ITO. At the ITO surface, oxygen is released by reduction process when ITO accepts electrons. Oxygen is then dissolved in moisture that was absorbed in the pin-hole of OLEDs. The concentration of oxygen is increased. Referring to equation (5.5), the electrode corrosion rate or the dark spots growth rate increases when the oxygen concentration increases. This explains the fast growth rate of dark spots in ITO/NPB/Ca/Ag device.

In section 4.3, it is shown that dark spot in ITO/Alq_3/Ca/Ag grows much slower than the ITO/NPB/Ca/Ag device, while Alq_3 is also an electron conducting material. This reveals that carrier mobility of organic materials might play an important role in determining the growth rate of dark spots. The mobility of hole in NPB is a few orders of magnitude higher than that of electron in Alq_3. However, results discussed in section 4.4 suggest that the carrier mobility in organic materials does not seem to play a critical role. If the mobility of carriers plays a role, it would expect that the dark spots growth rate in the devices with the structure of ITO/NPB/Alq_3/NPB/Ca/Ag and ITO/NPB/Alq_3/Ca/Ag would be similar to that of ITO/Alq_3/Ca/Ag device, as the lower mobility determines the overall mobility.

From the XPS experiment on the investigation at Alq_3/ITO interface (section 5.2.1), it was found that upon deposition on ITO, Alq_3 fragmented and formed Al_xO_y at the Alq_3/ITO interface. The formation of Al_xO_y, an insulating layer, prevented the electrons transfer from bulk Alq_3 to the ITO. This hypothesis is verified in a device with a thin insulating (photo resist) between ITO and NPB in ITO/NPB/Ca/Ag. The corrosion rate measured for this device was in the range of about 1μm^2/min.

Chapter 7

Anode Modification

7.1 Enhancement of EL Efficiency

Charge injection from the electrodes to organic materials and charge transport in the organic layers play the crucial roles in determining both the operating voltage and luminance efficiency in OLEDs. Apart from synthesizing new organic materials with different charge mobilities to improve device performance, electrode modification is another commonly used approach to achieve hole-electron current balance in OLEDs. The effect of metals having different work functions, used as cathode, has been widely investigated. [Tang and VanSlyke 1987, Hung et al. 1997, Jabbour et al. 1997, 1998, Stossel *et al.* 1999, 2000] Nevertheless, the modification of indium-tin-oxide (ITO), the commonly used anode in OLED, is also employed to improve the device performance. [VanSlyke *et al.* 1996, Wu *et al.* 1997, Kim *et al.* 1998, Nuesch *et al.* 1999, Forsythe and Abkowitz 2000, Hung *et al.* 2001]

In this section, the effect of adding thin Alq_3 buffer layer between the ITO and NPB on the OLED performance is investigated. Two sets of multilayer OLEDs with the structure of ITO/Alq_3(x nm)/NPB(60nm)/Alq_3(75nm)/Ca(5nm)/Ag(150nm) were made simultaneously, where x was varied from 0 – 5 nm. After the devices were made, one set of the devices was transferred to nitrogen grove box with oxygen and moisture levels lower then 1.0 ppm for current density-voltage-luminescence (I-V-L) measurement. After I-V-L measurement, lifetime measurement was started at a current density of 25 mA/cm^2 in the grove box. The other set of the devices, which was kept in the vacuum chamber and non-operated, was monitored using optical image analysis technique that developed for studying the growth of dark spots in an ambient environment (~25^{o}C and ~60% RH) without encapsulation.

Figures 7.1 (a) and (b) show the current density – voltage and luminance – current density curves for a set of OLEDs with the structure of ITO/Alq_3(x nm)/NPB/Alq_3/Ca/Ag, where x was varied from 0 – 5 nm. The control device denoted as x = 0 nm. It is expected that increase in the thickness of Alq_3 buffer layer would increase device driving voltage due to higher energy barrier and holes blocking effect by Alq_3 buffer layer. However, the increase in voltage was not significant when ultra-thin layer of Alq_3 (1 nm and 2 nm) were used. The voltage increased for only about 0.15 V at a current density of 100mA/cm^2 when comparing the control device with device with 1 nm Alq_3 buffer. Huge increase in voltage was observed when the thickness of buffer layer was 3 nm or above. Nevertheless, the current efficiency of these devices increases as the thickness of Alq_3 increases. For example, at a current density of 100 mA/cm^2, the current efficiency of 2.08 cd/A for a control device was increased to 2.62 cd/A for a device with 1 nm thick Alq_3 buffer layer, and it was further increased to 3.55 cd/A when the Alq_3 buffer was 5 nm. The current efficiency and the corresponding operating voltage at a current density of 100 mA/cm^2 are summarized in Table 4.

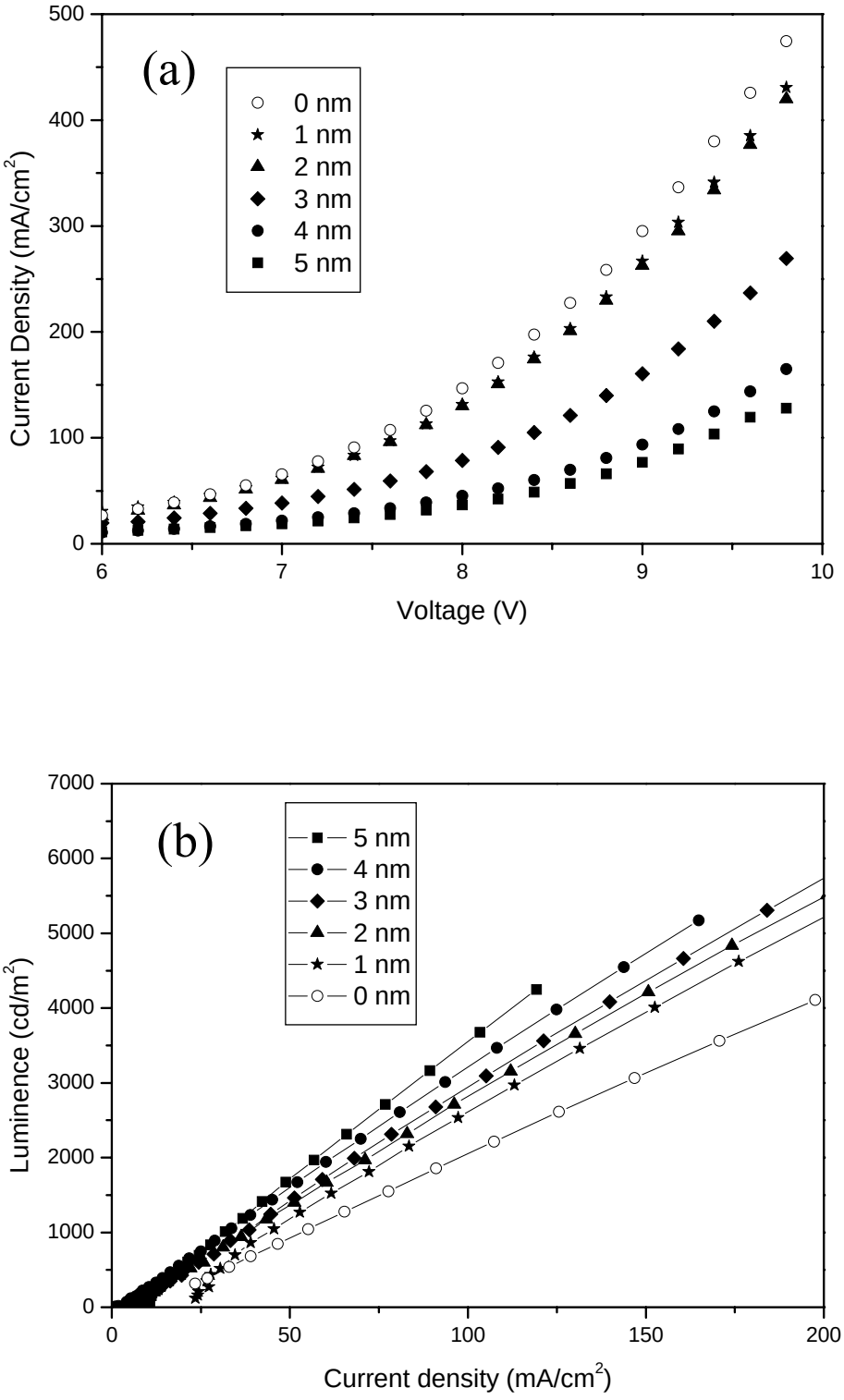

Figure 7.1: (a) Current density – voltage and (b) luminance – current density characteristics of OLEDs with a configuration of ITO/Alq_3 interlayer/NPB/Alq_3/Ca/Ag. The thickness of the Alq_3 interlayer was varied over a range of 0-5.0 nm.

Alq_3 thickness (nm)	Voltage (V)	Current efficiency (cd/A)
0	7.52	2.08
1	7.64	2.62
2	7.66	2.82
3	8.32	2.94
4	9.10	3.21
5	9.36	3.55

Table 4: Current efficiency and the corresponding voltage at current density of 100 mA/cm^2, for devices with different thickness of Alq_3 buffer layer.

The enhancement in the current efficiency by inserting a buffer layer between ITO and NPB is mainly due to the reduction of hole injection from ITO to NPB. The current efficiency, η, can be defined as the ratio of recombination current, J_r, to the device current, J_{tot}.

$$\eta = \frac{J_r}{J_{tot}} \ , \qquad (7.1)$$

where J_{tot} is the sum of hole current and electron current, $J_{tot} = J_h + J_e$. In NPB-Alq_3 based device, $J_h >> J_e$, this is attributed to a higher hole mobility in NPB compared to that of electron in Alq_3, $\mu_h >> \mu_e$, hence the total current can be simplified as $J_{tot} \approx J_h$. Therefore equation (7.1) can be expressed as:

$$\eta \approx \frac{J_r}{J_h} \ . \qquad (7.2)$$

The recombination current J_r, depends on the electron–hole pair generated, and it is limited by the minority charge carrier, in this case, the electron. Under this

assumption, J_r can be regarded as a constant if every electron-hole pair decayed by emitting light. When the thickness of Alq_3 interlayer increased, fewer holes were injected into the NPB and thus J_h decreased leading to an increase in current efficiency.

7.2 Extension of Device Lifetime

In addition to a higher device efficiency, stability is another important factor that determines the EL performance of OLEDs. The gradual decrease in electroluminescence efficiency and increase in operating voltage remain the major hurdles that limit the long-term stability of the OLEDs. [Adachi *et al*. 1995, Hamada *et al*. 1995, VanSlyke *et al.* 1996, McElvain *et al*. 1996, Aziz *et al*. 1999] Apart from the intrinsic instability of the organic materials, the growth of non-emissive areas known as dark spots in OLEDs, is another limiting factor that deteriorates the device performance. [Burrows *et al*. 1994, McElvain *et al*. 1996, Do *et al*. 1996, Aziz *et al*. 1998-a, 1998-b, Liew *et al.* 2000, Kolosov *et al.* 2001, Murase *et al.* 2001, Scheblykin *et al.* 2001, Kim *et al.* 2002]

In this section, the effect of adding thin Alq_3 buffer layer between the ITO and NPB on the device stability is investigated. The experimental details were described in section 7.1.

7.2.1 Retardation of Dark Spot Growth

As discussed in the chapter 4, it is worthwhile to note that the use of Alq_3 buffer in OLEDs is also demonstrated to have better storage stability over the control device. Figure 7.2 shows the dark spot growth rate for the ITO/Alq_3(x nm)/NPB/Alq_3/Ca/Ag devices with different thickness of Alq_3 buffer. The inset is the graph of dark spot area as a function of storage time. By using optical image analysis, the area of dark spots was measured without applying any electrical field. It is clearly shown from Figure 7.2 that, with the use of only an ultra-thin layer of Alq_3 buffer (1 nm), dark spot growth rate in the device reduces for more than 6 times compared to the control device. The dark spot growth rates do not change significantly when the thickness of Alq_3 buffer increases, at least in the range of our interest from 1 nm to 5 nm. Figure 7.3 shows the EL images taken through the glass side of the corresponding control device and the ones with a 2 nm thick Alq_3 buffer, after 24 hours exposure in ambient.

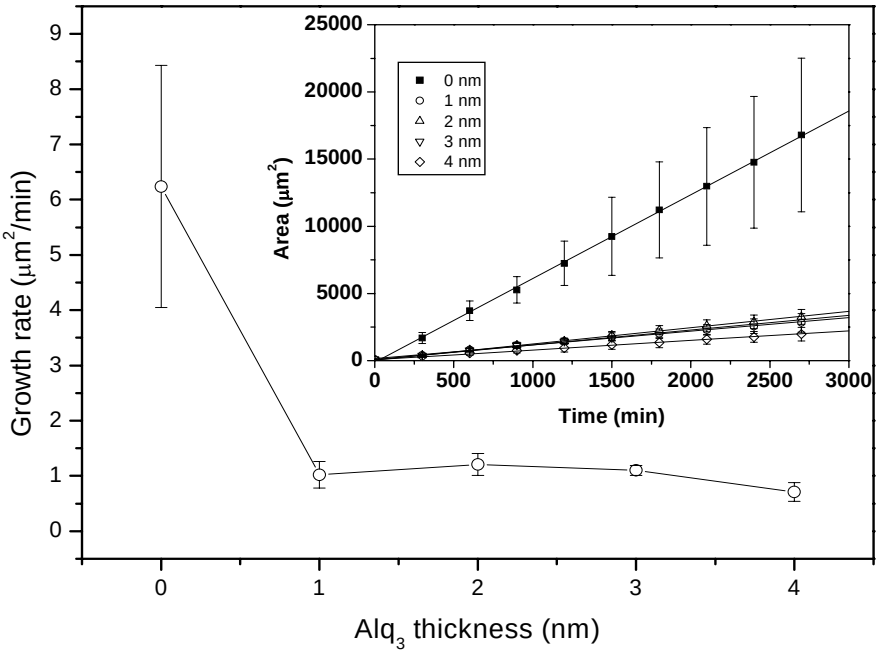

Figure 7.2: Growth rate Dark spots in ITO/Alq_3(x nm)/NPB/Alq_3/Ca/Ag devices with Alq_3 interlayer having different thicknesses of 0 – 4 nm. The inset is the graph of dark spots area as a function of time for these devices.

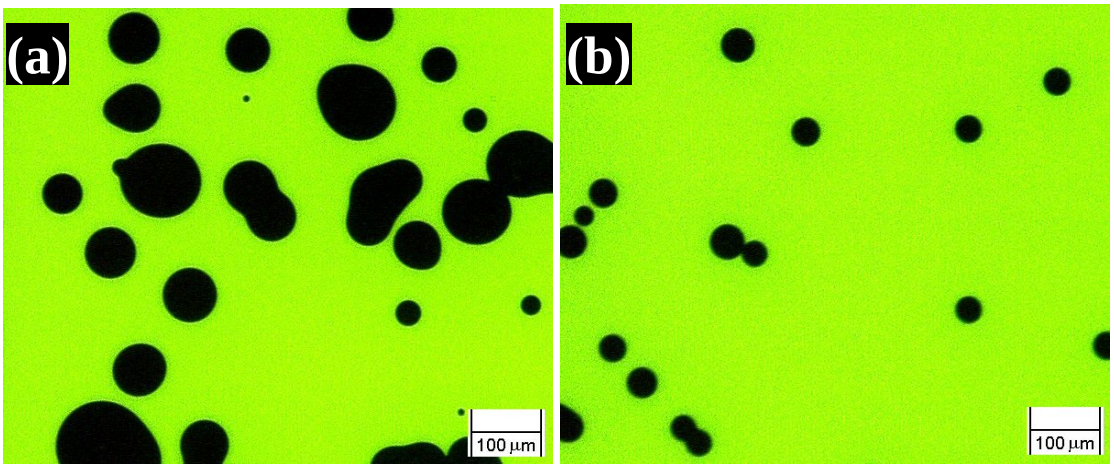

Figure 7.3: EL images for (a) control device with the structure of ITO/NPB/Alq_3/Ca/Ag and (b) Alq_3-modified ITO device with the structure of ITO/Alq_3(2 nm)/NPB/Alq_3/Ca/Ag, measured 24 hours after they were exposed in ambient.

7.2.2 Intrinsic Stability

Besides improvement in environmental stability, devices made with Alq_3 interlayer also show improvement in the intrinsic stability. Figure 7.4 shows the normalized luminance (L/L_o) plotted against operating time, for the control device and the device with 2 nm thick Alq_3 buffer. Both devices were driven, in nitrogen grove box, at 25 mA/cm^2, with their initial luminance and voltage of 563 cd/m^2, 6.9 V and 608 cd/m^2, 7.2 V respectively. From Figure 5.28, it is found that the luminance of the control device decreased by 37% from its initial values after 24 hours, while the Alq_3-modified device experienced a drop of only 18%. From the results of prolonging device lifetime and enhanced current efficiency, it indicates that less holes were injected to the Alq_3-modified ITO device. These results support the current balance mechanism described by Aziz et. al..[Aziz *et al.* 1999]

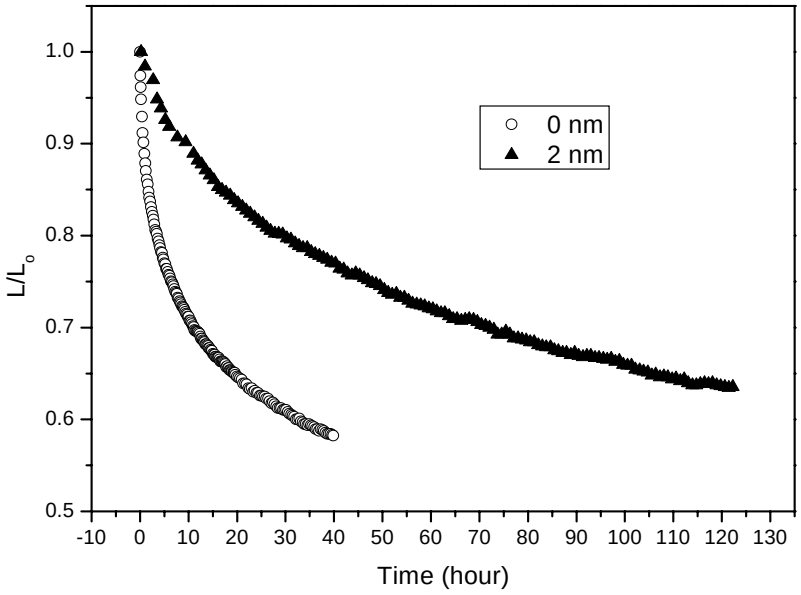

Figure 7.4: Normalized luminance as a function of operation time for (a) control device with the structure of ITO/NPB/Alq_3/Ca/Ag and (b) Alq_3-modified ITO device with the structure of ITO/Alq_3(2 nm)/NPB/Alq_3/Ca/Ag.

The device efficiency increased as thickness of Alq_3 buffer increased, the driving voltage also increased. The increase in voltage is not significant when the buffer layer become ultra-thin i.e., 1-2 nm thick, but the current efficiency increased by about 25%. Most importantly, the additional layer of Alq_3 also helps to enhance storage and operational stability of the devices. The growth of dark spots is retarded and the operational lifetime of the device also extended by adding buffer layer of Alq_3 between ITO and HTL in OLEDs.

In conclusion, the presence of an Alq_3 interlayer between ITO and HTL is shown to improve the current balance leading to an efficient operation of OLEDs. Besides enhancing the current efficiency, the Alq_3-modified ITO devices also show improved storage and operational stability. Adding ultra-thin layer of Alq_3 buffer (1 – 2 nm) in OLEDs did not lead to a significant increase in operating voltage, but the growth rate of dark spots was retarded by more than 6 times, and the operational lifetime was increased by a few times.

Chapter 8

Conclusion

Investigation of the evolution of dark spot formation in small molecule based OLEDs has been carried out. An optical image analysis technique has been developed to study the growth of dark spots in OLEDs under non-biased condition. Under reflected light of a microscope, a direct relationship between dark spots, found in the emitting area of the OLEDs, and circular features, seen in the same locations of non-operated devices, is identified. In addition to the understanding of dark spots induced by electrical stress or joule heating, this work demonstrates that dark spots also grow in OLEDs without the presence of an external electric field. By using the optical image analysis technique, the electrical field effect on dark spot formation is eliminated. Therefore, the nature of dark spot formation in OLEDs before device operation can be studied.

Through the optical image analysis, experimental results reveal that the growth of dark spots is not dependent on the thickness of organic layers used in the devices. However, adhesion at organic/electrode interface might play an important role in determining the growth of dark spots in OLEDs, due to the fact that no growth of dark spot was observed in device made without the organic layers.

For the first time, results of this research show that the growth of dark spots is dependent on the first organic layer on the substrate, or the anode/organic contact property. The organic/cathode interface does not seem to affect the growth rate of dark spots. The growth rate of dark spots in devices made of ITO/Alq_3/Ca/Ag, ITO/Alq_3/NPB/Ca/Ag and ITO/Alq_3/NPB/Alq_3/Ca/Ag are in the same range, which is at the slower rate of about 0.6 μm^2/min compared to devices made of ITO/NPB/Ca/Ag, ITO/NPB/Alq_3/Ca/Ag and ITO/NPB/Alq_3/NPB/Ca/Ag, which have

a faster growth rate of about 6 μm^2/min. It is well known that the site of dark spots formation in OLEDs is at the organic/cathode interface. The finding on the correlation between anode/organic interface and the growth of dark spots has added new knowledge in this field.

Since the growth of dark spots is also related to the organic/anode interface, AFM is used to investigate the correlation between the anode and organic film surface morphologies and dark spots growth rate. Results reveal that the organic films become smoother as the thickness increases. However, the variation in the RMS roughness as thickness increases is not relevant to the growth rate of dark spots in corresponding OLEDs, because the growth rate of dark spots does not depend on organic layer thickness. Furthermore, the RMS roughness of NPB from ITO/Alq_3/NPB and ITO/NPB films are similar, with 1.07 nm and 1.09 nm respectively. Inserting either a thin or thick Alq_3 layer in between ITO and NPB does not change the NPB film morphology significantly. However, the presence of even a nanometer thin Alq_3 interlayer between ITO and NPB in a device, i.e. of ITO/Alq_3/NPB/Ca/Ag can dramatically reduce the growth rate of dark spot as compared to ITO/NPB/Ca/Ag device. Therefore, the observed variation in the RMS roughness on ITO or at organic/ITO surface is not the main reason for initiating the dark spots in OLEDs.

In addition to the effect of film surface morphology on the dark spot formation, the interfacial properties at anode/organic and organic/cathode interfaces were investigated using XPS. In order to investigate the chemical interaction between the organic films and ITO at the organic/ITO interface, XPS studies were carried out

for the organic films with different layer thicknesses. Using samples with different films thicknesses avoid the need to use sputtering to reach the region where organic films and ITO interaction has taken place. Organic films and ITO interaction can be resolved when the film thickness approaches zero. From the XPS data, it was found that there was a chemical interaction at the Alq_3/ITO interface. Alq_3 breakdowns at the interface releasing the free Al^{3+} ions which then are bounded with the oxides to form Al_xO_y. However, there was no apparent chemical reaction observed at the NPB/ITO interface.

The XPS depth profiles of OLEDs reveal that, oxidation of calcium occurred at the organic/cathode interface for ITO/NPB/Ca/Ag device. Nevertheless, reduction of ITO was observed at the organic/anode interface. There were also no evidence of oxygen and indium diffusion from either ITO to cathode or from cathode to ITO. In the XPS depth profiles of both fresh and degraded devices, oxygen and indium signals were not detectable in the organic layer. This confirms that the formation of dark spots occurs at the organic/cathode interface. However, it has great influence from the anode/organic interface.

From the XPS experiments, it was shown that oxidation occurred at the cathode/organic interface and reduction took place at the ITO/organic interface. This research work also reveals that there exists a galvanic cell between the calcium cathode and the ITO anode. The growth rate of dark spots was accelerated due to a corrosion process in the galvanic cell, which is attributed to the built-in potential caused by different potentials in the two electrodes. The presence of a pair of dissimilar electrodes and an electrolyte forms a galvanic cell. For a galvanic cell, the

low electrode potential calcium is the anode, since calcium is corroded, and the high electrode potential ITO in the cathode, since it is protected. By offsetting the built-in potential in the galvanic cell using an external bias, the growth rate of dark spots is reduced to the slower growth rate, which is about 0.6 μm^2/min. Slow growth rate of dark spot was also observed when ITO was replaced by Au, Ag, Al and Ca in the device with a configuration of ITO/NPB/Ca/Ag. The main reason for the slower growth rate is due to the fact that the metals used are difficult to be reduced.

Based on the results obtained, a model of dark spot formation in OLEDs under non-operating condition is proposed. In this model, corrosion of the active metal cathode (in this case the calcium) is mainly responsible for the growth of dark spots. Since it is a corrosion process, moisture and oxygen in air made the major contribution in the corrosion process which aids the growth rate of dark spot. Moisture is absorbed by OLED through the pre-existing pin-holes, and acts as the electrolyte in the galvanic cell formed between the ITO and Ca electrodes. When oxidation occurs at calcium electrode, electrons are transported to the ITO through the conducting organic layers. This process is driven by the internal built-in potential between Ca and ITO. At the ITO, oxygen is released by a reduction process when ITO accepts electrons. Oxygen is then dissolved in moisture that was absorbed through the pin-hole. The corrosion rate for calcium increases since oxygen concentration increases. This explains the fast growth rate of dark spot in ITO/NPB/Ca/Ag device. In the case of ITO/Alq_3/Ca/Ag, low dark spot growth rate was observed. From the XPS experiments, Alq_3 was fragmented and formed Al_xO_y at the Alq_3/ITO interface. The formation of Al_xO_y insulation layer prevented the

formation of galvanic cell between the ITO and Ca. Therefore a low corrosion rate was observed.

In the last section, the results on the high performance OLEDs made with Alq_3-modified ITO are presented. The presence of an ultra thin (1-2 nm) Alq_3 interlayer in between ITO and NPB has an advantage of retarding the growth of dark spots. Comparing with a conventional OLED of ITO/NPB/Alq_3/Ca/Ag, current efficiency of the OLED made with Alq_3-modified ITO anode can be increased by approximately 25% without a significant increase in the operating voltage. Most importantly, the addition of Alq_3 interlayer also enhances the devices operational stability.

References

References

Adachi C., Tsutsui T., Saito S., *Appl. Phys. Lett.*, **56**, 799, 1990

Adachi C., Hagai K., Tamoto N., *Appl. Phys. Lett.*, **66**, 2679, 1995

Aria M., Nakaya K., Onitsuka O., Inoue T., Codama M., Tanaka M., Tanabe H., *Synth. Met.*, **91**, 21, 1997

Aziz H. and Popovic Z., *Chem. Mater.*, **16**, 4522, 2004

Aziz H., Popovic Z., Xie S., Hor A., Hu N., Tripp C., Xu G., *Appl. Phys. Lett.*, **72**, 756, 1998-a

Aziz H., Popovic Z., Hu N., Hor A., Xu G., *Appl. Phys. Lett.*, **72**, 2642, 1998-b

Aziz H., Popovic Z.D., Hu N-X., Hor A-M., Xu G., *Science*, **283**, 1900, 1999

Baldo M.A., O'Brien D.F., You Y., Shoustikov A., Sibley S., Thompson M.E., Forrest S.R., *Nature*, **395**, 151, 1998

Baldo M.A., Thompson M.E., Forrest S.R., *Pure Appl. Chem.*, **71**, 2095, 1999

Baldo M.A., Thompson M.E., Forrest S.R., *Nature*, **403**, 750, 2000

Braun D. and Heeger A.J., 1991, *Appl. Phys. Lett.*, **58**, 1982

Burroughes J.H., Bradley D.D.C., Brown A.R., Marks R.N., Mackay K., Friend R.H., Burns P.L., Holmes A.B., *Nature*, **347**, 539, 1990

Burrows P.E., Bulovic V., Forrest S.R., Sapochak L.S., McMarty D.M., Thompson M.E., *Appl. Phys. Lett.*, **65** ,2922, 1994

Burrows P.E. and Forrest S.R., *Appl. Phys. Lett.*, **64**, 2285, 1994

Burrows P.E., Forrest S.R., Thompson M.E., Sibley S.P., *Appl. Phys. Lett.*, **69**, 2959, 1996

Burrows P.E., Gu G., Bulovic, Forrest S.R., Thompson M.E., *IEEE Trans. Electron Devices*, **44**, 1188, 1997

Chen C.H., Shi J., Tang C.W., *Macromol. Symp.*, **125**, 1, 1997

Chen B.J., Lai W.Y., Gao Z.Q., Lee C.S., Lee S.T., Gambling W.A., *Appl. Phys. Lett.* **75**, 4010, 1999

Colvin V.L., Schlamp M.C., Allvisatos A.P., *Nature* **370**, 354, 1994

Dabbousi B.O., Bawendi M.G., Onitsuka O., Rubner M.F., *Appl. Phys. Lett.*, **66**, 1316, 1995

Deng Z.B., Ding X.M., Lee S.T., Gambling W.A., *Appl. Phys. Lett.* **74**, 2227, 1999-a

Deng Z.B., Lee S.T., Webb D.P., Chan Y.C., Gambling W.A., *Synth. Met.* **107**, 107, 1999-b

Destriau G., *J. Chem. Phys*., **33**, 587, 1936

Do L.M., Han E.M., Niidome Y., Fujihira M., Kanmo T., Yoshida S., Maeda A., Ikushima A.J., *J. Appl .Phys.*, **76**, 5118, 1994

Do L.M., Han E.M., Yamamoto N.Y., *Mol. Cryst. Liq Cryst.*, **280**, 373, 1996

Doi S., Osada T., Tsuchida Y., Noguchi T., Ohnishi T., *Synth. Met*., **85**, 1281, 1997

Fatemi D.J., Murata H., Merritt C.D., Kafafi Z.H., *Synth. Met*., **85**, 1225, 1997

Forsythe E.W., Abkowitz M.A., *J. Phys. Chem. B* **104**, 3948, 2000

Frederiksen P., Bjornholm T., Madsen H.G., Bechgaard K., *J. Mater. Chem*., **4**, 675, 1994

Friend R.H., Gymer R.W., Holmes A.B., Burroughes J.H., Marks R.N., Taliani C., Dos Santos D.D.C., Bradley D.A., Bredas J.L., Logdlund M., Salaneck W.R., *Nature*, **397**, 121, 1999

Fujihira M., Do L.M, Koike A., Han E.M., *Appl. Phys. Lett.*, **68**, 1787, 1997

Gao Z.Q., Lee C.S., Bello I., Lee S.T., Chen R.M., Luh T.Y., Shi J., Tang C.W., *Appl. Phys. Lett*., **74**, 865, 1999

Glinski J., Godlewski J., Kalinowski J., *Mol. Cryst. Liq. Cryst*., **48**, 1, 1978

Granström M., Inganäs O., *Appl. Phys. Lett*., **68**, 147, 1996

Greenham N.C., Friend R.H., *Solid State Physics Advances in Research and Applications*., **49**, 2, 1995

Gu G., Forrest S.R., *IEEE J. of Selected Topics in Quantum Electronics*, **4**, 83, 1998

Gutmann F., Lyons L.E., *Organic Semiconductor*, John Wiley & Sons, Inc. , 1967

Gymer R.W., *Endeavour*, **20**, 115, 1996

Hamada Y., Sano T., Fujita M., Fujii T., Nishio Y., Shibata K., *Jpn. J. Appl. Phys*., **32**, L514, 1993-a

Hamada Y., Sano T., Fujita M., Fujii T., Nishio Y., Shibata K., *Chem. Lett*., 905, 1993-b

Hamada Y., Sano T., Shibata K., Kuroki K., *Jpn. J. Appl. Phys*., **34**, L824, 1995

Hamada Y., Sano Y., Fuji H., Nishio Y., Takahashi H., Shibata K., *Jpn. J. Appl. Phys.*, **35**, L1339, 1996

Hamada Y., Sano T., Fujii H., Nishio Y., Takahashi H., Shibata K., *Appl. Phys. Lett.*, **71**, 3338, 1997

Hamada Y., Kanno H., Sano T., Fujii H., Nishio Y., Takahashi H., Usuki T., Shibata K., *Appl. Phys. Lett*., **72**, 1939, 1998

Hamada Y., Kanno H., Tsujioka T., Takahashi H., Usuki T., *Appl. Phys. Lett*., **75**, 1682, 1999

Hamaguchi M., Fuji A., Ohmori Y., Yoshino K., *Jpn. J. Appl. Phys*., **35**, L1462, 1996

Han E.M., Do L.M., Niidome Y., Fujihira M., *Chem Lett*., 969, 1994

Han E.M., Do L.M., Yamamoto N.Y., Fujihira M., *Mol. Cryst. Liq. Cryst*., **267**, 411, 1995-a

Han E.M. Do L.M., Yamamoto N.Y., Fujihira M., *Chem. Lett*., 57, 1995-b

Han E.M. Do L.M., Yamamoto N.Y., Fujihira M., *Thin Solid Films*, **273**, 202, 1996

Haskal E.I., *Synth. Met*., **91**, 187, 1997

Holonyak N.Jr., Bevacqua S.F., *Appl. Phys. Lett*., **1**, 82, 1962

Hosokawa C., Tokailin H., Higashi H., Kusumoto T., *Appl. Phys. Lett.* **60**, 1220, 1992

Hosokawa C., Higashi H., Nakamura H., Kusumoto T., *Appl. Phys. Lett*., **67**, 3853, 1995

Hosakawa C., Eida M., Matsuura M., Fukuoka K., Nakamura H., Kusumoto T., *Synth. Met*., **91**, 3, 1997

Hu N-X., Xie S., Popovic Z., Ong B., Hor A-M., *J. Am., Chem. Soc*., **121**, 5097, 1999

Hung L.S., Tang C.W., Mason M.G., *Appl. Phys. Lett.* **70**, 152, 1997

Hung L.S., Zheng L.R., Mason M.G., *Appl. Phys. Lett.* **78**, 673, 2001

Hung L.S, Chen C.H., Materials Science and Engineering: Report, **39**, 144, 2002

Itano K., Tsuzuki T., Ogawa H., Appleyard S., Willis M., Shirita Y., *IEEE Transactions on Electron Devices*, **44**, 1218, 1997

Jabbour G.E., Kawabe V., Shaheen S.E., Wang J.F., Morrell M.M., Kippelen B., Peyghambarian N., *Appl. Phys. Lett.* **71**, 1762, 1997

Jabbour G.E., Kippelen B., Armstrong N.R., Peyghambarian N., *Appl. Phys. Lett.* **73**, 1185, 1998

Jang M-S., Song S-Y., Shim H-K., Zyung T., Jung S-D., Do L-M., *Synth. Met*., **91**, 317, 1997

Jiang H.J., Zhou Y., Ooi B.S., Chen Y.W., Wee T., Lam Y.L., Huang J.S., Liu S.Y., *Thin Solid Films* **363**, 25, 2000

Jordon R.H., Dodabalapur A., Strukelj M., Miller T.M., Appl. Phys. Lett., **68**, 1192, 1996

Kalinowski J., Di Marco P., Cocchi M., Fattoru V., Camaioni N., Duff J., *Appl., Phys. Lett*., **68**, 2317, 1996

Kao K.C., Hwang W., *Electrical Transport in Solids: with Particular Reference to Organic Semiconductors*. Pergamon Press, 1981

Katsuma K., Shirota Y., *Adv., Mater*., **10**, 223, 1998

Kawaharada M., Ooishi M., Saito T., and Hasegawa E., *Synth. Met.*, **91**, 113, 1997

Kepler R.G., Beeson P.M., Jacobs S.J., Anderson R.A., Sinclair M.B., Valencia V.S., Cahill P.A., *Appl. Phys. Lett*. **66**, 3618, 1995

Kido J., Kimura M., Nagai K., *Science*, **267**, 1332, 1995

Kido J. and Endo J., *Chem. Lett*., 593, 1997

Kido J., Iizumi Y., *Appl. Phys. Lett*., **73**, 2721, 1998

Kijima Y., Asai N., Kishii N., Tamura S., *IEEE Transactions on Electron Devices*, **44**, 1222, 1997

Kim J.S., Granström M., Friend R.H., Johansson N., Salaneck W.R., Daik R., Feast W.J., Cacialli F., *J. Appl. Phys.*, **84**, 6859, 1998

Kim J.S., Ho P.K.H., Murphy C.E., Baynes N., Friend R.H., *Adv. Mater.*, **14**, 206, 2002

Kolosov D., English D.S., Bulovic V., Barbara P.F., Forrest S.R., Thompson M.E., *J. Appl. Phys.,* **90**, 3242, 2001

Kraft A., Gimsdale A.C., Holmes A.B., *Angew. Chem. Int. Ed.* **37**, 402, 1998

Liao L.S., Sun X.H., Cheng L.F., Wong N.B., Lee C.S., Lee S.T., *Chem. Phys. Lett.*, **333**, 212, 2001

Liew Y.F., Aziz H., Hu N.X., Chan H.S.O., Xu G., Popovic Z., *Appl. Phys. Lett.*, **77**, 2650, 2000

McElvain J., Antoniadis H., Hueschen M.R, Miller J.N, Roitman D.M, Moon R.L., *J. Appl. Phys.*, **80**, 6002, 1996

Mitschke U. and Buerle P., *J. Mater. Chem*., **10**, 1471, 2000

Mori T., Obata K., Imaizumi K., Mizutani T., *Appl. Phys. Lett*., **69**, 3309, 1996

Mori T., Obata K., Mizutani T., *Synth. Met*., **91**, 199, 1997

Murase A., Ishii M., Tokito S., Taga Y., *Anal. Chem.*, **73**, 2245, 2001

Murata H., Merritt C.D., Mattoussi H., Kafafi Z.H., *Proc. SPIE Int. Soc. Opt. Eng*., **3474**, 88, 1998

Naka S., Shinno K., Okada H., Onnagawa H., Miyashita K., *Jpn. J. Appl. Phys*., **33**, L1772, 1994

Nguyen T.P., Jolinat P., Destruel P., Clergereuux R., Farenc J., *Thin Solid Films*, **325**, 175, 1998

Nuesch F., Rothberg L.J., Forsythe E.W., Le Q.T., Gao Y., *Appl. Phys. Lett.* **74**, 880, 1999

Oktusu S., Onikubo T., Tamano M., Enokida T., *IEEE Transactions on Electron Devices*, **44**, 1302, 1997

Papadimitrakopoulos F., Zhang X-M., Thompson D.L., Higginson K.A., *Chem. Mater*., **8**, 1363, 1996

Papadimitrakopoulos F., Zhang X-M., Higginson K.A., *IEEE Journal of Selected Topic on Quantum Electronic*, **4**, 49, 1998

Pope M., Kallmann H.P., Magnante P., *J. Chem. Phys*., **38**, 2042, 1963

Pope M.and Swenberg C.E., *Electronic Process in Organic Crystals*, Oxford University Press, 1982

Popovic Z.D., Xie S., Hu N., Hor A., Fork D., Anderson G., Tripp C., *Thin Solid Films*, **363**, 6, 2000-a

Popovic Z.D., Aziz H., Hu N-X., Hor A-M, Xu G., *Synth. Met*., **111-112**, 229, 2000-b

Saito S., Tsutsui T., Era M., Takada N., Adachi C., Hamada Y., Wakimoto T., *Proc. SPIE*, **1910**, 212, 1993

Sakakibara Y., Okutsu S., Enokida T., Tina T., *Appl. Phys. Lett*., **74**, 2587, 1999

Salbeck J., *Ber. Bunsenges. Phys. Chem*., **100**, 1667, 1996

Sato Y., Kanai H., *Mol. Cryst. Liq. Cryst*., **253**, 143, 1994

Sato Y., Ogata T., Ichinosawa S., Murata Y., *Synth. Met*., **91**, 103, 1997

Sato Y., Ichinosawa S., Kanai H., *IEEE Journal of Selected Topics in Quantum Electronics*, **4**, 40, 1998

Schaer M., Nuesch F., Berner D., Leo W., Zuppiroli L., *Adv. Funct. Mater.*, **11**, 116, 2001

Scheblykin I.G., Arkhipov V.I., van der Auweraer M., De Schryver F., *Helv. Chim. Acta*, **84**, 3616, 2001

Sheats J.R., Antoniadis H., Hueschen M., Leonard W., J Miller., Moon R., Roitman D., Stocking A., *Science* **273**, 884, 1996

Shi J. and Tang C.W., *Appl. Phys. Lett*., **70**, 1665 , 1997

Shirota Y., Kuwabara Y., Inada H., Wakimoto T., Nakada H., Yonemoto Y., Kawami S., Imai K., *Appl. Phys. Lett*., **65**, 807, 1994

Shoustikov A., You Y., Burrows P.E., Thompson M.E., Forrest S.R., *Synth. Met*., **91**, 217, 1997

Shoustikov A.A., You Y., Thompson M.E., *IEEE Journal of Selected Topics in Quantum Electronics*, **4**,3, 1998

Sibley S., Thompson M.E., Burrows P.E., Forrest S.R., Chapter 2, *Electroluminescence in Molecular Materials*, in Optoelectronic Properties of Inorganic Compounds, edited by D. Max Roundhill and John P. Fackler, Jr., Plenum Press, New York, 1999

Stossel N., Staudigel J., Steuber F., Blassing J., Simmerer J., Winnacker A., Neuner H., Metzdorf D., Johannes H.-H., Kowalsky W., *Synth. Met.* **111-112**, 19, 2000

Stossel N., Staudigel J., Steuber F., Simmerer J., Winnacker A., *Appl. Phys. A.* **68**, 387, 1999

Tanaka H., Tokito S., Taga Y., Okada A. *Chem Commun*., **18**, 2175, 1996

Tang C.W., VanSlyke S.A., *Appl. Phys. Lett*., **51**, 913, 1987

Tang C.W., VanSlyke S.A., Chen C.H., *J. Appl. Phys*., **65**, 3610, 1989

Tao X.T., Suzuki H., Wada T., Miyata S., Sasabe H., *J. Am. Chem. Soc*., **121**, 9447, 1999

Tian P.F., Burrows P.E., Forrest S.R., *Appl. Phys. Lett*., **71**, 3197, 1997

Tokito S., Taga Y., Tsutsui T., *Synth. Met*., **91**, 49, 1997

VanSlyke S.A., Chen C.H., Tang C.W., *Appl. Phys. Lett*., **69**, 2160, 1996

Vestweber H., Rieb W., *Synth. Met*., **91**, 181, 1997

Wakimoto T., Yonemoto Y., Funaki J., Tsuchida M., Murayama R., Nakada H., Matsumoto H., Yamamura S., Nomura M., *Synth. Met*., **91**, 15, 1997

Wang J.F., Jabbour G.E., Mash E.A., Anderson J., Zhang Y., Lee P.A., Armstrong N.R., Peyghambarian N., Kippelen B., *Adv. Mater*., **11**, 1266, 1999

Wu C.C., Wu C.I., Sturm J.C., Kahn A., *Appl. Phys. Lett.* **70**, 1348, 1997

Yamashita K., Mori T., Mizutani T., *Synth. Met*., **91**, 203, 1997

Yang Y., Pei Q., *Appl. Phys. Lett*., **68,** 2708, 1996

Yang Y., Jiang H., Liu S., Zhou X., Wu F., Tian W., Ma Y., Shen J., *Synth. Met.*, **91**, 335, 1997

Yang J.P., Heremans P.L., Hoefnagels R., Tachelet W., Dieltiens P., Blockhuys F., Geise H.J., Borghs G., *Synth. Met.*, **108**, 95, 2000

Yoshida M., Fuji A., Ohmori Y., Yoshino K., *Jpn. J. Appl. Phys.*, **35**, L397, 1996

Zhang Z., Jiang X., Xu S., Nagatomo T., Omoto O., *Synth. Met.*, **91**, 131, 1997

Zhang Z., Jiang X., Xu S., Nagatomo T., Omoto O., *J. Phys. D: Appl. Phys.*, **31**, 32, 1998